Recent glacier change (1965 - 2021) and identification of surge-type glaciers on Severnaya Zemlya, Russian High Arctic

HOLLY ELIZABETH WYTIAHLOWSKY

Holly Elizabeth Wytiahlowsky

Recent glacier change (1965 - 2021) and identification of surge-type glaciers on Severnaya Zemlya, Russian High Arctic

Glaciers in the Russian High Arctic are rapidly losing mass due to strong atmospheric and oceanic warming of the Barents-Kara Sea region. However, most studies have concentrated on Novaya Zemlya, despite a 29% acceleration in mass loss on Severnaya Zemlya (SZ) in the past decade (2003-2009 to 2010-2017). Research on SZ has formerly been hindered by its inaccessibility and limited data availability, with long-term trends in glacier change largely unknown. Moreover, records of glacier change on SZ may be complicated by evidence of surging, rather than solely due to climatic perturbations. In this thesis, an assessment of recent glacier change (1965 to 2021) on SZ is presented, along with a new inventory of surge-type glaciers from a high-resolution digital elevation model (Arctic DEM), declassified spy-satellite photography (KH-7/9 Hexagon), and optical satellite imagery (Sentinel 2, ASTER & Landsat 8 & TM). A total of 190 glaciers were mapped at five dates and surveyed for glaciological and geomorphological criteria indicative of former or active surging (e.g., thrust-block moraines and looped medial moraines). The results show that the glacierised area reduced from 17,053 km^2 in 1965 to 16,275 in 2021 (-778 km^2) and retreat rates accelerated post-1997. There is no evidence of summer air temperature warming on northern SZ, with most glacier retreat occurring in the south of SZ where land-terminating glaciers have retreated (some up to 30%), attributed to emerging summer air temperature warming trends. Further north, glacier retreat is attributed to rising ocean temperatures and strong annual atmospheric warming which has likely lengthened the melt season. Additionally, four glaciers are classified as surge-type, seven as likely and nine as possible, comprising 11% of SZ's glaciers. These glaciers occupy larger basins and are more likely to be marine or lake terminating.

Holly Elizabeth Wytiahlowsky

Recent glacier change (1965 - 2021) and identification of surge-type glaciers on Severnaya Zemlya, Russian High Arctic

Thesis submitted for MSc by Research degree

Department of Geography

Durham University

2022

Table of Contents

List of figures

List of Tables

List of Abbreviations

RHA - Russian High Arctic

SZ - Severnaya Zemlya

NZ - Novaya Zemlya

GrIS - Greenland Ice Sheet

FJL - Franz Josef Land

SLR - Sea level rise

SST - Sea surface temperature

NAO - North Atlantic Oscillation

CSR - Crevasse squeeze ridge

AoSIC - Academy of Sciences Ice Cap

LGM - Last Glacial Maximum

LIA - Little Ice Age

MIS - Matusevich Ice Shelf

RGI - Randolph Glacier Inventory

DEM - Digital Elevation Model

ASTER - Advanced Spaceborne Thermal Emission and Reflection Radiometer

RMS - Root mean square

NOAA - National Oceanic and Atmospheric Administration

NCEP - National Centres for Atmospheric Prediction

Acknowledgements

Firstly, I would like to thank Professors Chris Stokes and David Evans for their guidance and support throughout this degree. I have learnt a lot this year and it would not have been without the help of my supervisors.

I would also like to thank those that helped me settle into the department and joined me for excessively long coffee breaks. To my family and friends, you have been fantastic and thank you for all your support and company.

Chapter 1: Introduction

1.1 Arctic glacier change

Arctic glaciers and ice caps are rapidly losing mass due to strong atmospheric and oceanic warming (Carr et al., 2017a; Cook et al., 2019; Tepes et al., 2021a). Due to Arctic amplification, temperatures have risen faster than the global mean, with the Arctic warming by ~3.5 ˚C compared to the global mean of 0.85˚C, between 1880 and 2012 (Moon et al., 2018; Rantanen et al., 2022). In recent years, climatic warming has already accelerated glacier and ice sheet contributions to sea level rise (SLR) (Mengel et al., 2016; The IMBIE Team, 2020; Edwards et al., 2021), which, according to the IPCC will result in irreversible impacts (e.g., glacier melt and SLR) if global warming exceeds 1.5 ˚C above pre-industrial levels (Pörtner et al., 2022). Resulting SLR contributions are anticipated to exceed 51 cm by 2100 under an unchecked emission growth scenario (Bamber et al., 2019). Between 2010 and 2017, Arctic glaciers (excluding the Greenland Ice Sheet (GrIS) and peripheral glaciers) lost 609 ± 7 Gt of ice, equating to a SLR of 0.240 ± 0.007 mm a^{-1} (Tepes et al., 2021a). During this period (excluding the GrIS and peripheral glaciers), the largest mass losses in the Arctic occurred in the southern Canadian Arctic (-606 ± 44 kg m^{-2} a^{-1}) and in the Russian High Arctic (RHA) (Noël et al., 2018; Zemp et al., 2019; Tepes et al., 2021a), which is primarily dominated by mass loss from Novaya Zemlya (NZ) (-385 ± 18 kg m^{-2} a^{-1}) (Tepes et al., 2021b).

Atmospheric warming is the primary driver of Arctic glacier loss, whereas oceanic warming has been largely restricted to Atlantic-influenced Greenland and the eastern Arctic, in the Barents-Kara Sea region (Straneo & Heimbach, 2013; Carr et al., 2017a; Sommer et al., 2018; Tepes et al., 2021b). The inflow of warmer Atlantic waters into the Eurasian Basin is a key driver of glacier retreat in the RHA and has been proposed as the primary driver of glacier retreat on Severnaya Zemlya (SZ), whereas NZ is complicated by ocean-atmospheric forcing (Polyakov et al., 2017; Tepes et al., 2021b). For example, warmer waters and reduced sea ice concentrations surrounding NZ allow heat fluxes to rise through the water column, interacting with the atmosphere (Carr et al., 2017; Tepes et al., 2021b). By comparison, there are higher sea ice concentrations and a more pronounced ocean stratification towards SZ, reducing such ocean-atmosphere heat transfer (Tepes et al., 2021b). Increasing oceanic temperatures in the RHA threaten to accelerate the rate of glacier loss andSLR, notably on SZ, a region thought to

be less sensitive to ocean-climate warming, but which has undergone a 29% increase in specific mass loss from 2003 to 2009 and 2010 to 2017 (Tepes et al., 2021b).

In recent years, SZ has not only undergone accelerated mass loss (Sommer et al., 2022) but also increasing glacier flow speeds, with some notable 'surging' activity linked to a switch in basal thermal regime, potentially attributed to climatic changes (Strozzi et al., 2017). Most notable of these was the destabilisation of the western basin of the Vavilov Ice Cap, which transitioned from land to marine-terminating and advanced >8 km (Willis et al., 2018). In general, however, research on SZ has been hindered by inaccessibility and poor data availability, hence both the very recent and long-term trends in glacial retreat/advance are largely unknown compared to elsewhere in the European High Arctic (e.g., NZ, Svalbard). The recent availability of new high-resolution imagery (e.g., Sentinel 2 and the Arctic DEM Version 3(Arctic digital elevation model)) and gravimetry and altimetry data (e.g., GRACE and ICESat) has led to an increase in research on SZ, which has focused on glacier elevation changes and overall mass balance estimates (e.g.,Ciraci et al., 2018; Tepes et al., 2021b). However, whilst mass balance estimates are known for the last few decades, it is not known how changes in mass balance manifest as changes in surface area, nor how different types of glaciers on SZ (e.g., marine or land-terminating glaciers and potential surge-type glaciers) are responding to climatic drivers. This can be understood by interpreting a record of glacier area change, but no long-term record exists, despite the availability of decommissioned KH-7 1960s imagery and a range of medium to high-resolution imagery through to the present-day.

However, a record of long-term glacier change may be complicated by the presence of surge-type glaciers on SZ (Dowdeswell & Williams, 1997; Glazovsky et al., 2015; Sánchez-Gámez et al., 2019). Surge-type glaciers are believed to be uncommon in the eastern Russian High Arctic as climate is the primary control on surging and dictates that glaciers in cold and dry environments are less likely to be surge-type, although they have been documented, particularly in the Canadian High Arctic (e.g., Copland et al., 2003; Frappé and Clarke, 2007) (Sevestre and Benn, 2015; Benn et al., 2019). However, the precise trigger of a surge is not necessarily linked to regional climate, and instead may be due to changing basal conditions. The recent destabilisation of the Vavilov Ice Cap and the identification of two surge-diagnostic looped medial moraines on SZ are significant in that they provide clear evidence of glacier surging on SZ (Dowdeswell & Williams, 1997; Willis et al., 2018; Zheng et al., 2019). However, the wider distribution/existence of surge-type glaciers on SZ is largely unknown and an assessment of this is required in order to separate surge-driven glacier changes from the

impact of climatic change on glacier extent. However, it should be acknowledged that surge activity can be linked to climatic changes (e.g., Małecki et al., 2013; Kochtitzky et al., 2020). Additionally, an improved knowledge of surge-type glacier distribution and their characteristics on SZ can assist in improving the wider understanding of glacier surging, especially as glaciers on SZ are predominantly cold-based whereas most research on surging focuses on temperate and polythermal glaciers (e.g., Kamb et al. 1985; Raymond, 1987; Frappé & Clark 2007; Quincey et al., 2011; Benn et al., 2019; Thøgersen et al., 2019).

1.2 Aim, objectives, and research questions

1.2.1 Project aim

The main aim of this project is to provide the first long-term (1965 to 2021) record of glacier change on SZ in relation to climate change. A secondary aim is to provide a new inventory of surge-type glaciers in order to understand their wider distribution in the RHA and further the state of knowledge of surging in predominantly cold-based glaciers.

1.2.2 Objectives

To meet the aims of the thesis, the objectives are as follows:

1. Acquire and process imagery (e.g., georeferencing KH-7 imagery) from KH-7 (1965), KH-9 (1979), Landsat TM (1986 and 1997), ASTER (2011), Sentinel-2A (2021), and Landsat 8 (2021), including Arctic DEM strips at a 2 m resolution (2018) in order to visualise and map glaciers and glacial geomorphology.
2. Delineate changes in glacier area from the imagery at five different time-steps.
3. Analyse climatological data (1936 to 2021) to explore possible links between glacier change and ocean-climate forcing.
4. Classify glaciers as either non-surge or confirmed surge-type, including categories of “likely to have surged” and “possible” from previously published criteria (see Grant et al., 2009 and Copland et al., 2003).
5. Examine the distribution/absence of surge-type glaciers, their characteristics, and the dynamics of surging on SZ.

1.2.3 Research Questions

The research questions that this study will address are as follows:

1. How extensively, and at what rate has the glacierised area on SZ changed since 1965? How does this compare to elsewhere in the Arctic?
2. What are the climatic controls on glacier dynamics on SZ? How does this explain observed patterns of glacial change?
3. Are there surge-type glaciers on SZ? If so, how prevalent are they, and what are the characteristics of surging on SZ?

1.3 Thesis structure

This thesis begins by reviewing the literature on Arctic glacier change in Chapter 2, including the contribution of glaciers and ice caps to sea level rise, a review of glacier mass balance, and rates of glacier change. The focus of the literature review is then narrowed down to the RHA and surge-type glaciers. Chapter 3 begins by outlining the study area and then summarises the changes in glacier extent on SZ since the LGM, followed by a review of recent (~100 yr) glacier changes. Chapter 4 describes the methods employed in this study, beginning with the methods used for glacier delineation, the calculation of error margins, and the methods used for identifying surge-type glaciers. The results of this study are presented in Chapter 5 and are subdivided into glacier changes, climatic changes, and the identification of surge-type glaciers. Chapter 6 firstly contextualises glacier changes with climate, and then discusses the existence and characteristics of surge-type glaciers on SZ. This chapter concludes with suggestions for further research on SZ. Lastly, Chapter 7 summarises the conclusions of this thesis.

Chapter 2: A Review of Arctic Glacier Change and Surge-Type Glaciers

2.1. Recent (post-20th Century Arctic Glacier Change)

2.1.1. Patterns of Arctic Glacier Change

Glaciers and ice caps in the Arctic are rapidly losing mass (Gardner et al., 2013; Wouters et al., 2019; Hugonnet et al., 2021; Tepes et al., 2021a), and are anticipated to substantially contribute to sea level rise throughout the 21st century (Mengel et al., 2016; Bamber et al., 2019; Edwards et al., 2021). Between 2010 and 2017, Arctic glaciers and ice caps (excluding the GrIS and peripheral glaciers) contributed 0.240 ± 0.007 mm a^{-1} to global SLR, almost doubling from 0.13 mm a^{-1} in ~1997 (Dowdeswell et al., 1997; Tepes et al., 2021a). In recent history (1971 to 2017), the regions dominating SLR contributions (excluding Greenland) have been Alaska, the Canadian Arctic (north and south), and the Russian High Arctic, which is dominated by mass loss from NZ (Fig. 2.1; Gardner et al., 2013; Box et al., 2018; Wouters et al., 2019). Over the next century, these regions are projected to dominate Arctic contributions to global SLR behind Greenland(Oerlemans et al., 2005; Edwards et al., 2021).

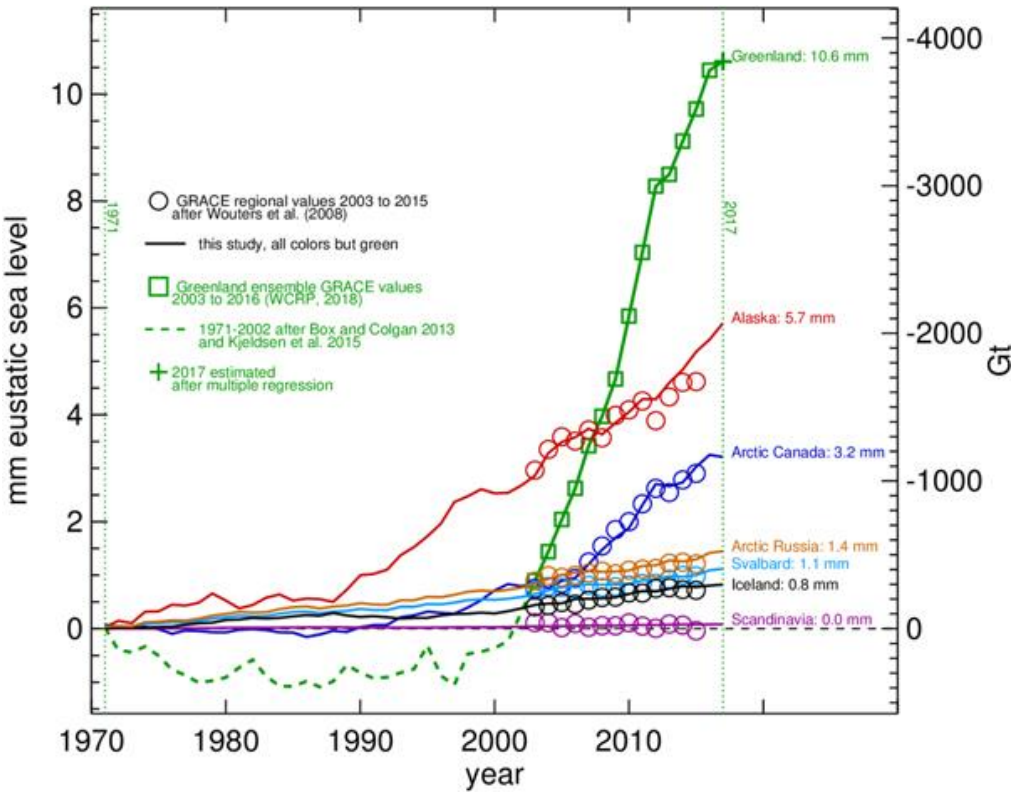

Fig. 2.1. *Arctic land ice contributions to SLR from 1971 to 2017 (from Box et al., 2018). The squares and circles show values obtained during the 2003 to 2015 GRACE observational period.*

Within the Arctic, Greenland is projected to dominate Arctic contributions to global SLR (2006 to 2100), with the GrIS and periphery glaciers predicted to contribute 120 mm to SLR under an RCP 8.5 emission scenario (Fig. 2.2; Moon et al., 2018). The highest SLR contributions mostly correspond with the most negative glacier mass budgets, with Arctic Canada North (-35.8 ± 3.5 Gt a^{-1}, 2002 to 2016) and South (-32.8 ± 7.8 Gt a^{-1}, 2002 to 2016) being the combined second largest contributor to projected SLR (33 mm, 2006 to 2100) (Moon et al., 2018; Wouters et al., 2019). In contrast, the recent mass budget of the RHA (-14.0 ± 0.5 Gt a^{-1}, 2010 to 2017) has remained relatively low by comparison to the Canadian Arctic yet poses a risk of a similar SLR contribution within the next century (28 mm, 2006 to 2100) (Moon et al., 2018; Tepes et al., 2021a). However, within the RHA, most of this mass loss is concentrated on NZ (-8.5 ± 0.4 Gt a^{-1}, 2010 to 2017), which is projected to have higher SLR contributions than further east on SZ, which has a substantially lower mass budget (-1.7 ± 0.1 Gt a^{-1}) (Oerlemans et al., 2005; Tepes et al., 2021a).

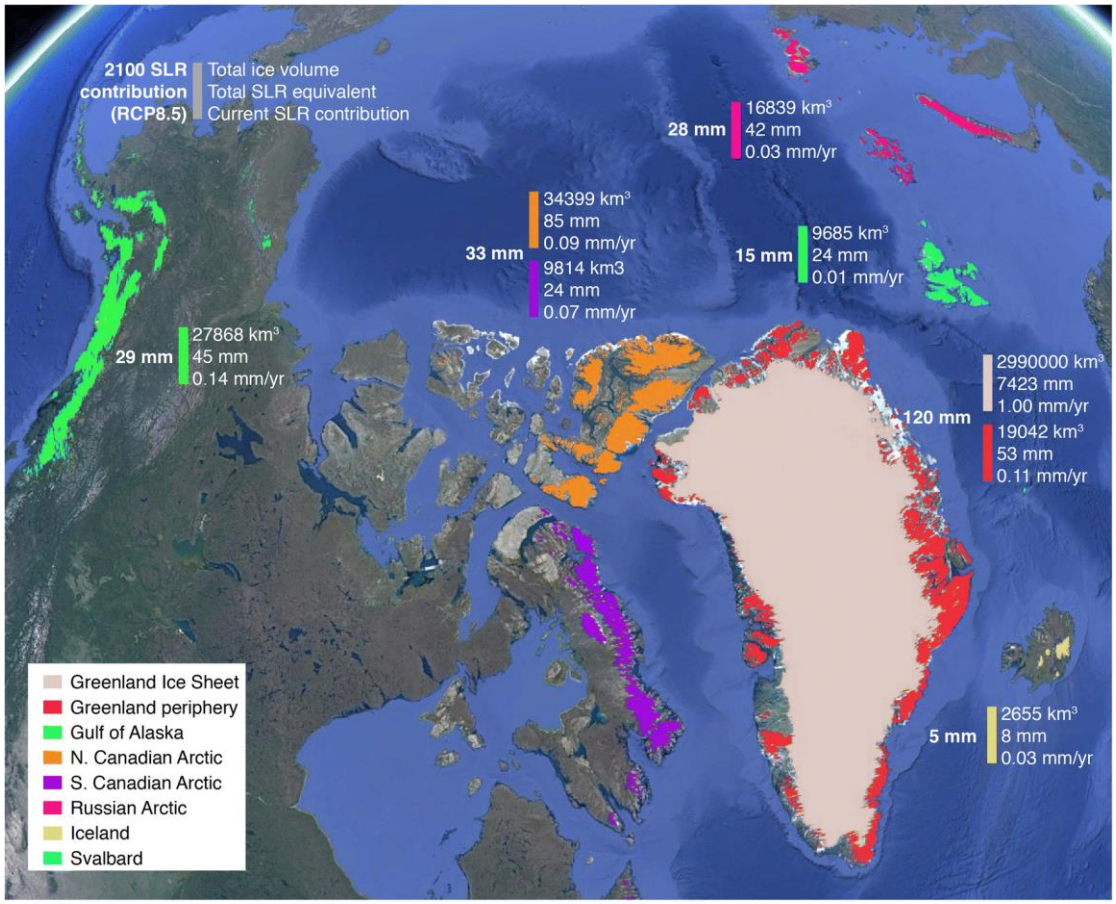

Fig. 2.2. *Projected 2100 SLR contributions, sub-divided to reflect projected regional contributions (from Moon et al., 2018). The data for each region follows the format shown in grey in the top left.*

Within the Arctic, not all regions are undergoing an acceleration in mass loss. Despite exhibiting the most negative mass balance in the Arctic, the GrIS has undergone a deceleration in mass loss, having peaked in 2011 (356 ± 66 billion tonnes a^{-1}) and since slowed to 220 ± 30 billion tonnes a^{-1} (2013 to 2017) (The IMBIE Team., 2020). Additionally, the Canadian Arctic has shown no statistically significant acceleration in mass loss between 2002 and 2019 (Ciracì et al., 2020). In contrast, the RHA recorded a statistically significant increase in mass loss (10 ± 2 Gt/a), with Franz Josef Land (FJL) undergoing an acceleration in mass loss, doubling between 1953 to 2011 (-2.18 ± 0.72 Gt a^{-1}) and 2011 to 2015 (-4.43 ± 0.78 Gt a^{-1}) (Zheng et al., 2018). FJL showed evidence of negative mass balance as early as 1953, which is significant as it provides evidence of a response to climatic changes in a region thought to have maintained a relatively stable mass balance (Zheng et al., 2018). However, further into the Atlantic-influenced domain, Svalbard and NZ have exhibited significant temporal variability in rates of mass loss, with average mass loss (between 2004 and 2012) peaking between 2004 and 2008 (32.9 ± 19.2 Gt a^{-1}) (Matsuo & Heki, 2013). The only region outside the GrIS to experience a deceleration in mass loss was Iceland (Ciracì et al., 2020). The fact that regions in the RHA are now experiencing accelerations in mass loss suggests that they are undergoing a shift in regime and hence require further monitoring to assess their potential impact on SLR in the near future.

2.1.2. Drivers of Arctic Glacier Change

2.1.2.1. Atmospheric warming

Over the last two decades, Arctic surface air temperatures have disproportionately warmed by over double the global average due, at least partially and potentially mostly, due to anthropogenic greenhouse gas emissions, with winter temperatures between 2016 and 2018 recorded at 6 °C above the 1981 to 2010 average (Meredith et al., 2019). Until the early 1980s, temperature anomalies were not observed in the Arctic, but annual air temperatures have since begun to strongly deviate from the long-term mean (up to 7°C from the 1981-2010 mean) (Rantanen et al., 2022). This is due to Arctic amplification, whereby anthropogenically-induced greenhouse gas emissions have increased atmospheric temperatures, in turn creating a positive feedback cycle related to the albedo of sea-ice. Warming temperatures have reduced the concentration of Arctic sea-ice, which in turn, lowers the surface albedo and results in the warming of the lower atmosphere and decreases north-south pressure gradients (Overland et al., 2019). In addition, Arctic warming has led to thawing of permafrost in the Arctic, further

accelerating warming; permafrost is anticipated to contribute 20 ± 85 Gt of carbon emissions by 2100 (Schaefer et al., 2014). When combined, these factors form the positive feedback cycle of Arctic amplification, accelerating the rate at which the Arctic warms. However, this amplification is not uniform, and amplification has disproportionately occurred in the RHA region of the Barents-Kara Sea, where sea-ice is known to be declining (Fig. 2.3c; Rantanen et al., 2022).

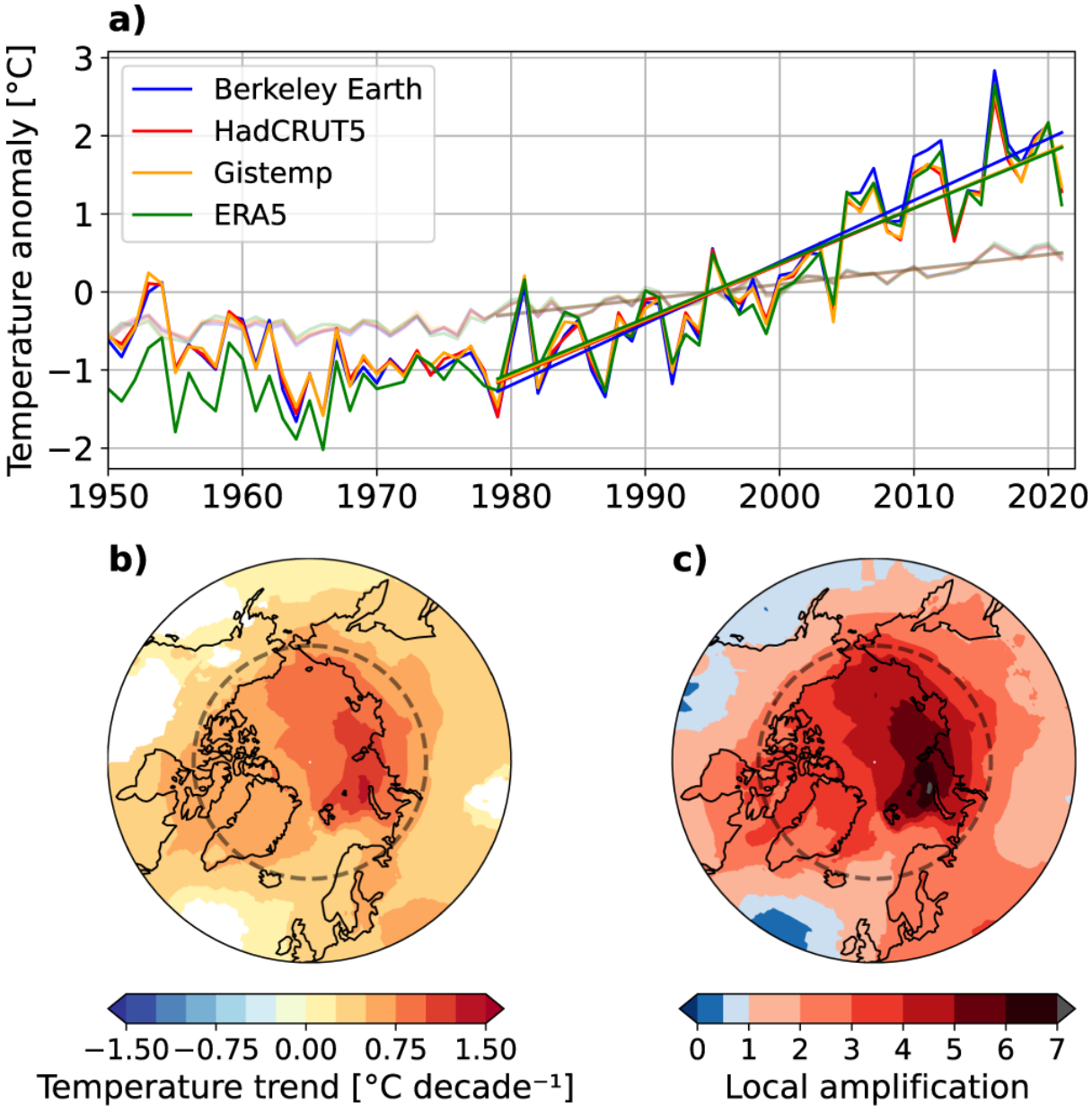

Fig. 2.3. *Trends in Arctic air temperature anomalies and amplification (from Rantanen et al., 2022). (a) Air temperature data from 1950 to 2021 was used, with anomalies calculated against a 30-year period between 1981 and 2010. (b) Annual mean temperature trends between 1979 and 2021, with trends derived from the average temperature of the observational period. (c) Local amplification ratio for 1979 to 2021, derived from the average of the observation period.*

Within the Arctic, winter atmospheric warming is occurring at a faster rate than summer warming. The Canadian Arctic recorded winter warming of 3.1 °C per century, whereas summer warming trends are considerably lower at 1.6 °C per century (van Wijngaarden, 2015). Warming was not uniform between 1895-2014 but occurred for 15 years post-1900, followed by a period of negligible warming and then warming initiating again in the late 1990s and then decelerating after 2000 (van Wijngaarden, 2015). Compared to the Canadian Arctic, annual warming trends on Svalbard are occurring at a slower rate of 2.6 °C per century, with the strongest decadal trend of warming occurring in spring (3.9 °C) instead of summer (1.0 °C) or winter (2.9 °C) (Nordli et al., 2014). On Svalbard, between 1898 and 2012, the coldest minimum occurred during the 1910s followed by a warmer 1930s, albeit of less intense warming than current temperatures (Nordli et al., 2014). The 1960s were characterised by a colder climate and preceded the upward trend of warming that extends to the present and which started in the 1970s (Nordli et al., 2014). On NZ, no significant trend of summer warming (June to August) was apparent between 1990 to 2011 (Carr et al., 2014). However since 2010, NZ has shown a progressive increase in summer warming anomalies (Ciracì et al., 2018), in accordance with the summer warming observed in Svalbard and the Canadian Arctic.

Atmospheric warming is identified to be a key control on the increasingly negative mass balance of Arctic glaciers (Carr et al., 2013). In the Canadian Arctic, summer near-surface atmospheric warming has been identified to be the primary control on the rapid retreat and negative mass balance of both land and marine-terminating glaciers (Cook et al., 2019). However, along with anthropogenic warming, much of the Atlantic Arctic is complicated by changes in atmospheric circulation patterns. Notably, in 2012 the GrIS underwent record surface melting due to abnormally high atmospheric temperatures (Hanna et al., 2012). This was attributed to a blocking local high-pressure feature due to negative North Atlantic Oscillation (NAO) conditions (Hanna et al., 2012). There has since been a reduction in mass loss due to cooler atmospheric conditions between 2013 and 2018 (The IMBIE Team., 2020), followed by anomalously warm summer air temperatures again in 2019 and subsequent high mass loss (Cullather et al., 2020). This suggests that high summer air temperatures are a key control of glacier mass loss, however, air temperature trends are subject to higher variability in regions highly influenced by the NAO.

2.1.2.2. Ocean warming

Over the past two decades, the Barents Sea region has experienced pronounced warming and is undergoing 'Atlantification' (Asbjørnsen et al., 2020). Atlantification refers to the eastward movement of conditions characteristic of the western Eurasian Basin and involves the northward movement of sea ice in the Barents Sea, increased vertical mixing, and weakening of ocean stratification (Fig. 2.4; Polyakov et al., 2017). Drivers of Atlantification were found to be regionally dependent, with the strongest warming trends occurring in the southern Barents Sea, south of the winter ice margin, due to the inflow of warmer Atlantic water (Asbjørnsen et al., 2020). However, in the northern Barents Sea, ocean advection and air-sea heat fluxes work in tandem to drive gradual warming (Asbjørnsen et al., 2020). Ocean temperature is found to influence calving rates at tidewater glaciers and, at depth, has been found to control c.50% of glacier frontal ablation on Svalbard (Luckman et al., 2015; Holmes et al., 2019), with alteration of ocean temperatures due to Atlantification posing a substantial threat to accelerated glacier retreat in the Eurasian Arctic.

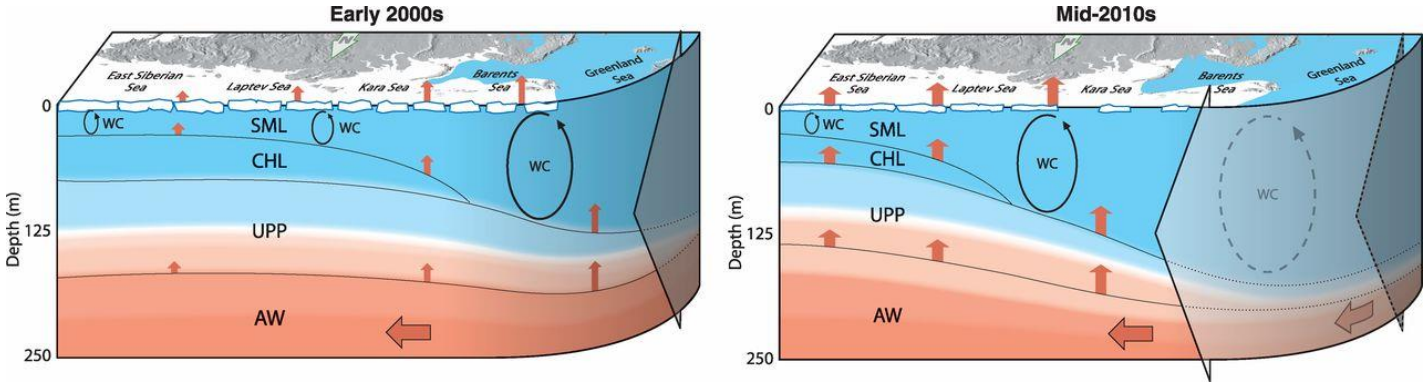

Fig. 2.4. *A schematic of Atlantification of the eastern continental margin of the Eurasian Basin in recent years (from Polyakov et al., 2017). The schematic shows the intrusion of Atlantic waters (AW) into the east Eurasian Basin, which has resulted in a reduction in ice cover, increased surface heat, moisture flux and increased depth of winter penetrative convection. This has transformed the permanent cold halocline layer (CHL) to a seasonal halocline. Other abbreviations show the surface mixed layer (SML), upper permanent pycnocline (UPP) and winter convection (WC), with heat fluxes shown by red arrows. Note the increased eastward movement of winter convection, reduced sea ice and increased heat flux transfer from the early to mid-2000s.*

2.1.2.3. Reduced sea-ice concentrations

Across the Atlantic Arctic, retreat rates of marine-terminating glaciers have increased threefold between 1992 to 2000 and 2000 to 2010, correlating with changes in sea-ice concentrations (Carr et al., 2017a). The largest increases in marine-terminating glacier frontal position change (from 1992 to 2000 and 2000 to 2010) are observed around Greenland, whereas by comparison, marine-terminating glaciers in north Svalbard have undergone the least frontal position change (Carr et al., 2017a). This disparity between regions has commonly been attributed to changes in sea ice and mélange concentrations (e.g., Carr et al., 2013, 2014; Moon et al., 2015; Bevan et al., 2019). For example, during two abnormally warm winters in SE Greenland, the lack of sea-ice buttressing allowed Kangerlussaq Glacier to calve uninterrupted, increasing its ice flow velocity by 35% and thinning it by 35 m (Bevan et al., 2019). Additionally, southeast Greenland is particularly vulnerable to anomalously high sea surface temperatures (SST) during warm phases of the Atlantic Multi-decadal Oscillation, further amplifying glacier retreat and reducing sea ice concentrations (Howat et al., 2008). Thus, sea ice is a vital control on glacier retreat rates, with the effect of sea ice decline likely to be amplified at marine-terminating outlets around Atlantic-influenced Greenland.

Similar trends can be anticipated at marine-terminating outlets as sea ice concentrations across the Arctic decline (Fig. 2.4; Fig. 2.5). The trend in Arctic sea ice decline is most prominent in September, which had a linear rate of decline of $-12.9 \pm 1.47\%$ per decade between 1978 - 2011 and equates to a 30% reduction in September sea ice since the late 1970s (Stroeve et al., 2012; Onarheim et al., 2018). The proportion of thick sea ice >5 years old has declined by >90% since 1979, with its demise attributed to an increase in greenhouse gas concentrations (IPCC, 2019). Declining Arctic sea-ice concentrations not only threaten rates of marine-terminating glacier retreat (Carr et al., 2013, 2014) but are also proposed as the primary driver of Arctic Amplification due to a decrease in Arctic surface albedo (Kim et al., 2016; Wunderling et al., 2020), reinforcing the significance of sea ice decline.

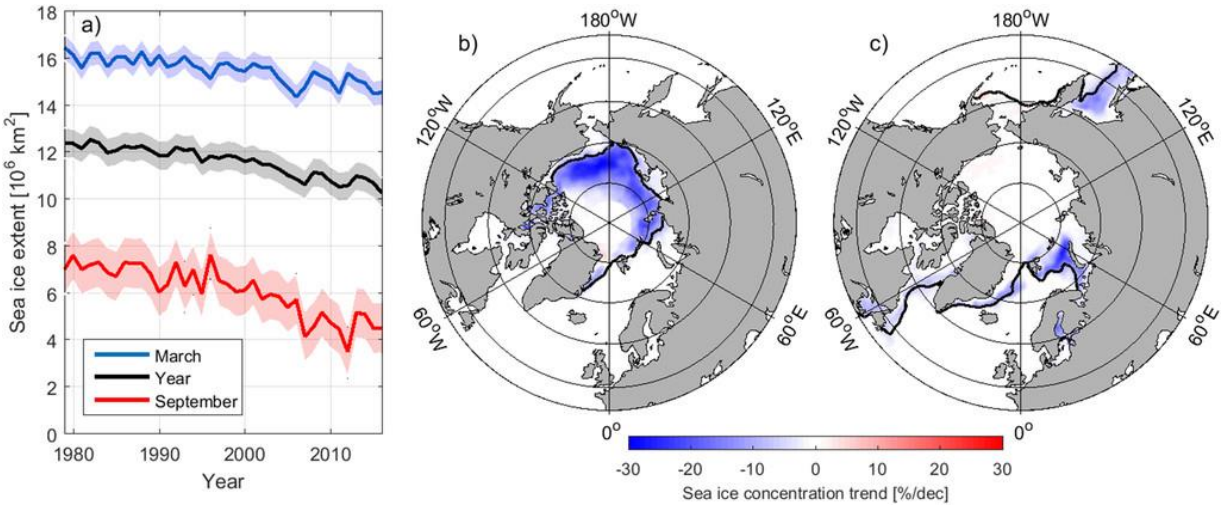

Fig. 2.5. *Changes in Northern Hemisphere sea ice extent from 1979 to 2016 (from Onarheim et al., 2018). (a) Trends in annual, March and September sea ice extent. Linear sea ice concentration trends (% decade^{-1}) in (b) September and (c) March. The black line indicates the mean sea ice edge.*

2.2. Glacier Change in the Russian High Arctic

The most recent survey of the RHA (~1999-2010), which includes FJL, NZ and SZ, identified 1069 glaciers, covering a combined area of ~52,000 km^2 (Fig. 2.6; Pfeffer et al., 2014), a decline from ~56,000 km^2 in ~1949-1968 (Grosval'd & Kotlyakov et al., 1969). However, since 2010, strong atmospheric and oceanic warming in the Eurasian Basin has resulted in increased surface ablation and mass loss (Tepes et al., 2021b). Across the RHA, gravimetric measurements estimate average ice loss rates to be 6.9 ± 7.4 Gt a^{-1} (2004-2012) (Matsuo & Heki, 2013), with recent SLR contributions of 0.06 ± 0.02 mm a^{-1} (2010-2017) (Sommer et al., 2022). However, mass loss is not regionally equal, with mass balance more negative further west in NZ (-431 ± 22 kg m^{-2} a^{-1}, 2010 to 2018) (Moholdt et al., 2012a; Tepes et al., 2021b). Eastwards, the mass balance was closer to equilibrium over SZ (-97 ± 8 kg m^{-2} a^{-1}) during the same period (Tepes et al., 2021b). The mass balance of FJL is intermediate between NZ and SZ (−297 ± 23 kg m^{-2} a^{-1}), with its annual surface air temperatures ~2°C warmer than SZ, but colder than NZ (Zheng et al., 2018). The same intermediate conditions are experienced with oceanic temperatures, resulting in a gradient of increasingly negative mass balance across SZ - FJL - NZ (Tepes et al., 2021a).

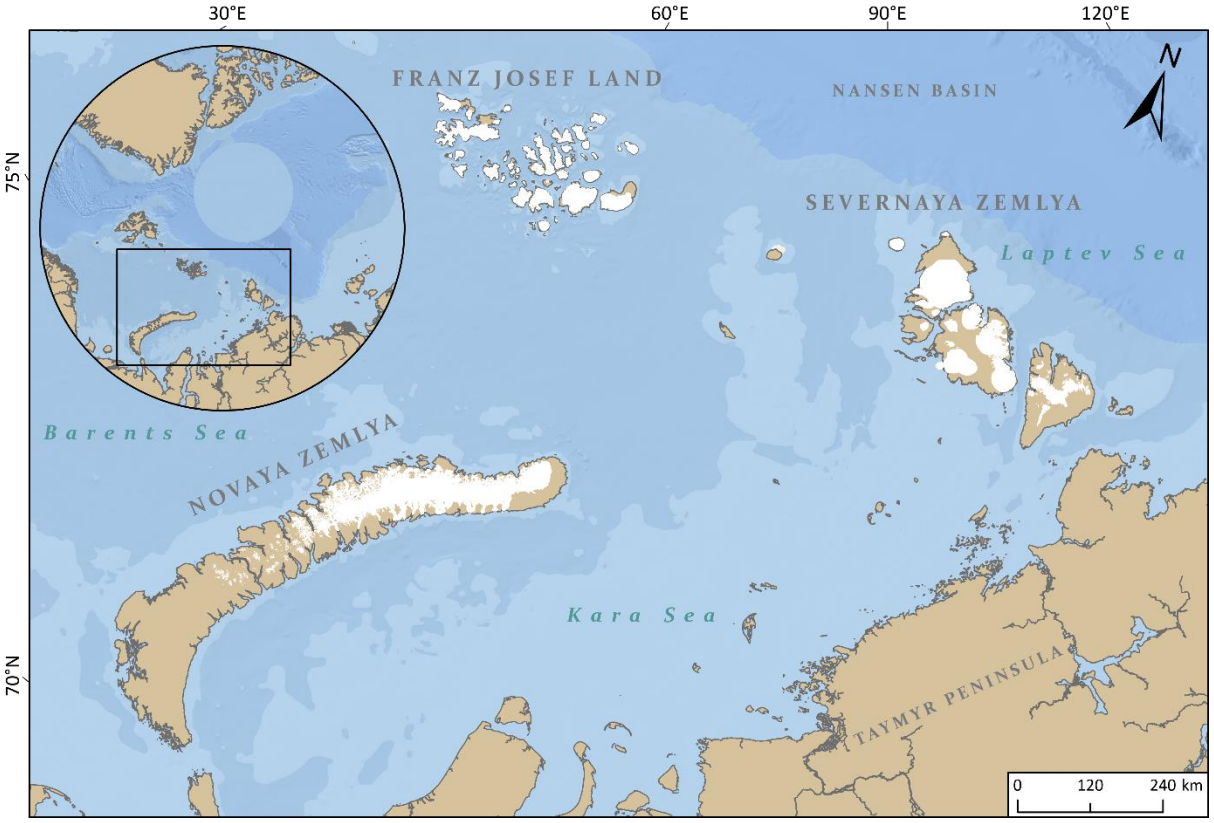

Fig. 2.6. *The location of the RHA archipelagos shown within the Arctic. Glacier outlines for SZ use the 2021 data produced by this study, and FJL (2016) and NZ (2013) glacier outlines were obtained from GLIMS.*

Regional variations in glacier mass loss within the RHA can be attributed to different climatic forcing mechanisms. Further west, NZ is characterised by increased intrusion of warmer Atlantic waters, which has reduced sea ice concentrations around NZ (Polyakov et al., 2017; Carr et al., 2017b). Declining sea ice around NZ has allowed for heat fluxes to rise into the atmospheric boundary layer from the water column, subsequently increasing the surface air temperature (Fig. 2.7; Rodrigues, 2008; Tepes et al., 2021b). Thus, mass loss on NZ is attributed to both ocean and atmospheric forcing. However, oceanic warming appears to be the primary control on mass loss, because marine marine-terminating glaciers there have retreated 3.5 times faster than land-terminating glaciers (Carr et al., 2017b; Tepes et al., 2021b). In contrast, this coupling is inhibited around SZ due to higher sea ice concentrations reducing the transfer of heat flux. Hence, air temperatures have remained much cooler than NZ, although there is evidence of ocean warming around SZ, which has begun to drive submarine melting at marine-terminating glaciers, albeit to a lesser degree than NZ (Tepes et al., 2021b).

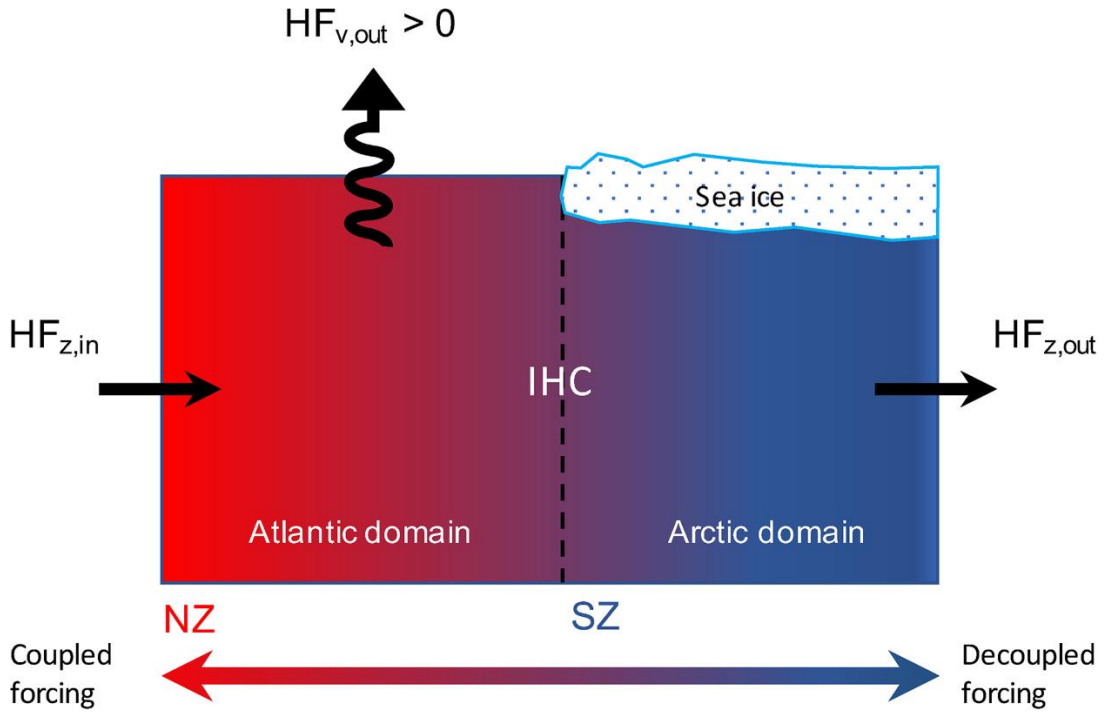

Fig. 2.7. *Heat flux schematic in the Barents-Kara Sea region (from Tepes et al. 2021b). Note the inhibition of heat flux transfer in the Arctic domain due to sea ice. This schematic represents the gradient between coupled and decoupled forcing as seen within the RHA, with NZ in the Atlantic domain, FJL in an intermediate domain, and SZ within the Arctic domain.*

Similarly, trends of reduced summer sea ice cover have been correlated with earlier surface snowpack melt on NZ and SZ and accelerated glacier retreat (Fig. 2.5; Carr et al., 2014; Zhao et al., 2014). Around NZ, sea ice concentrations declined post-2000 on the Barents Sea coast yet remained high on the Kara Sea coast (Carr et al., 2014). Declining sea ice was linked by Carr et al. (2014) to the preferential retreat of marine-terminating glaciers on the Barents Sea coast and identified to be a key control on marine-terminating glacier retreat because a lack of buttressing allows for higher calving rates. The same pattern is observed around FJL, with two periods of key sea ice decline in all seasons between 1995-99 and 2000-10 coinciding with accelerated glacier retreat (Carr et al., 2017b). Sea ice decline corresponds with periods of higher SST, which in the RHA have not solely been linked to climatic warming but also to positive phases of the NAO, which is known to increase the intrusion of warmer Atlantic waters further north (Carr et al., 2017b; Luo et al., 2019). The rate of sea ice decline in the RHA increased at a higher rate between 2001 and 2006 than any period after 1979 (Rodrigues, 2008), with a possible September ice-free Arctic by 2037 being likely if emissions are limited to, or

exceed 2°C (Wang & Overland, 2009; Screen & Williamson, 2017). This will inevitably affect glacier mass loss in the RHA.

2.3. Glacier Surging in the Arctic

2.3.1. Distribution

Within the Arctic, not all patterns of glacier advance and retreat can be attributed solely to climatic perturbations. Surge-type glaciers are widespread in the Arctic (Jiskoot et al., 2000; Copland et al., 2003; Sevestre et al., 2015; Farnsworth et al., 2016). Unlike non-surge-type glaciers, they are characterised by velocity increases and rapid transfer of mass downglacier, often manifesting as a cyclical pattern of advance and retreat, which results from glacier mass and energy are not being in balance (Sevestre & Benn, 2015; Benn et al., 2019). The global distribution of surge-type glaciers is uneven amongst glaciated regions, and they occur in large clusters in Alaska, Arctic Canada, Svalbard, Greenland, and Iceland, with others clusters of surge-type glaciers outside of the Arctic, notably in High Mountain Asia(Fig. 2.8;Sevestre & Benn, 2015). Within a surge cycle, glaciers alternate between a quiescent phase, characterised by slow flow, until the initiation of an active phase, whereby ice that has built up in the reservoir area is rapidly transferred down glacier (Kamb, 1987). Quiescent phase duration is regionally variable, with Svalbard surge-type glaciers characterised by a long ~50 to 100-year quiescent phase and a ~3 to 10-year active surge phase (Dowdeswell et al., 1991). This contrasts with those in Alaska and Yukon, where the active phase is typically 1 to 3 years and the quiescent period is ~20 to 40 years (Dowdeswell et al., 1991; Sun & Qiao, 2021).

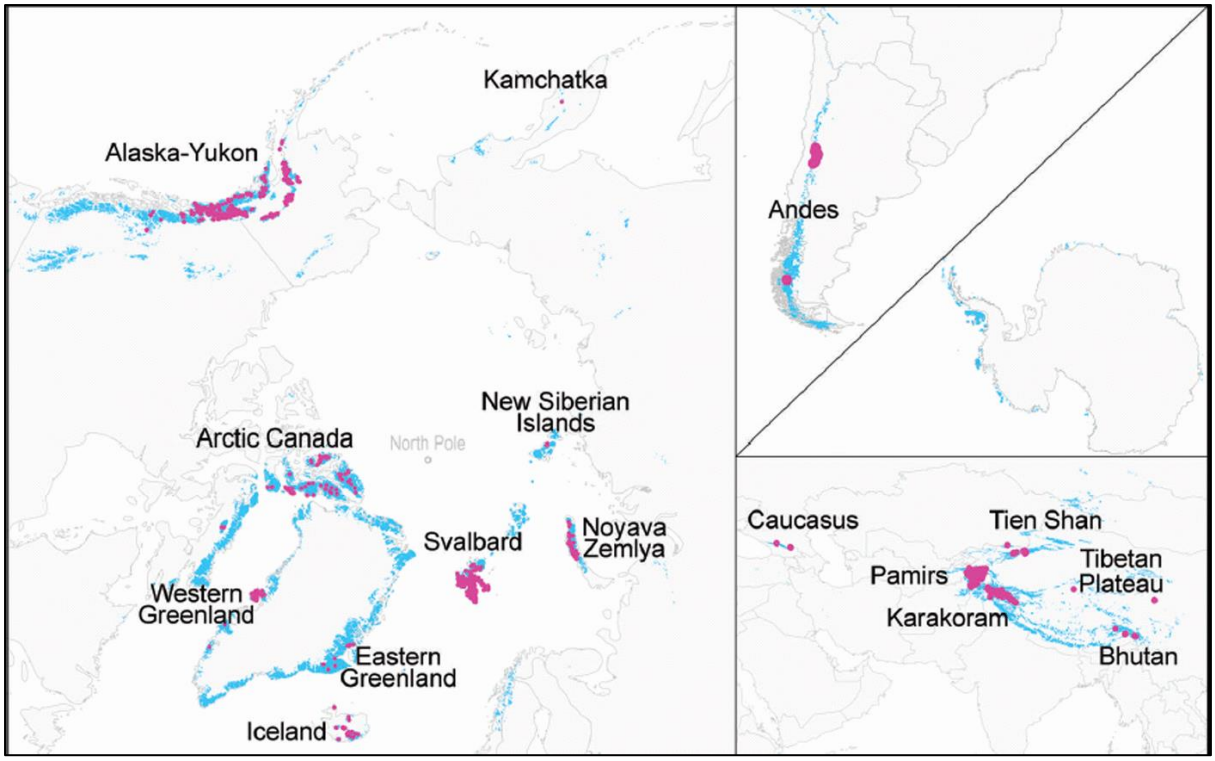

Fig. 2.8*. The known global distribution of surge-type glaciers (pink) and non-surge type glaciers (blue) (from Sevestre & Benn, 2015). Note that surge-type glaciers most commonly occur in clusters, with the highest density of surge-type glaciers occurring in Svalbard and Alaska but do occur in lesser numbers in the RHA.*

2.3.2. Mechanisms

The mechanisms driving surge-type behaviour have been heavily disputed and, until 2015, there was no unifying theory of surging for both temperate and polythermal glaciers (Sevestre & Benn, 2015; Benn et al., 2019) with most theories invoking surging as being dependent on basal thermal regime and/or the reorganisation of subglacial drainage systems (e.g., Kamb, 1987; Sharp, 1988; Flower et al., 2001; Fowler et al., 2001). Initial observations of surge-type glaciers focused on temperate glaciers in Alaska (e.g., Variegated Glacier) and propose changes in basal hydrology from an efficient to inefficient drainage system as the driver of surge initiation and termination (Kamb, 1987). Velocity variations during active surging are attributed to subglacial cavity linkage and varying pressurisation of water at the glacier bed. Surge termination occurs when high hydraulic gradients lead to the collapse of the cavity system which transitions into large conduits that drain subglacial water, terminating the surge (Kamb et al., 1985; Humphrey & Raymond, 1994). In temperate glaciers, it has been suggested

that this water is primarily routed to the bed during winter from englacial water storage and gravitational movement of water to the bed (Lingle and Fatland, 2003). However, this theory implies that surging only occurs on bedrock rather than on thicker sediment beds,, whereas surging behaviour is observed to have occurred on a variety of subglacial substrates (Kamb, 1987; Benn & Evans, 2010).

The mechanisms of surging are thought to differ in colder, polythermal glaciers (e.g., Svalbard), with surging occurring due to changes in the basal thermal regime (Fowler et al., 2001; Benn & Evans, 2010). Increased accumulation in the reservoir area during the quiescent period results in increasing driving stresses and creep rates, with ice creep generating heat and thereby increasing the proportion of warm-based ice. The presence of warm-based ice results in meltwater production at the bed, with the glacier front remaining predominantly cold-based (Murray et al., 1998; Smith et al., 2002). The active phase of surging occurs when basal water pressure increases enough for basal sliding and terminates once subglacial water has drained. The thermal switch model of surging was applied to Svalbard to test its applicability but failed to explain the surges of large glaciers (Sevestre et al., 2015). This is because it cannot explain surging due to thermal cycling where tidewater glaciers lack a cold-based frozen terminus. However, the model appears to be more applicable to smaller glaciers with cold-based termini (Sevestre et al., 2015). Instead, the concept of enthalpy is used to explain the variations in surge-type behaviour on Svalbard (Sevestre et al., 2015).

The concept of enthalpy provides the first theory of glacier surging that includes temperate and polythermal glaciers (Benn et al., 2019). According to this theory, surging occurs when mass and energy are not in balance, resulting in an unsteady state due to the glacier being unable to keep variables such as ice discharge and accumulation in equilibrium (e.g., if sufficient energy cannot be lost through drainage or conduction). A steady state is most easily maintained in cold, dry, and warm, humid environments with the intermediate (polythermal) condition most prone to surging. Climate, glacier geometry, and bed properties were all once hypothesised to independently drive surging behaviour (e.g., Hamilton & Dowdeswell, 1996; Jiskoot et al., 2001; Eisen et al., 2001). However, enthalpy theory states that together they determine whether glaciers are stable (normal) or in an unsteady state (surge-type). Factors such as climate can be linked to quiescent period duration, with snowfall accumulation hypothesised to dictate the length of the quiescent period and whether a glacier can build-up sufficient mass to surge (Eisen et al., 2001; Małecki et al., 2013). This results in the existence of an optimal climatic envelope

controlled by temperate and rates of precipitation (Sevestre & Benn, 2015). For example, Svalbard has lower rates of snowfall than Alaska, thus surging should occur less frequently due to the longer period required to replenish the reservoir zone. However, no one factor can solely predict whether a glacier is of surge-type or not.

Using a species distribution model, Sevestre & Benn (2015) were able to accurately predict the major distribution of surge-type glaciers using common surging climatic conditions and variables (Fig. 2.9). Additionally, they found surging was predicted in regions traditionally perceived to be mostly devoid of surge-type glaciers, notably the RHA (Dowdeswell & Williams, 1997; Grant et al., 2009), albeit mostly on NZ, and on the Antarctic Peninsula where no surging is presently known to occur. However, the model was found to underpredict glacier surging outside of the climatically optimal surge zone, in regions known to have surge-type glaciers. Thus, uncertainties remain as to where and under what conditions glaciers surge.

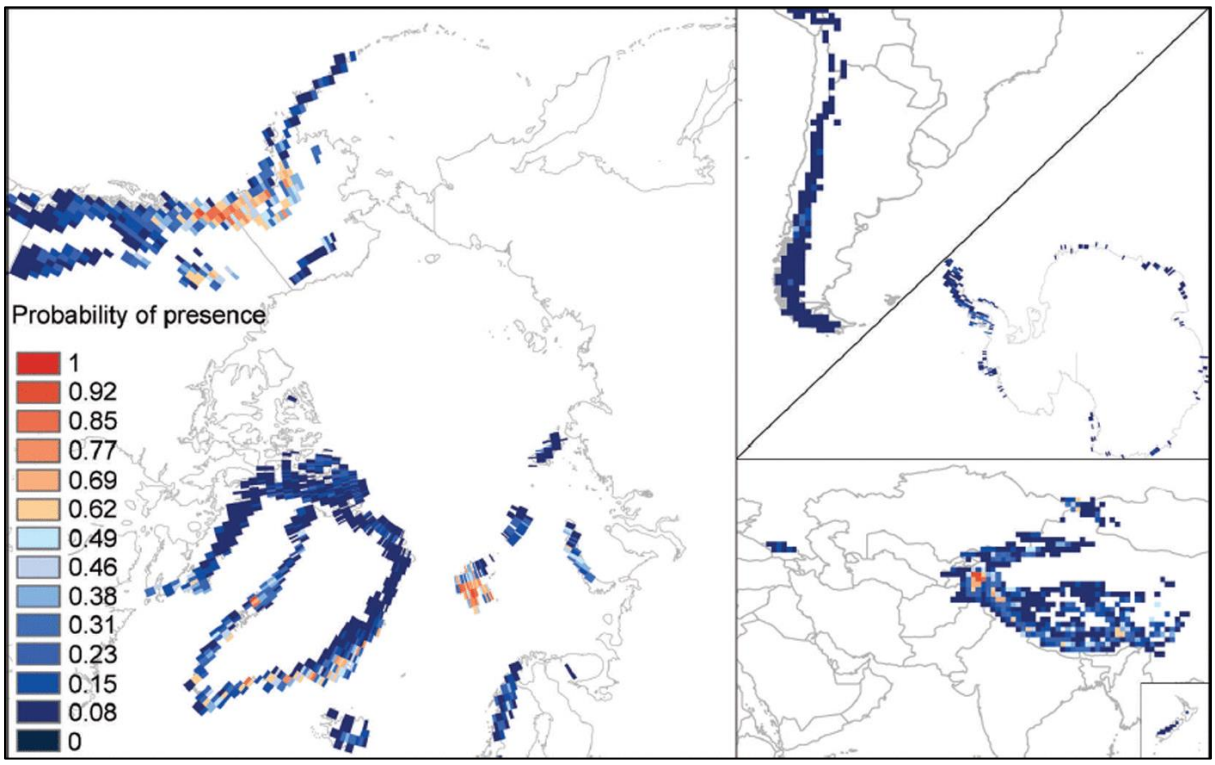

Fig. 2.9. *The prediction of surge-type glaciers using a species distribution model based upon optimal climatic and glacier geometry variables (from Sevestre & Benn, 2019). Note that the highest probability of surge-type glacier presence is in Svalbard. In the RHA, surge-type glaciers are predicted in FJL, NZ and in a small area of eastern SZ.*

2.3.3. Glaciological Evidence of Surging

Within the Arctic, surge-type glaciers are commonplace and have been observed in most regions (Fig. 2.8). Surging most frequently occurs in polythermal regimes, notably in abundance on Svalbard, where at least 32.6% of glaciers are likely to have surged (Lovell & Boston, 2017). However, surging is also known to have occurred in colder, dryer environments such as the Canadian High Arctic, following the identification of 51 surge-type glaciers there by Copland et al. (2003). Copland et al. (2003) systematically surveyed each glacier for geomorphological and glaciological criteria (e.g., looped medial moraines and digitate termini) indicative of surging and classified them by their likelihood of being surge-type. Subsequently, Grant et al. (2009) used the same methodology to identify surge-type glaciers on NZ in the RHA, which was previously assumed to be devoid of surging, except for a few looped medial moraines on NZ and SZ identified by Dowdeswell & Williams (1997). Thus, as no such survey has been conducted for FJL and SZ, the RHA remains one of the few regions in the Arctic where the presence of surge-type glaciers remains relatively unknown, despite some clear evidence suggesting that it does occur.

The initial survey of the RHA by Dowdeswell and Williams (1997) from 30-80 m Landsat TM imagery found limited evidence of surging. They aimed to identify the presence of ice surface features that indicate past/active surging, including looped medial moraines, potholes, and heavily crevassed surfaces. Subsequently, they identified three potential surge-type glaciers on NZ, two on SZ and none on FJL, contrasting with the >80 surge-type glaciers known to exist on Svalbard at the time (Dowdeswell & Williams., 1997). However, rapid retreat and iceberg production from Znemity Glacier in FJL was recorded by Kloster (1991), with Dowdeswell and Williams (1997) acknowledging that this may be evidence of surging in the archipelago, despite no surge indicative features found in FJL by their study. No further surge-type glaciers in the RHA were identified en-masse until Grant et al. (2009) classified 32 glaciers as potential surge-type on NZ.

Grant et al. (2009) demonstrated that surging was more common on NZ than initially thought, with 4.6% of NZ's glaciers and 18% of glacier area subsequently classified as surge-type. They utilised a large number of features diagnostic of surging, with glaciological features including: (1) looped medial moraines, (2) deformed ice structures, (3) shear margins, (4) heavy surface crevassing, (5) high surface velocities, (6) rapid terminus advance, (7) digitate terminus, (8)

ice-marginal strandlines and (9) surface potholes. Geomorphological features used are detailed in section 2.3.4. Most evidence of surging was concentrated in western NZ, in areas of higher precipitation, where large ice caps feed longer outlets with low slope angles. The detection of new surge-type glaciers is attributed to the use of imagery with a higher spatial resolution (> 4 m) by Grant et al. (2009) that allowed smaller-scale features to be identified.

Unlike NZ, no re-survey of FJL or SZ has been conducted utilising higher-resolution imagery, although both show some evidence of surge-like behaviour, including recent frontal destabilisations (Strozzi et al., 2017; Willis et al., 2018). On SZ, the western margin of the Vavilov Ice Cap, on the Kara Sea coast, had been slowly advancing since observations began in 1952 (Fig. 2.10; Willis et al., 2018). In 2000, rates of advance were steady, and the western margin had transitioned from land- to marine-terminating. By 2010, ice flow velocity had accelerated, reaching >1,000 m a^{-1} between 2014 and 2015, with the terminus splaying to form multiple grounded or partially grounded digitate ice tongues (Willis et al., 2018). The causation of this surge-like behaviour is attributed by Willis et al. (2018) to changing resistive stresses at the glacier bed and the removal of resistance at the ice front, with sliding aided by weakly consolidated, low-friction marine sediments at the glacier bed. It has been suggested that, due to the magnitude of mass loss (-11% of the basin), the Vavilov is unlikely to regain sufficient mass to 'surge' again and has instead transitioned into an ice stream-like regime (Zheng et al., 2019). The observation of surge-like behaviour in a predominantly cold-based ice cap suggests that surging does take place on SZ and that such instabilities may also exist elsewhere.

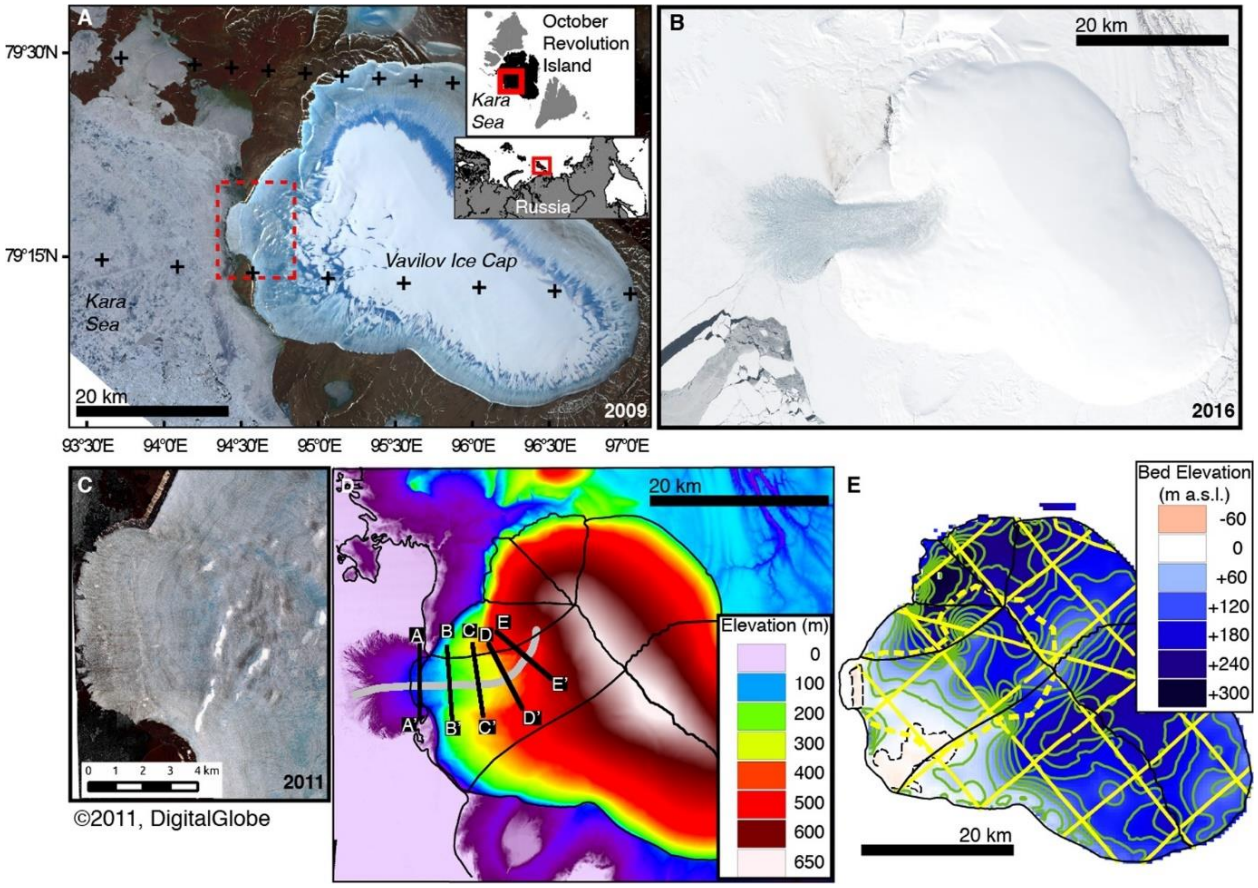

Fig. 2.10. *The 'surge' of the Vavilov Ice Cap, Severnaya Zemlya (from Willis et al., 2018). (A) ASTER imagery of the Vavilov Ice Cap in late summer 2009. (B) True colour Landsat-8 imagery from 2016. (C) True colour imagery of the Vavilov terminal moraine in 2011. (D) 2016 DEM elevation of the Vavilov Ice Cap. (E) Bed elevation derived from airborne radio echo sounding. The scale used in panel A is the same for panels B, D, and E.*

Elsewhere on SZ, the presence of surging in the Academy of Sciences Ice Cap (AoSIC) on Komsomolets Island, northern SZ, has been debated, with Dowdeswell et al. (2002) finding no evidence of surging within the residency time of the ice. However, Moholdt et al., (2012b) note that it may be more complicated because multiple basins appear to undergo oscillations in flow speed. Additionally, Basin A is characterised by a post-surge geometry and has undergone surge-like elevation changes (Moholdt et al., 2012b). Due to the apparent absence of heavy surface crevassing and relatively stable post-1960s terminus position, Basin A has not been classified as surge-type by the literature. However, the causation of the flow oscillation and surge-like features remain unknown and may be indicative of surging.

On FJL, Simony Glacier has exhibited a Vavilov-style frontal destabilisation, albeit of a smaller magnitude (Strozzi et al., 2017). FJL has had a negative mass balance since 1953, with most glaciers in net retreat, accompanied by increased frontal velocities (Zheng et al., 2018). Despite this, Simony Glacier is observed to have advanced between 1998 and 2014, with an increase in ice flow velocity and higher concentrations of crevasses (Strozzi et al., 2017). Strozzi et al. (2017) do not explicitly classify it as surge-type due to the absence of earlier synthetic-aperture radar images from which to assess whether it exhibits surge-like changes in ice flow velocity. This does, however, suggest that surge-type glaciers may exist on FJL, despite no prior record of surging there.

2.3.4. Geomorphological Evidence of Surging (Surging Landsystems)

Identifying where surging occurs is essential for understanding records of glacier change and the factors that control surging. Initial studies on surge-type glaciers identified individual features indicative of surge behaviour (e.g., Meier & Post, 1969; Sharp, 1988). Since then, the development of a holistic landsystem approach provides the most effective and convincing method for identifying surge-type glaciers (Evans & Rea, 1999). Landforms produced during surging can include (1) thrust block/push moraines, (2) overridden thrust block moraines, (3) zig-zag eskers, (4) looped medial moraines, (5) long flutings and (6) crevasse squeeze ridges (CSR) or geometric ridge networks (Fig. 2.11; Evans & Rea, 1999; Copland et al., 2003; Evans et al., 2007; Roberts et al., 2009). As the genesis of each individual surge indicative landform can be a product of equifinality, the presence of multiple surge-diagnostic landforms (a surging landsystem signature) are required to confidently identify former surges.

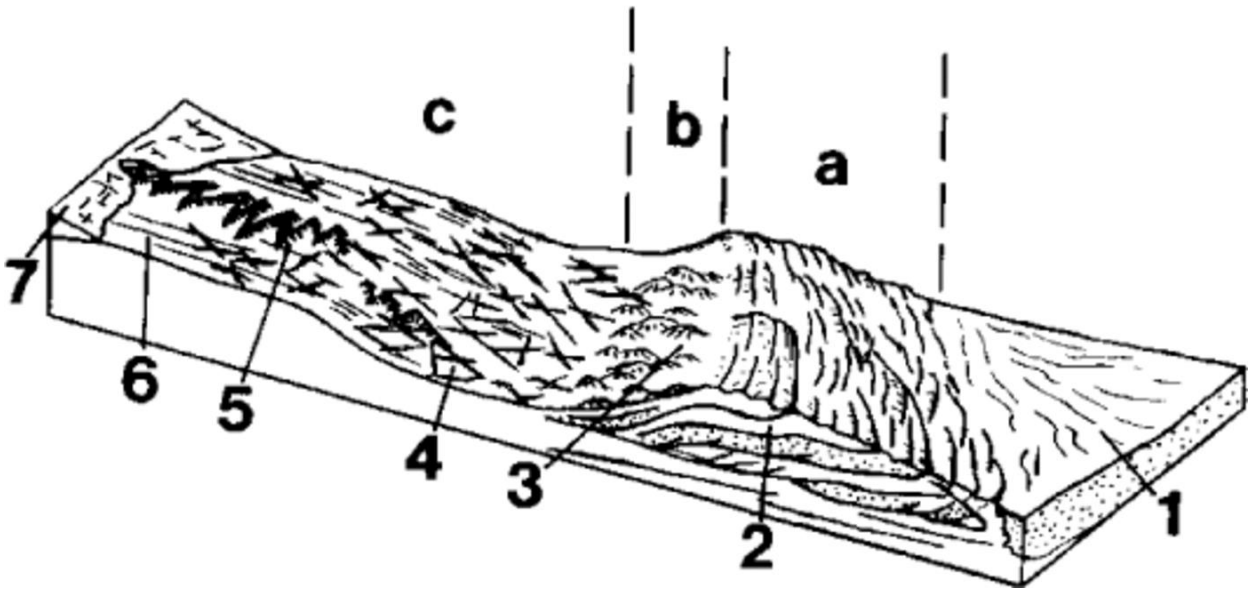

Fig. 2.11. *The surging glacier landsystem model (from Evans & Rea, 2003). (A) outer zone of proglacially thrust pre-surge sediment. (B) zone of weakly developed hummocky moraine. (C) zone of flutings, crevasse-squeeze ridges and zig-zag eskers. (1) proglacial outwash fan. (2) thrust-block moraine. (3) hummocky moraine. (4) crevasse- squeeze ridge. (5) zig-zag esker. (6) fluting. (7) glacier ice margin.*

Surge-indicative features are each of varying diagnostic power, with thrust-block moraines, zig-zag eskers, looped medial moraines (glaciological feature) and geometric ridge networks being the strongest (Meier & Post 1969; Lawson, 1996; Evans & Rea, 1999, 2003; Hewitt, 2007; Paul, 2015). Glacier advances into proglacial sediments produce arcuate thrust ridges and, in High Arctic environments, predominantly occur in coastal lowlands with thinner permafrost (Evans & England, 1991). Glaciotectonic thrust-block or composite moraines are strongly associated with surge-type glacier advances (Evans & Rea, 1999), although they have also formed at the margin of non-surging dry-based Antarctic glaciers (Fitzsimons, 1996). Despite equifinality, the success of using glaciotectonic moraines for identifying surge-type glaciers is highlighted by Lovell & Boston (2017) who identified 50 new glaciotectonic composite ridge systems and found that 49 were associated with known surge-type glaciers (Fig. 2.12). Of similarly high confidence are zig-zag eskers, which are assumed to form during a short-lived, high-discharge event shortly after surge termination (Fig. 2.13; Evans & Rea,

2003). They have been observed in glacier forelands on NZ (Grant et al., 2009), Iceland (Schomacker et al., 2014) and Svalbard (Hansen, 2003) and are not known to form in non-surge settings. Likewise, terminus-wide geometric ridge networks (CSRs) are thought to be unique to surging glacier forelands (Fig. 2.13; Rea and Evans, 2011; Evans et al. 2016), and have been used to identify 431 previously undocumented surge-type glaciers on Svalbard (Farnsworth et al., 2016), although they have a relatively low preservation potential due to active landscape modification in glacial forelands (Farnsworth et al., 2016). Despite the high diagnostic potential of some landforms, not all will form or be preserved in a surge-type glacier foreland. Hence, a landsystems approach is the most effective for identifying surging, as, despite equifinality, an array of multiple surge-indicative features in one foreland strengthens the likelihood of a glacier being of surge-type.

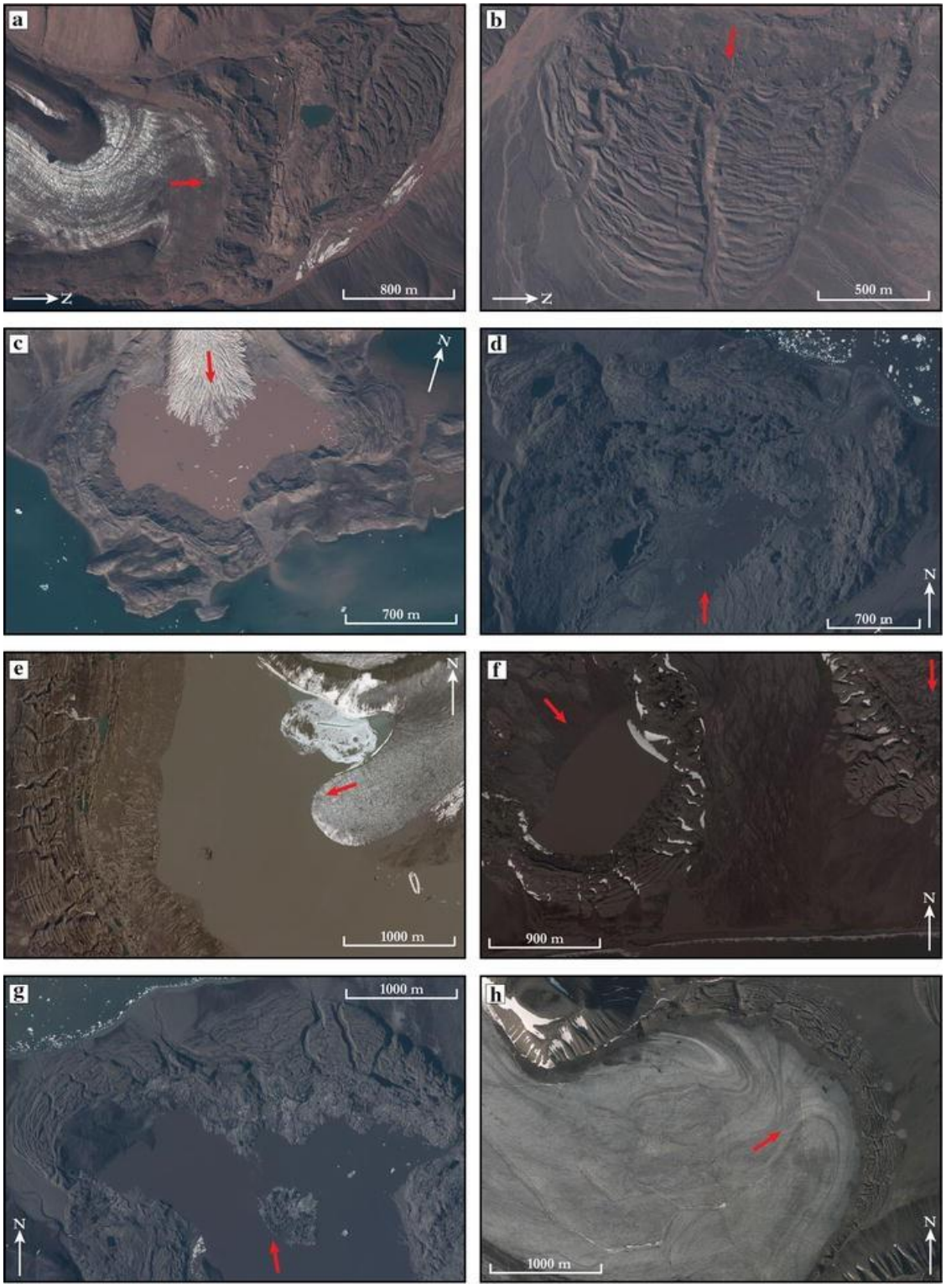

Fig. 2.12. *Examples of composite ridge systems within surge-type glacier forelands in Svalbard (from Lovell & Boston, 2017). The red arrows indicate the direction of glacier flow. Note the presence of additional surge diagnostic criteria, e.g., (a) looped medial moraine, (b) digitate terminus and (d) zig-zag eskers.*

Fig. 2.13. *The foreland of Brúarjökull, a surge-type outlet of Vatnajökull Ice Cap in southeast Iceland (from Evans et al., 2007). Note the zigzag esker network on the right and adjacent flutings and CSRs. The ice flow direction is towards the NNE as recorded by flutings and the distance across the photograph is 1.2 km.*

Of lowest confidence for definitive surge-type classification are flutings and hummocky moraine. Flutings are a common subglacial landform, providing evidence of fast flow but not always surging. However, when present in association with CSRs, they can provide strong evidence of surging (Evans & Rea 1999, 2003; Evans et al., 2007). Although hummocky moraine is found at the margins of surge-type glaciers, it is a common feature also of high debris supply, non-surge-type glaciers. In surge-type glaciers, the supply of supra- and englacial debris through thrusting is thought to be responsible for debris supply to the terminus, which when undergoing stagnation produces hummocky moraine (Evans & Rea, 2003). Sedimentological investigations may aid in establishing hummocky moraine genesis, but when identified remotely using only aerial imagery, it is not a reliable record of surging when used in isolation (i.e., not in a landsystem context).

On Svalbard, high-resolution swath bathymetry has been used to document the subglacial imprint of glacier surges (Ottesen et al., 2008, 2017; Dowdeswell & Ottesen, 2016). Tidewater glaciers were found to have well-defined landform assemblage, which was subsequently formulated into a landsystem model by Ottesen and Dowdeswell (2006). Landforms observed in the following sequence can be linked to a surge-cycle: (1) MSGL; (2a) terminal moraines and (2b) lobe-shaped debris flows; (3) isolated areas of crevasse-fill ridges; (4) eskers and (5) annual retreat ridges (Fig. 2.14; Ottesen and Dowdeswell, 2006; Ottesen et al., 2008; Dowdeswell & Ottesen, 2016). However, this method of surge-type glacier identification is typically limited to Svalbard and areas with high-resolution bathymetric data, thus the tidewater glacier landsystem cannot be used for surge-identification in regions with lower data availability such as the Russian High Arctic. Therefore, there may be a bias for the overidentification of land-terminating glaciers due to a larger observable criteria of surge-indicative geomorphology.

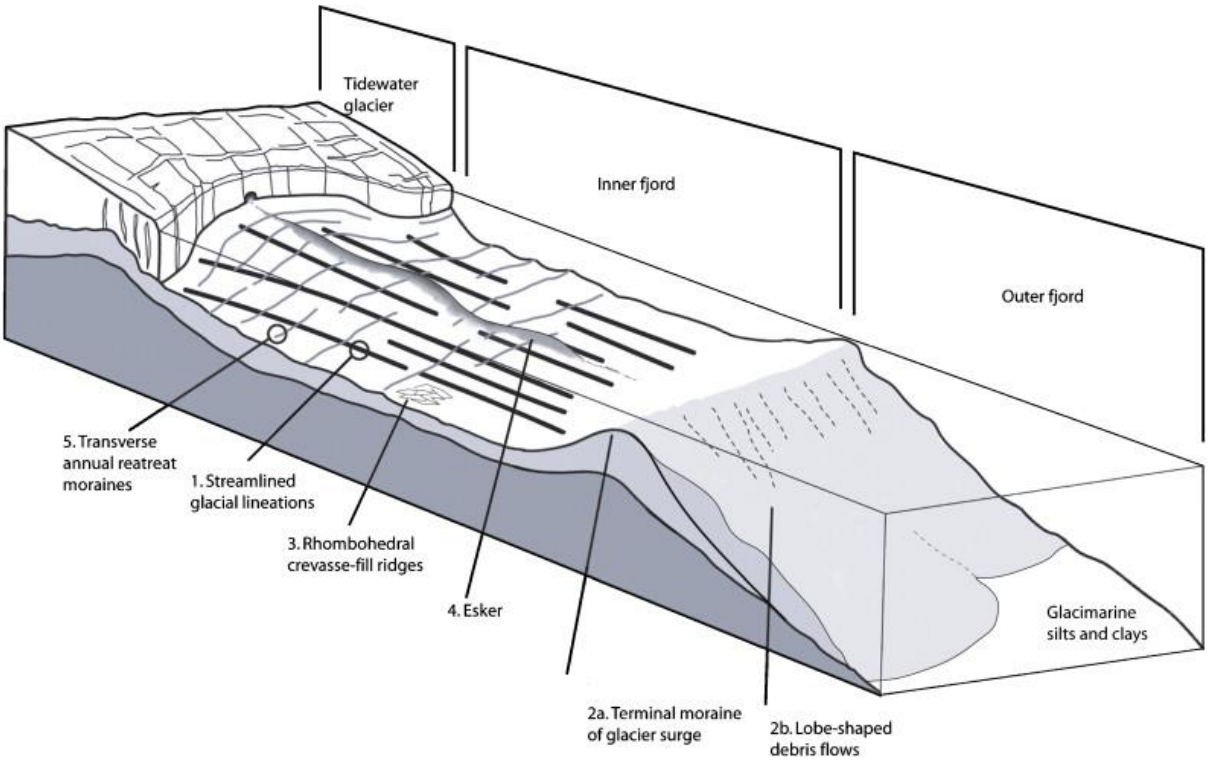

Fig. 2.14. *A landsystem schematic model for tidewater surge-type glaciers in Svalbard, based upon swath bathymetry data from Van Keulenfjorden and Rindersbukta, Spitsbergen (Ottesen et al., 2008).*

2.4. Summary

Atlantification of the Barents-Kara region has led to accelerated glacier melt in the European Arctic, driven by ocean-atmospheric coupling and a decline in sea ice concentrations (Asbjørnsen et al., 2020; Tepes et al., 2021b). This coupling is reduced further east due to higher sea ice concentrations, inhibiting the transfer of heat fluxes to the atmosphere (Tepes et al., 2021b). However, SZ has undergone a 29% increase in specific mass loss from the previous decade (between 2003 to 2009 and 2010 to 2017) and shows evidence of glacier instability (e.g., the Vavilov surge) (Willis et al., 2018; Tepes et al., 2021b). Despite the recent increase in mass balance studies in the region (e.g., Bassford et al., 2006a, b, c; Tepes et al., 2021b), no record of long-term terminus positions and surface area changes exist for the region. This record is crucial for understanding the long-term impact of climatic warming and how shifts in mass balance manifest as changes in terminus positions. Additionally, localised evidence of surging exists on the archipelago, but no recent and systematic survey of surging has been conducted from newly available high-resolution imagery. The task of identifying surging would be aided by a long-term record of glacier surface area changes. Identifying surging is

essential for understanding the drivers of glacier area change on SZ and the impact of climate change on glacier retreat, which bears implications for glacier surging, if and where it exists,

Chapter 3: Study Area and Previous Work

3.1. Geographic Setting

SZ is situated north of the Taymyr Peninsula, with FJL and NZ to the west and southwest, respectively (Fig. 3.1). The archipelago is located between the Kara and Laptev seas and is less influenced by warmer Atlantic waters than NZ to the west, with lower rates of precipitation than in the Barents-Kara Seas (Timokhov, 1994; Schaeur, et al., 2002). Mean annual precipitation and temperature as recorded at the Vavilov Station (Fig. 3.1) are 423 mm water equivalent and -16.5 °C for the period 1974-1988, respectively (Bassford et al., 2006b).

The study area encompasses all glaciers on SZ, which covered a total area of 17, 500 km^2 in the glacier inventory of the USSR compiled between 1940 and 1970 (Grosval'd & Kotlyakov, 1969). A re-survey from imagery acquired between 2000 and 2010 for the Randolph Glacier Inventory (RGI) 6.0 estimated the glacierised area to be 16,700 km^2, which is the most up-to-date and only record of glacier area for the region prior to this study(Moholdt et al., 2012a; Khromova et al., 2014).

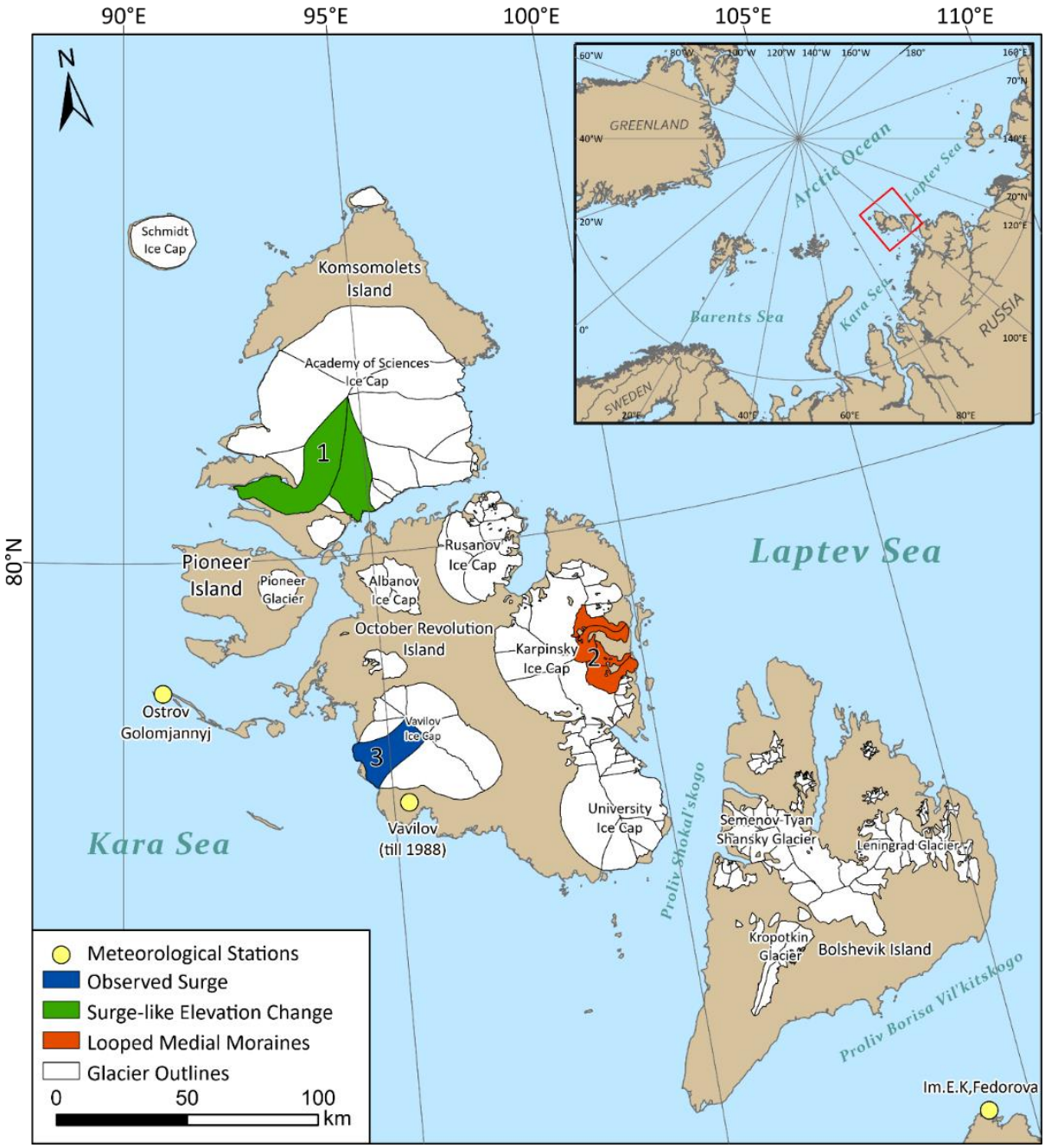

Fig. 3.1. *Map of SZ and its distribution of glaciers. The location of SZ is shown with glaciers from the 2001 - 2010 Randolph Glacier Inventory (RGI Consortium, 2017). The locations of previously identified surge-type glaciers are mapped as follows: (1) basins A & B of the AoSIC where surge-like elevation changes were identified by Sánchez-Gámez et al. (2019); (2) The two looped medial moraines identified by Dowdeswell & Williams (1997). (3) The location of the observed surge of the Vavilov Ice Cap documented by Glazovsky & Nosenko (2015).*

The 1940-70 USSR inventory estimated mean glacier thickness and volume to be 200 m and 3,500 km^3, respectively (Grosval'd & Kotlyakov, 1969). Glacier coverage increases towards the north, with glaciers covering 99.7% on the northwesternmost island, Schmidt Island, and the largest ice cap being the Academy of Sciences Ice Cap (AoSIC) on Komsomolets Island (Fig. 3.1; Sharov & Tyukavina, 2009). To the southeast of the AoSIC, the highest elevation is the peak of the Karpinsky Ice Cap, which reaches an altitude of 963 m (Sharov & Tyukavina, 2009). Most of the larger glaciers drain towards the eastern coast, with 26 outlet glaciers terminating in the Laptev Sea and displaying generally higher velocities (AoSIC Basins C & D – avg. 543 m a^{-1} (2016-17)) than the 5-6 slow-moving outlet glaciers flowing into the Kara Sea to the west (AoSIC Basin A – 240 m a^{-1}) (Sharov & Tyukavina, 2009; Sánchez Gámez et al., 2019).

3.2. Glacial History

The extent of the Late Pleistocene glaciation during Marine Isotope Stage 2 (including the last glacial maximum (LGM)) is controversial on SZ as the eastern margins of the former Barents-Kara Ice Sheet are unknown but are generally assumed to have reached the Taymyr Peninsula, not extending onto SZ (Fig. 3.2; Svendsen et al., 1999, 2004; Polyak et al., 2008; Hughes et al., 2015). The interpretation of lacustrine proxies on October Revolution suggests that it has not been covered by extensive glaciation since marine isotope stage 5d-4 (Early Middle Weichselian; Raab et al., 2003). A change to colder, drier conditions at ~22 ka following an interstadial period triggered ice cap growth, with the LGM in the Russian Arctic being reached around 20-15 ka BP (Hubberten, et al., 2004). However, the LGM on SZ was likely constrained close to modern margins, with the Vavilov Ice Dome believed to be small or non-existent (Raab et al., 2003; Svendsen et al., 2004). No evidence of glacial deposits was found in a lake core from southern Bolshevik Island, supporting these assumptions (Cherezova et al., 2020). Additionally, local evidence for ice grounding on the East Siberian continental margin during the LGM suggests that the purported East Siberian ice sheets did not extend to SZ (Niessen et al., 2013). This reinforces the theory that SZ has not been completely glaciated since pre-LGM times.

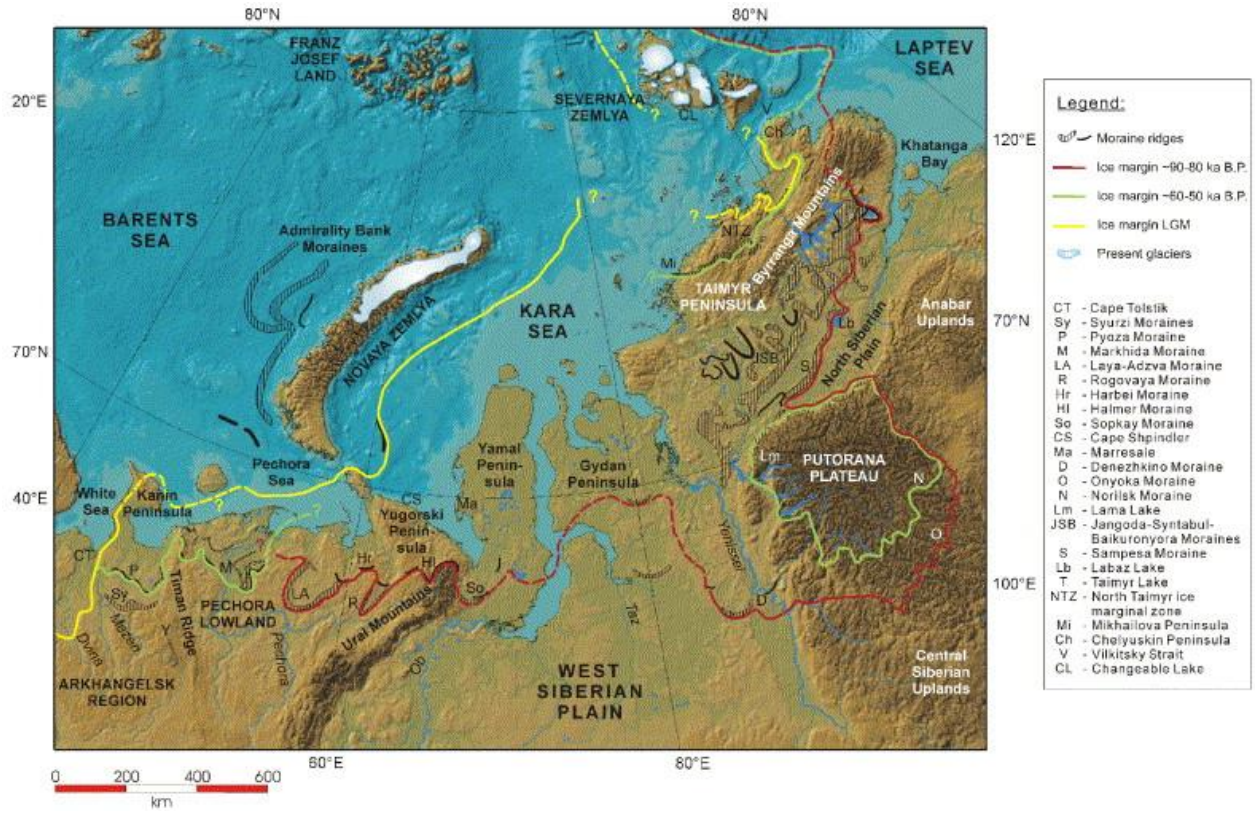

Fig. 3.2. *The margins of the former Barents-Kara Ice Sheet (from Svendsen et al., 2004). Note the uncertainty of the ice margin during the LGM on eastern SZ. However, the ice margin is known to have extended onto the Taymyr Peninsula during the LGM.*

In the RHA, the Pleistocene - Holocene transition was characterised by warming, punctuated with cooling correlated with the Younger Dryas. This was followed by an early Holocene warming peak at 10,000-9,700 yr BP, reaching the Boreal then Holocene thermal maxima at ~8500 and ~5500 yr BP, respectively (Andreev & Klimanov, 2000). On FJL, glaciers remained behind present margins from ~9.4 - 4.4 kyr, advancing to reach present margins by 2 kyr (Lubinski et al., 1999). Prominent neoglacial advances are recorded at ca. 1 kyr on FJL and, on NZ, neoglacial moraine sequences are situated within 4 km of present margins and dated to 1300 and 800 yr BP. This was followed by the Little Ice Age (LIA) advances on FJL and NZ and subsequent widespread retreat (Forman et al., 1999; Lubinksi et al., 1999). No distinct signal of the Medieval Climate Anomaly or the LIA is readily detectable in the $\delta^{18}O$ ice core record from the AoSIC (SZ), suggesting they may have not been pronounced in the Barents-Kara Sea region (Opel et al., 2013). A cold period at ~1800 followed by subsequent warming is interpreted to mark the termination of the LIA (Opel et al., 2013), although without

establishing a chronology on moraine formation on SZ this cannot be correlated with moraine stabilisation at surrounding localities.

3.3. Recent Glacier Change

3.3.1. Kosmomolets Island

Few studies have assessed long-term changes in glacier extent on SZ, with research primarily focusing on short-term changes in mass balance and ice flow dynamics (e.g., Bassford et al., 2006a, b, c; Tepes et al., 2021b). Several studies have used gravimetry and laser altimetry to assess recent volumetric changes of ice caps. These have been concentrated on the AoSIC and Komsomolets Island (e.g., Moholdt et al., 2012b; Sánchez-Gámez et al., 2019; Sánchez-Gámez et al., 2020; Tepes et al., 2021a, b).

The climatic mass balance of the AoSIC has remained close to zero over the last four decades (0.21 ± 0.68 Gt a^{-1}), with small changes in total mass balance controlled by ice discharge variations attributed to ice cap characteristics (e.g., subglacial topography and changes in floatation conditions; Sánchez-Gámez et al. 2019). Since 1988, the mass of the AoSIC has reduced by 3%, equating to 0.16 mm in SLR (Moholdt et al., 2012b). A large proportion (~40%) of its total mass loss occurs due to iceberg calving at a rate of ~0.65 km^3 a^{-1}, predominantly from the major outlet glaciers, with the remaining proportion (~60%) from surface melting (Dowdeswell et al., 2002). Most mass loss on SZ is attributed to three outlets (ice streams *sensu lato*) on the AoSIC which have thinned by > 1 m a^{-1} and remained in a period of fast flow since 1995, notably Basins C & D, with Basin A showing a three-fold increase in velocity and an increase in thickness its terminus (Fig. 3.3; Sharov & Tyukavina, 2009; Moholdt et al., 2012b; Nela et al., 2019; Sánchez-Gámez et al., 2019). These outlets exhibit highly variable seasonal changes in ice flow velocity, attributed to the routing of meltwater to the glacier bed, which allows for basal sliding, with high velocities sustained for 2 months until a decrease before the end of the melt season; this has been linked to a change in drainage system efficiency (Sánchez-Gámez et al., 2019). Despite the current low rates of discharge from the AoSIC, it shows evidence of some mass loss and much of its dynamics remain a subject of debate.

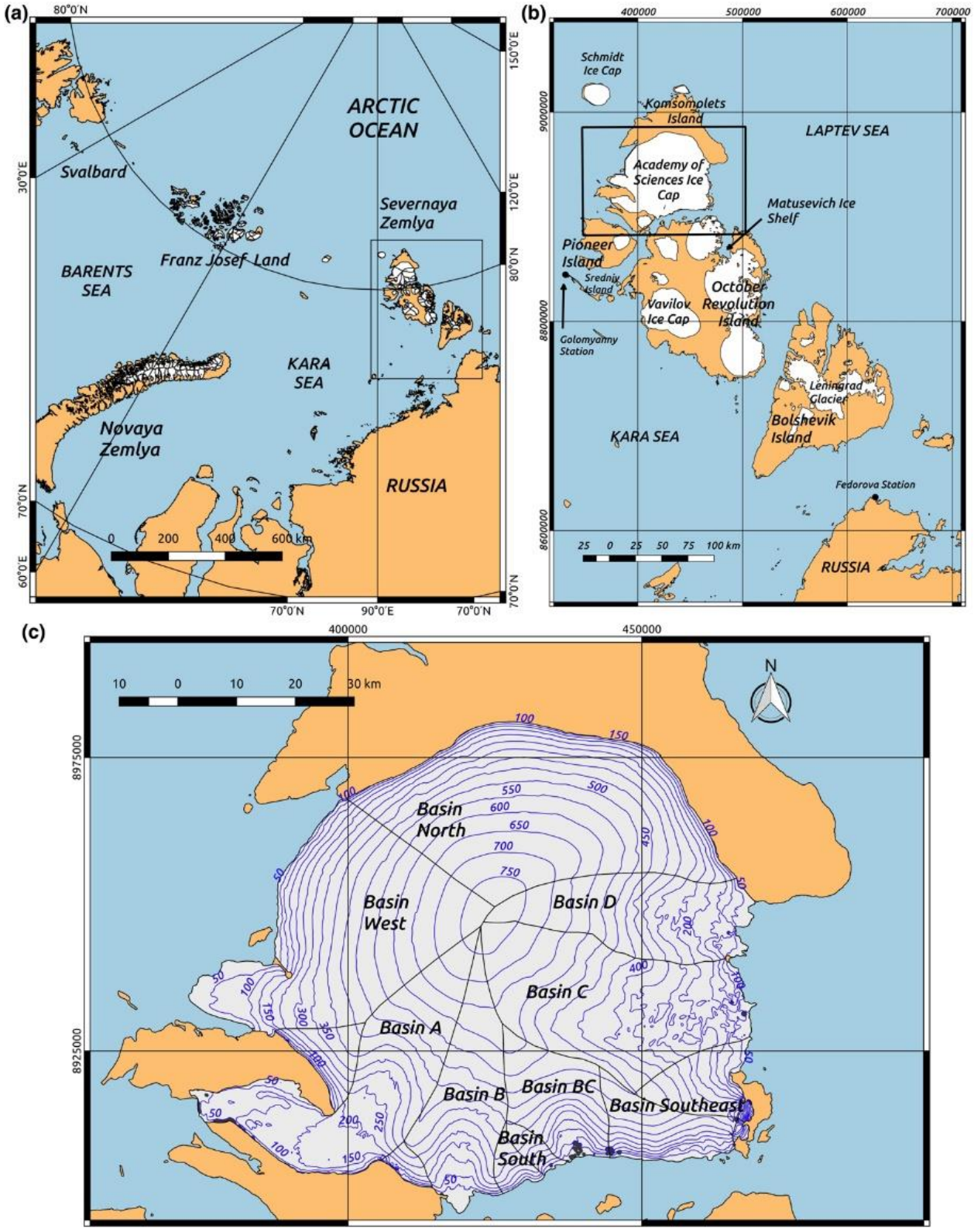

Fig. 3.3. *The location of the AoSIC, shown within the RHA and SZ (from Sánchez-Gámez et al., 2019). Note panel c, which details the basin names referred to throughout the text.*

3.3.2. October Revolution Island

The Matusevich Ice Shelf (MIS) was once the largest floating ice shelf in the Eurasian Arctic, fed by eight outlet glaciers on October Revolution Island and containing a floating area of 240 km^2 in 1955 (Dowdeswell, 2017). Historical observations (post-1931) of the ice shelf show that it undergoes cyclical terminus fluctuations of ~30 years, attributed to the nature of iceberg calving (Williams & Dowdeswell, 2001; Dowdeswell, 2017). However, the ice shelf collapsed in 2012, with its collapse proposed to be due to abnormally warm summer surface air temperatures in the years preceding the breakup, with 2012 being characterised by the highest annual air temperatures and precipitation (rain) since observations began (Sharov et al., 2015; Willis et al., 2015). Velocity increases of the Issledovateley Glacier, the largest outlet glacier, are recorded prior to the breakup which signalled that the ice shelf was undergoing changes beforethe collapse (Willis et al., 2015). Post-collapse, between 2012 and 2014, the main outlets of the Karpinsky Ice Cap thinned at a rate 3-4 times greater than the 30-year average (Willis et al., 2015). Willis et al. (2015) note that further observation of the tributary glaciers feeding the former ice shelf is recommended to see if it re-establishes, in accordance with its ~30-year cycle of collapse/re-establishment or whether climatic warming will prohibit its reformation.

No other large changes in elevation or mass loss have occurred on October Revolution except for the destabilisation of the western margin of the Vavilov Ice Cap (see section 2.3.3).

3.3.3. Bolshevik Island

Glaciers on Bolshevik had been observed to be retreating as early as 1952/75 by Govorukha et al. (1987), who compared the ice margins recorded by the first aerial survey of SZ in 1931 to later surveys. Ice dome margins were found to have retreated by up to 2-2.5 km in places, with the greatest retreat recorded around the Kropotkin Glacier and surrounding ice caps (Fig. 5.2). These limited surveys show that glacier mass balance was mostly positive during 1974-1977 but became increasingly negative during periods of high ablation and low accumulation from 1978-79, and hence glaciers retreated during this period (Govorukha et al., 1987). However, this mapping does not include any of the glaciers and cirques in north-eastern Bolshevik Island and has not been updated since 2010 (Moholdt et al., 2012a).

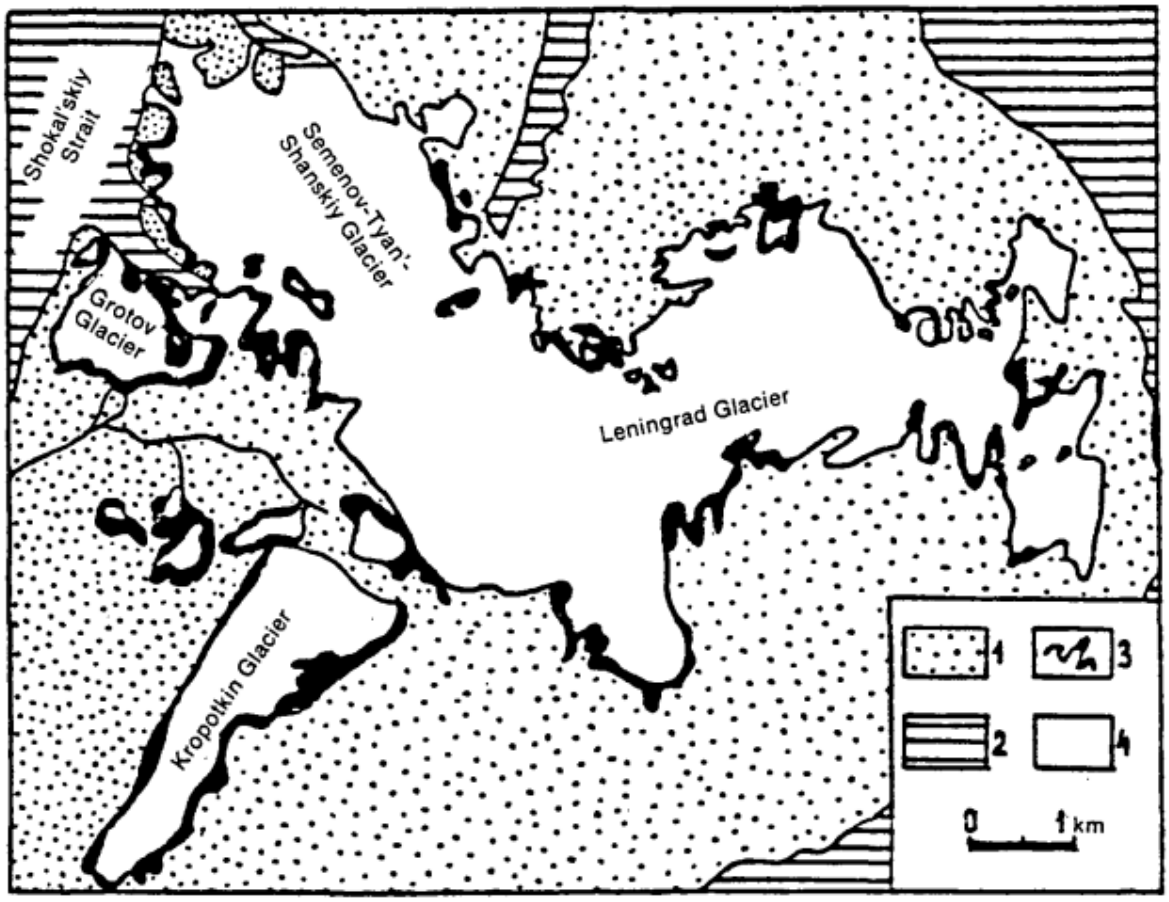

Fig. 3.4. *Shrinkage of glaciers on Bolshevik Island over the period 1952-1975. (1) land (2) sea (3) areas which have emerged from the ice (4) present glacier cover (from Govorukha et al., 1987)*

Additionally, climatic warming on Bolshevik Island has resulted in a series of glacial lake outburst floods at one glacier. The Spartakovskoye glacier-dammed lake on northern Bolshevik Island most recently burst in 2016, with the next outburst anticipated to occur between 2024 and 2025 (Chernov & Muraviev, 2020). Under current melt rates, it will refill every ~10 years and despite no direct human impacts, the duration between outbursts provides a visual record of glacier melt, which is likely to accelerate.

3.4 Summary

SZ is the coldest and driest region in the RHA, characterised by large ice domes (Timokhov, 1994; Schaeur, et al., 2002; Sharov & Tyukavina, 2009). During the LGM, it is unlikely that these ice domes coalesced and they are assumed to have been constricted close to their current

margins, with the Barents-Kara Ice Sheet unlikely to have grounded on western SZ (Fig. 3.2; Svendsen et al., 1999, 2004; Polyak et al., 2008). Due to the lack of an established chronology for moraine formation on SZ, it is unknown when glaciers on SZ last advanced and whether they underwent neoglacial or LIA advances. Since observations began (in the 1930s), no widespread period of advance has been observed. Glaciers in the north of SZ have shown little change in surface area, whereas glaciers on Bolshevik Island have been in a pattern of net retreat since the period between 1931 and 1952 (Fig. 3.4; Govorukha et al., 1987). Further north, the breakup of the former largest floating ice shelf in the RHA has been attributed to oceanic and atmospheric warming (Sharov et al., 2015; Willis et al., 2015). Thus, it can be assumed that glaciers on SZ are undergoing accelerated retreat due to climatic warming.

Chapter 4: Methods

4.1 Introduction

This chapter details the methods undertaken for glacier surface area change quantification and surge-type glacier identification. The first section outlines the process of image acquisition and data processing (including geocorrection) (section 4.2). This is followed by the methods utilised for manual glacier delineation and the calculation of error margins (section 4.3). The final sections then detail the acquisition and processing of climatological data (section 4.4) and the process of identifying surge-type glaciers (section 4.5).

4.2 Imagery Acquisition and Processing

4.2.1 Imagery

Satellite imagery was acquired for the years 1965/79, 1986, 1997, 2011, 2018 (DEM) and 2021 at intervals of ~10 years to capture long-term changes (see Appendix A). The earliest imagery available for SZ is 1965 (KH-7), before the launch of Landsat 1 in 1972 (80 m ground pixel resolution) and is used despite its lack of georeferencing as it provides high resolution (4.9 m) imagery. The dates used reflect the typically high cloud and snow cover of the archipelago, and some georeferencing errors in Level 2 Landsat imagery, hence the lack of dates between 1965 and 1986.

The imagery used is from KH-7 and KH-9 'Hexagon', Landsat TM, Advanced Spaceborne Thermal Emission and Reflection Radiometer (ASTER), Worldview 1-3 (ArcticDEM), Landsat 8 and Sentinel-2A (Fig. 4.1; see Appendix A). These sensors were chosen as they provide the highest-resolution open-access imagery available at each timestamp. Scenes were predominantly obtained from July to September, when sea ice and snow cover are at a minimum and filtered for low cloud cover (< 10%), to ensure accurate delineation of glacier margins. All years have full glacier coverage except for 1965, which only covers October Revolution and Bolshevik Island, and 1979 which only covers Komsomolet and Pioneer Island, which when combined provide high-resolution (< 7 m) full coverage of SZ (excluding Schmidt Island) during the 1960s and 70s.

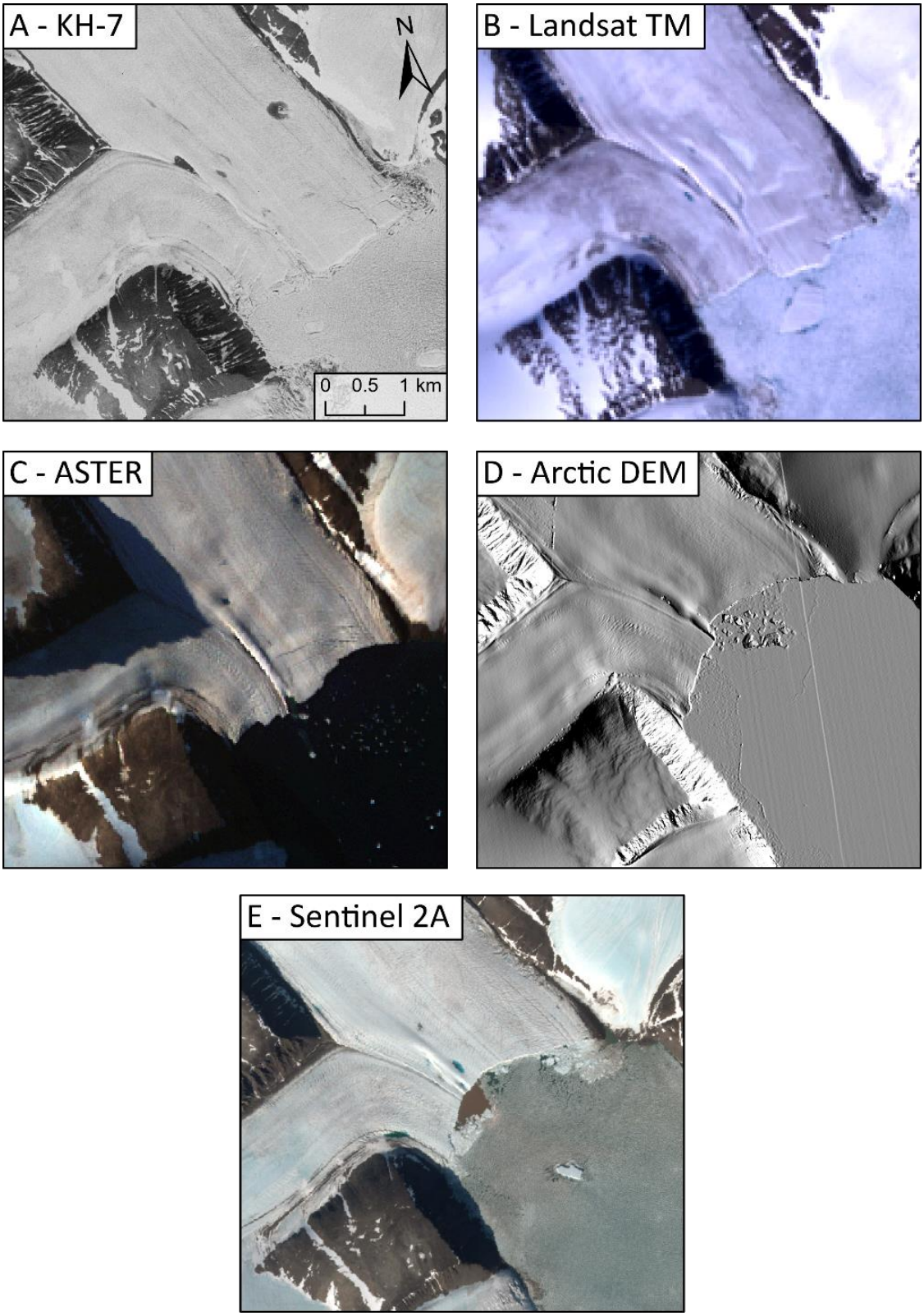

Fig. 4.1. *Examples of imagery used for glacier delineation and surge-type feature identification (Glaciers 36 (middle), 39 (top right), 83 (bottom left)). (A) 1965 KH-7 greyscale imagery; (B) 1997 Landsat TM RGB composite; (C) 2011 ASTER RGB composite; (D) 2018 Arctic DEM; (E) 2021 Sentinel-2A RGB composite.*

4.2.2 Geocorrection

KH-7 and KH-9 imagery were manually georeferenced using a 2021 Sentinel 2A base layer and co-registered to a WGS 1984 Arctic Polar Stereographic projection. A total of 23 KH-7 and 2 KH-9 scenes were used to cover SZ and were georeferenced using a spline transformation with ~30 control points per tile. Fixed points such as coastlines and bedrock features were used as ground control points, avoiding features subject to alteration (e.g., deltas and rivers). The transformations have a root mean square (RMS) value close to zero (~>0.001), providing a good assessment of the transformation accuracy, although minor errors in aligning control points may not be accounted for in the RMS value.

4.3 Glacier delineation

4.3.1 Method

Using the RGI (Randolph Glacier Inventory) 6.0 data as a guide, glaciers were manually delineated using ESRI ArcGIS software, giving a total of 190 individual glacier units. Ice divides from the RGI data were used but that inventory could not be utilized in the analysis because the year of measurement was not the same for each glacier. The long-term record of satellite imagery in this study also allowed for the rectification of misclassifications in the RGI inventory using some of the criteria in Leigh et al. (2019), including 16 new glaciers that may have been overlooked as snow patches in the RGI and one lake misclassified as a glacier in the RGI (Fig. 4.2). Thereafter, each glacier was manually digitised using a Lambert Equal Area Projection for 1965, 1979, 1986, 1997, 2011 and 2021 (Fig. 4.3). Each glacier was given an ID from 1-190 for identification purposes (see Appendix B). On Bolshevik Island, some linear snow patches may contain glacier ice, but do not meet the criteria for glacier identification (see Leigh et al., 2019) so are excluded from the mapped glaciated area for Bolshevik Island. Glacier change was calculated in km^2 using ESRI ArcGIS Pro to calculate the geometry of each glacier/basin. No classification of terminus type exists for SZ, so each glacier unit was classified into one of three terminus types: marine-terminating, land-terminating and lake-terminating.

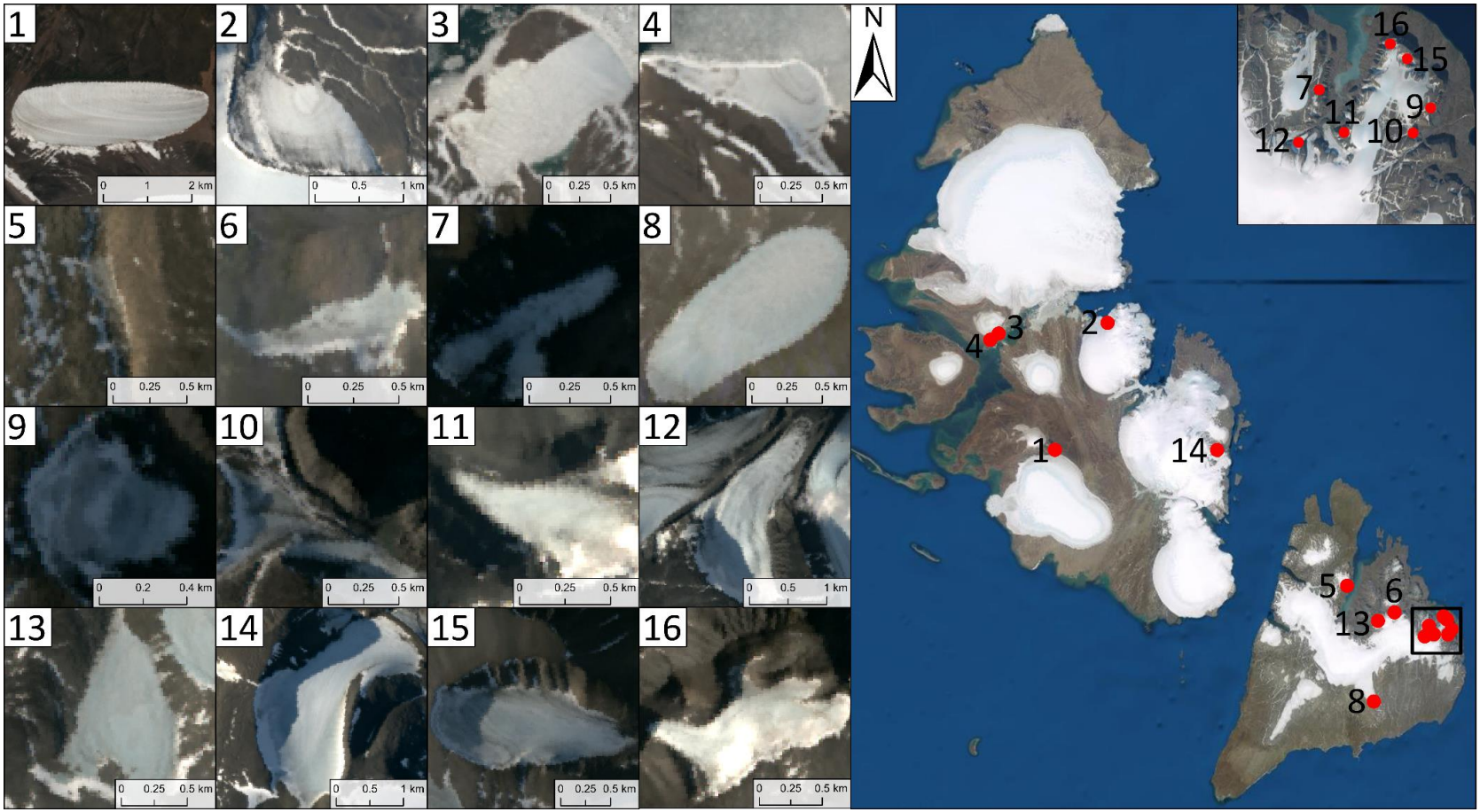

Fig. 4.2. *New glaciers identified and included in glacial change calculations. Glaciers (left) and numbered based on their name in the supplementary data (e.g., New Glacier 1, New Glacier 2 etc.). All glaciers have been identified following criteria proposed by Leigh et al. (2008) for identifying small glaciers. The glaciers are shown in 2021 Landsat 8 (15 ground pixel resolution) imagery. All glaciers still exist except for glacier 5 which has almost disappeared, although it was identified to be a glacier from 1965 high-resolution imagery, where it formerly covered 1.15 km^2.*

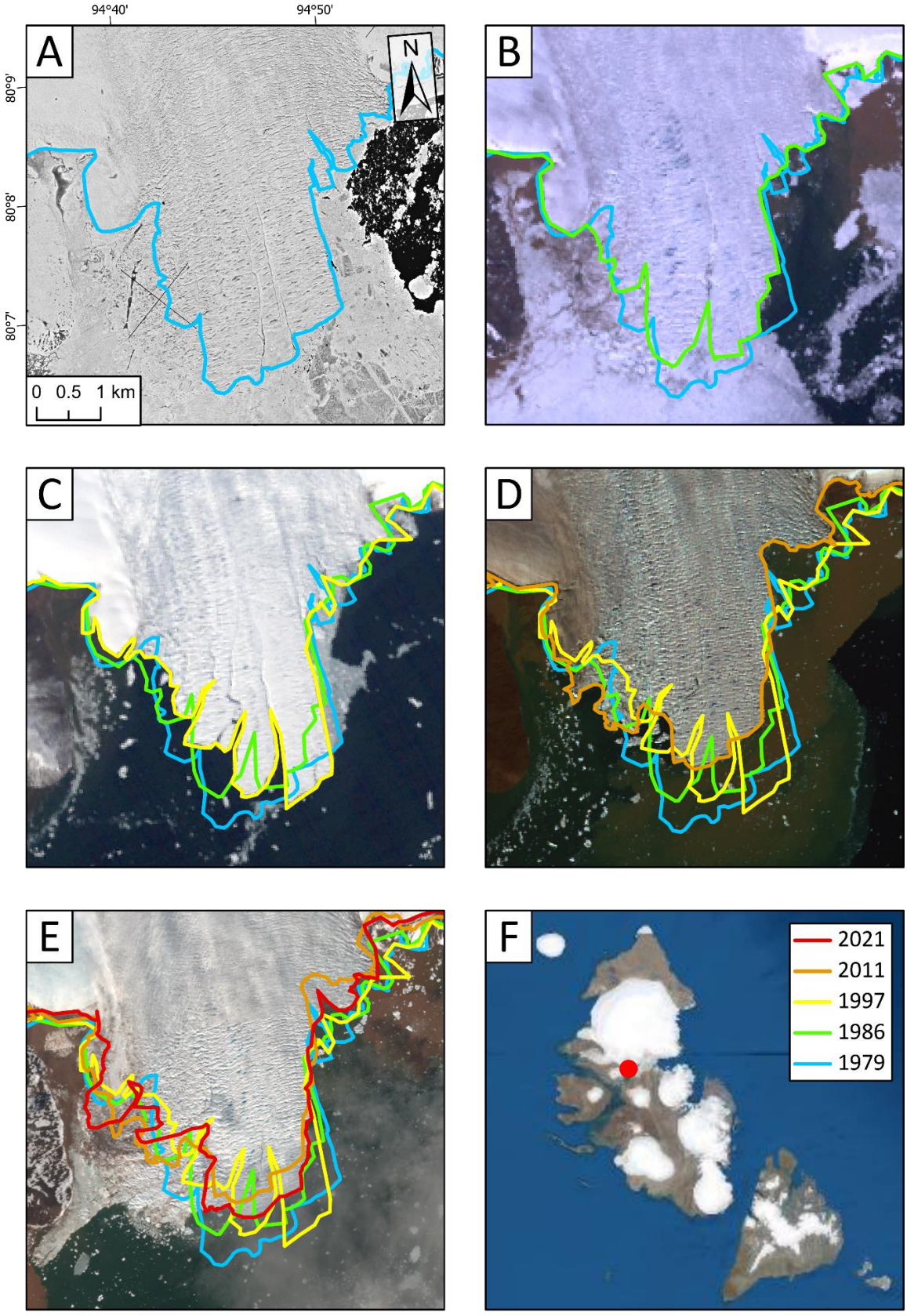

Fig. 4.3. *An example of manual glacier terminus delineation on Basin B of the AoSIC. (A) KH-7: 1979, (B) Landsat TM, 1986, (C) Landsat TM, 1999, (D) ASTER, 2011, (E) Sentinel 2A, 2021.*

4.3.2 Errors

Errors in manual glacier delineation were calculated following DeBeer and Sharp (2007), who assumed that line placement uncertainty is likely to be larger than the imagery resolution for debris-free glaciers on cloud-free imagery. Measurement error is thus equal to the polygon perimeter x pixel resolution; for example, the area of glacier 1 = 120 km^2 has a perimeter of 66307.4 m and was mapped from 10 m ground pixel resolution imagery. Thus, the line placement/mapping uncertainty is 120 ± 0.66 km^2. Errors are calculated for each glacier unit at each date (see Appendix B), with measurement errors for the total area detailed in Table 5.1.

4.4 Climate Data

Daily air temperatures were obtained from two stations: Im.E.K Fedorova (77.7°N, 104.3°E, 12 m a.s.l., 1936-2021) at the north of the Taymyr Peninsula, south of Bolshevik Island; and Ostrov Golomjannyj (79.6°N, 90.6°E, 8 m a.s.l., 1936-2021) on a small island 40-50 km west of October Revolution Island (see Fig. 3.1). Annual summer (1st June to 31st August) and winter (1st Dec - 28/29th February) means were computed for each station, with anomalies calculated against a 1936 - 2021 mean. Data were accessed from the National Oceanic and Atmospheric Administration (NOAA) (https://www.noaa.gov/). Long-term composite plots of SST, precipitation and air temperature were produced from NOAA plotting tools, which use National Centres for Atmospheric Prediction (NCEP) re-analysis data.

4.5 Surge-type glacier identification

Each of the 190 glaciers on SZ were examined for the presence of features that may be diagnostic of surging (Table 4.1; see sections 2.3.3 and 2.3.4). These criteria for identifying surge-type glaciers have been adapted from Grant et al. (2009) and updated to reflect advances in understanding surge-type glaciers (e.g., Farnsworth et al., 2016). Each criterion was weighted to reflect whether it is primarily diagnostic of surging (e.g., looped medial moraines) or may only be diagnostic of surging in conjunction with other criteria (e.g., high surface velocities) (Table 4.1). The highest weighting of 5 was assigned to looped medial moraines and localised abnormal advances as they are most indicative of surging (Meier & Post 1969; Lawson, 1996; Evans & Rea, 1999, 2003; Hewitt, 2007; Paul, 2015). Due to potential equifinality associated with thrust block/glacitectonic composite moraines (4) and crevassing

up glacier (3), they are not weighted high enough to individually result in a surge-type classification (Fitzsimons, 1996, 1997, 2003; Evans & Rea, 1999, 2003; Evans, 2009; Benn & Evans 2010). However, they are weighted more heavily than supraglacial ponding (1) and shear margins (1). Following weighting, each glacier is classified as either: confirmed surge-type (active phase observed) (>10), likely to have surged (7-9), possible surge-type (>7) or non-surge-type (0-3). Glaciers are only classified as surge-type if a localised abnormal advance has been observed during the study period, which is assumed to be the active phase, and three other surge-indicative criteria are present, increasing the likelihood that the glacier is in fact of surge-type. This method is biased towards the surge classification of land-terminating glaciers because of the additional criteria that may be present within their forelands, although without the availability of bathymetric datasets this cannot be rectified at this stage.

Table 4.1. *Criteria for identification of surge-type glaciers (following Grant et al., 2009).*

Criteria	Description	Weighting
Glaciological		
Looped moraines	Produced when medial moraines are deformed due to the combination of fast- and slow-flowing ice within adjacent glaciers	5
Localised abnormal advance	Indicative of the active phase of the surge cycle	5
Highly digitate terminus	Terminus is splayed into lobes by longitudinal crevasses	3
Heavy surface crevassing up-glacier	Indicative of the active phase of the surge cycle and develop due to increased longitudinal stresses	3
Deformed ice structures	Form in a similar manner to looped moraines	1
Shear margins	Develop at the boundary between fast- and slow-flowing ice	1
Heavy surface crevassing at the terminus	Formed during the surge phase	1
High surface velocities (>150 m a^{-1})	Occur during the surge phase	1
Surface Potholes	Typically appear during the quiescent phase; they form in crevasses formed during the surge phase or in depressions between transverse ridges	1
Geomorphological		
Thrust-block/composite moraines	Form as a result of marginal thrusting due to ice advance into proglacial sediments and can form in belts of arcuate thrust ridges. In areas where sediment in limited, low-amplitude push moraines develop	4
Overriden thrust-block moraines	Formed thrust blocks are overriden by ice and form ice-moulded 'cupola' hills	1
Hummocky moraine	Produced in belts at the margin of glaciers and consist of the product of melt-out of debris-mantled glaciers (however, other origins are possible)	1
Concertina eskers	Developed during short-lived, high-discharge flood events which occur prior to or immediately after surge termination	5
Crevasse squeeze ridges (CSR) or geometric ridge networks	Commonly form in response to a highly crevassed glacier. On termination of the surge, water-saturated sediments rise into the basal crevasses and are subsequently preserved in the foreland as a series of cross-cutting ridges.	4
Flutes	Can indicate evidence for rapid advance over significant distances but are not solely diagnostic of glacier surging. They often occur in association with geometric ridge networks.	2

4.6 Summary

Remote sensing techniques have been used to assess glacial change for 190 glaciers over 5 dates (1965/79, 1986, 1997, 2011 and 2021). Satellite imagery was acquired from KH-7/9, Landsat TM, ASTER, Landsat 8 and Sentinel-2A sensors and used to manually delineate glacier outlines, using the ice divides established by RGI 6.0. The record of glacier change was

then used in conjunction with a suite of surge indicative criteria (e.g., looped medial moraines and glaciotectonic thrust-block moraines) to classify glaciers based on the likelihood that they are of surge-type. External forcing data included the use of air temperature data (1936 - 2021) and SST, precipitation, and air temperature NCEP re-analysis plots from NOAA.

Chapter 5: Results

5.1 Introduction

The first section of this chapter (5.2) details the results of glacier area delineation (1965 to 2021), commencing with the overall spatial and temporal patterns of glacier change. This is followed by patterns of glacier change in the regions of SZ, ordered from north to south from Komsomolets Island to Bolshevik Island. The second section (5.3) details the trends in surface air temperatures at the two stations, Im.E.K.Fedorova on the Taymyr Penninsula and Ostrov Golomjannyj, situated closely offshore from October Revolution Island (Fig. 3.1). This is followed by an analysis of NCEP re-analysis data, providing larger scale spatial climatological patterns and anomalies. The final section (5.4) focuses on the glaciological and geomorphological features indicative of surging present on the glacier forelands and on the glacier surfaces.

5.2 Glacier Change

Between 1965 (17,053 ± 38 km^2) and 2021 (16,275 ± 69 km^2), glaciers on SZ lost a combined area of 778 km^2 (5% area decrease) at an average rate of 14.9 km^2 a^{-1} (Table 5.1; Fig. 5.1). By region, Bolshevik Island accounts for 55% of glacier area loss (-426 km^2), October Revolution Island for 30% (-230 km^2), and Komsomolet, Pioneer and Schmidt islands for 16% (-122 km^2). From 1965 to 2021, 95.7% of glaciers showed a decline in surface area and eight glaciers increased in overall area, with ten separate advances (> 0.5 km^2 and exceeding error margins) recorded between these dates (Table 5.1; see Appendix B for individual glaciers).

In terms of temporal changes, glaciers and ice caps retreated at a rate of -13.3 km^2 a^{-1} between 1965/79 and 1986, which decreased to -5.5 km^2 a^{-1} between 1986 and 1997. However, due to the larger error margins for 1986 and 1997, there is low confidence in a significant deceleration in retreat rate (Figure 5.1; Table 5.1). A notable acceleration in retreat is recorded between 1997 and 2011 (-20.3 km^2 a^{-1}), which continues through to 2011 - 2021 (-15.4 km^2 a^{-1}).

Table 5.1. *Summary statistics of glacier surface area change on SZ. Uncertainties are provided for the overall and regional total areas (for individual glaciers see Appendix B).*

	1965(*79)	1986		1997		2011		2021		1965 - 2021	
	Area (km^2)	Area (km^2)	Change (km^2 a^{-1})	Area (km^2)	Change (km^2 a^{-1})	Area (km^2)	Change (km^2 a^{-1})	Area (km^2)	Change (km^2 a^{-1})	Change (km^2)	Change (km^2 a^{-1})
All Glaciers	17053.4±38	16774.2±221	-13.3	16713.9±216	-5.48	16429.2±22	-20.34	16275.4±69	-15.4	-778.1	-13.9
Mean	90.1	90.2	-0.1	89.9	0.0	90.6	-0.1	85.7	-0.1	-2.2	-0.1
Median	21.8	21.8	0.0	21.6	0.0	22.4	-0.1	19.7	-0.1	-1.8	0.0
SD	173.4	174.1	0.3	174.3	0.2	175.0	0.2	171.6	0.1	16.1	0.3
Min	0.4	0.4	2.9	0.2	1.8	0.5	0.1	0	0.0	141.5	2.5
Max	1243.7	1246.2	-2.0	1246.1	-0.7	1243.7	-1.7	1243.1	-1	-42.8	-1.8
Komsomolets, Pioneer & Schmidt*	6407.8±7	6422.3±44	2.1	6395.8±44	-2.4	6328.7±22	-4.8	6285.5±30	-4.3	-122.3	-2.2
Mean	305.1	305.8	0.1	304.6	-0.1	301.4	-0.2	299.3	-0.2	-5.8	-0.1
Median	157.7	157.7	0.0	157.2	0.0	155.7	-0.1	154.8	-0.1	-0.7	0.0
SD	363.2	366.3	0.8	365.8	0.3	364.6	0.4	363.6	0.5	11.3	0.3
Min	1.3	1.4	2.9	1.9	0.4	0.7	0.2	0.5	0.4	3.9	0.1
Max	1243.7	1246.2	-1.1	1246.1	-0.7	1243.7	-1.1	1243.1	-1.6	-39.9	-3.0
October Revolution	7628.8±17	7507.6±101	-5.8	7513.2±98	0.5	7413.4±49	-7.1	7398.7±32	-1.5	-230.3	-4.1
(-Vavilov)	7285.4±16	7164.2±98	-5.8	7166.3±96	0.2	6903.02±47	-18.8	6913.6±30	1.1	-371.8	-6.7
Mean	117.4	115.5	-0.1	116.0	0.0	112.3	-0.1	112.1	0.0	-3.6	0.0
Median	58.2	55.6	0.0	55.3	0.0	54.4	0.0	53.8	0.0	-2.1	0.0
SD	144.6	142.6	0.3	144.0	0.3	142.5	0.3	143.4	1.8	23.3	0.4
Min	1.3	1.5	0.4	1.5	1.8	1.1	0.8	1.1	12.7	141.5	2.5
Max	594.1	594.8	-2.0	594.0	-0.4	593.3	-1.7	591.8	-5.4	-99.8	-1.8
Bolshevik	3016.6±13	2844.3±76	-8.2	2805.0±74	-3.6	2687.0±36	-8.4	2591.2±23	-9.6	-425.5	-7.6
Mean	30.8	28.4	-0.1	28.0	0.0	26.6	-0.1	25.2	-0.1	-4.5	-0.1
Median	11.3	9.8	0.0	9.6	0.0	8.2	0.0	7.4	-0.1	-2.0	0.0
SD	49.9	47.8	0.1	47.5	0.1	46.0	0.1	45.0	0.0	7.5	0.1
Min	0.5	0.4	0.0	0.2	0.0	0.2	0.0	0	0.0	1.2	0.0
Max	335.8	323.2	-0.8	320.0	0.0	306.5	-1.0	296.5	-1	-44.8	-0.8

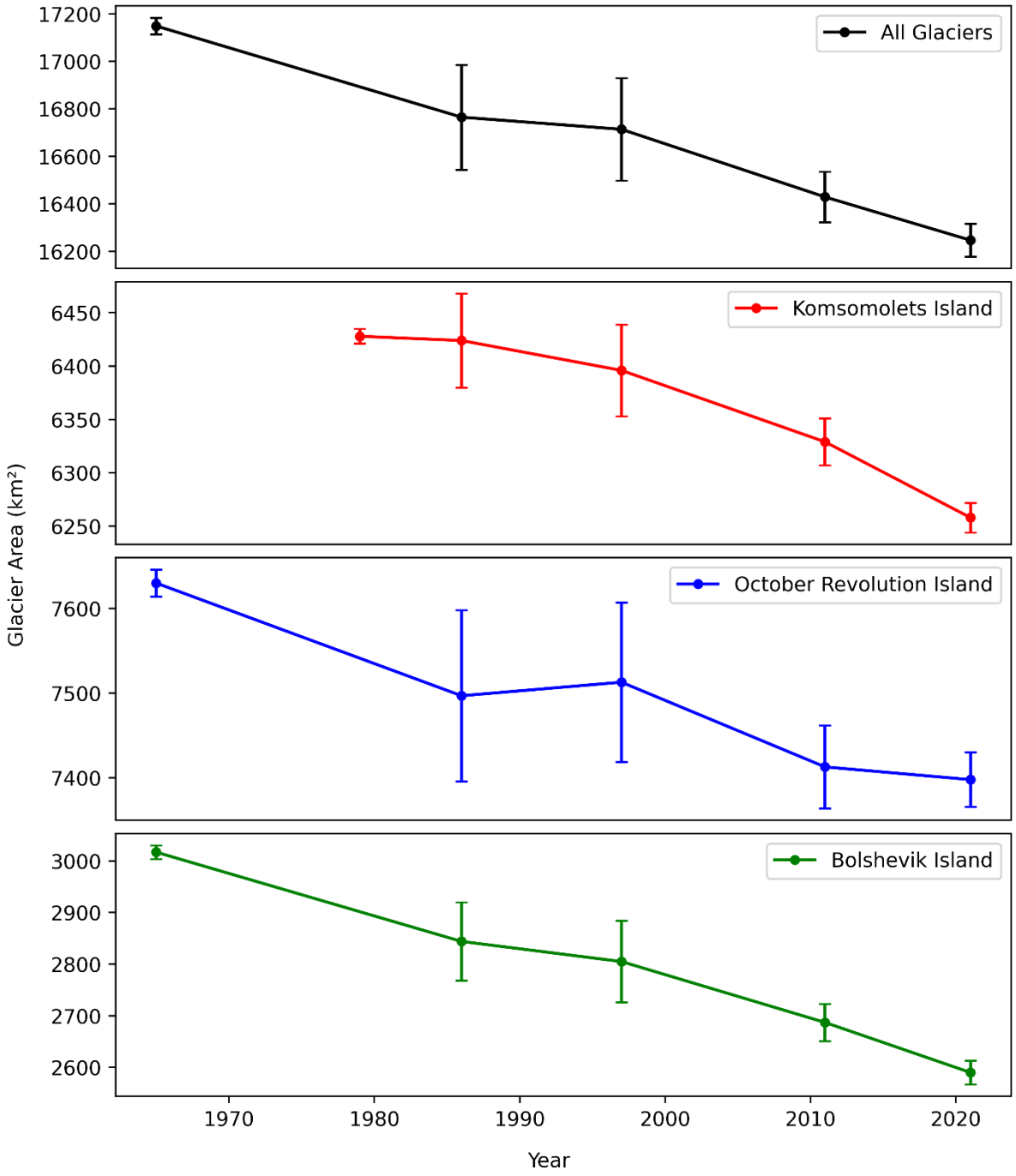

Fig. 5.1. *Changes in glacier area by region (see Fig. 3.3 for location). Error bars reflect the minimum and maximum possible extents of glacier area at each date. Imagery for Komsomolets Island is first available in 1979 and is grouped with the 1965 data in the total glacier area change plot.*

Komsomolets Island experienced the smallest amount of glacier retreat (-2.2 km^2 a^{-1}, 1979-2021 = 1.9% area decrease), compared to the southernmost Bolshevik Island (-7.6 km^2 a^{-1}, 1965-2021 = -14.1% area decrease; Table 5.1; Fig. 5.1). Nonetheless, glaciers and ice caps on

Komsomolets Island underwent a progressive acceleration in retreat rates between each date, with a small increase in area between 1979 and 1986 (2.1 km^2 a^{-1}), followed by an acceleration in retreat rate between 1986 and 1997 (-2.4 km^2 a^{-1}) (Fig. 5.2). Annual retreat rates increased by 92% between the periods 1986-1997 and 1997-2011 (-4.8 km^2 a^{-1}) and decelerated slightly to -4.3 km^2 a^{-1} between 2011-2021, which is lower than the rate of change on Bolshevik Island between 1965/79 and 1986 (-8.2 km^2 a^{-1}) (Fig. 5.2). The largest rates of retreat (in percentage terms) have preferentially occurred on the smaller Arctic Ice Cap (glacier 17) and Separate Ice Cap (glacier 147), with minimal retreat of the AoSIC (Fig. 5.3). Between 1965/79 and 2021, five seperate advances (that exceed error margins) are recorded for the AoSIC, although only Basin A (Fig. 5.4A) and Glacier 154 showed an overall net increase in area from 1965 - 2021.

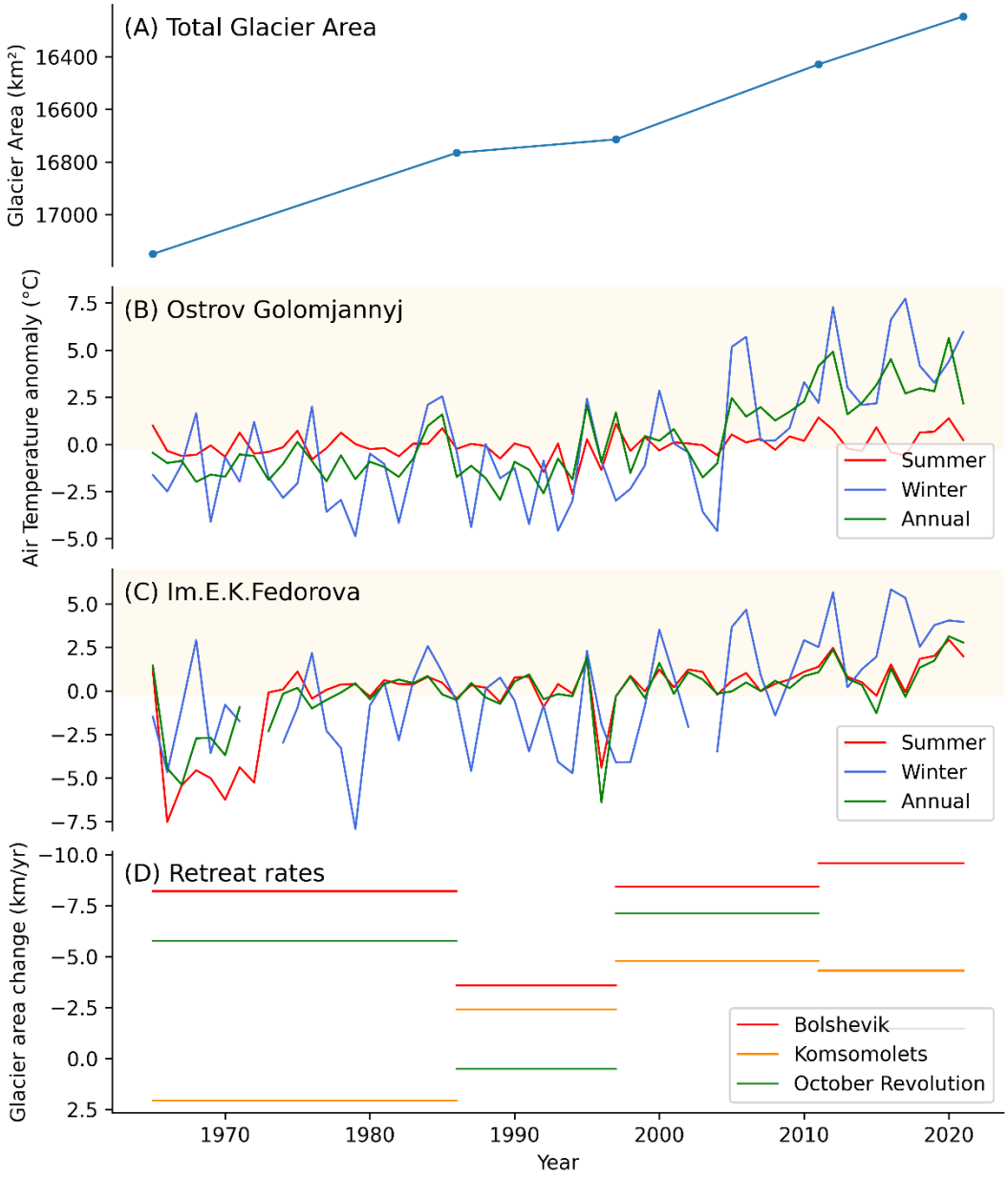

Fig. 5.2. *Changes in glacier area, retreat rates, and temperature anomalies on SZ from 1965 to 2021. (A) Changes in total glacier area, note that the y-axis is inverted. (B) Summer, winter and annual air temperature anomalies at Ostrov Golomjannyj, west of October Revolution Island (Fig. 3.1). (C) Summer, winter and annual air temperature anomalies at Im.E.K.Fedorova on the Taymyr Peninsula (Fig. 3.1). (D) Rates of retreat (km/yr) for each region.*

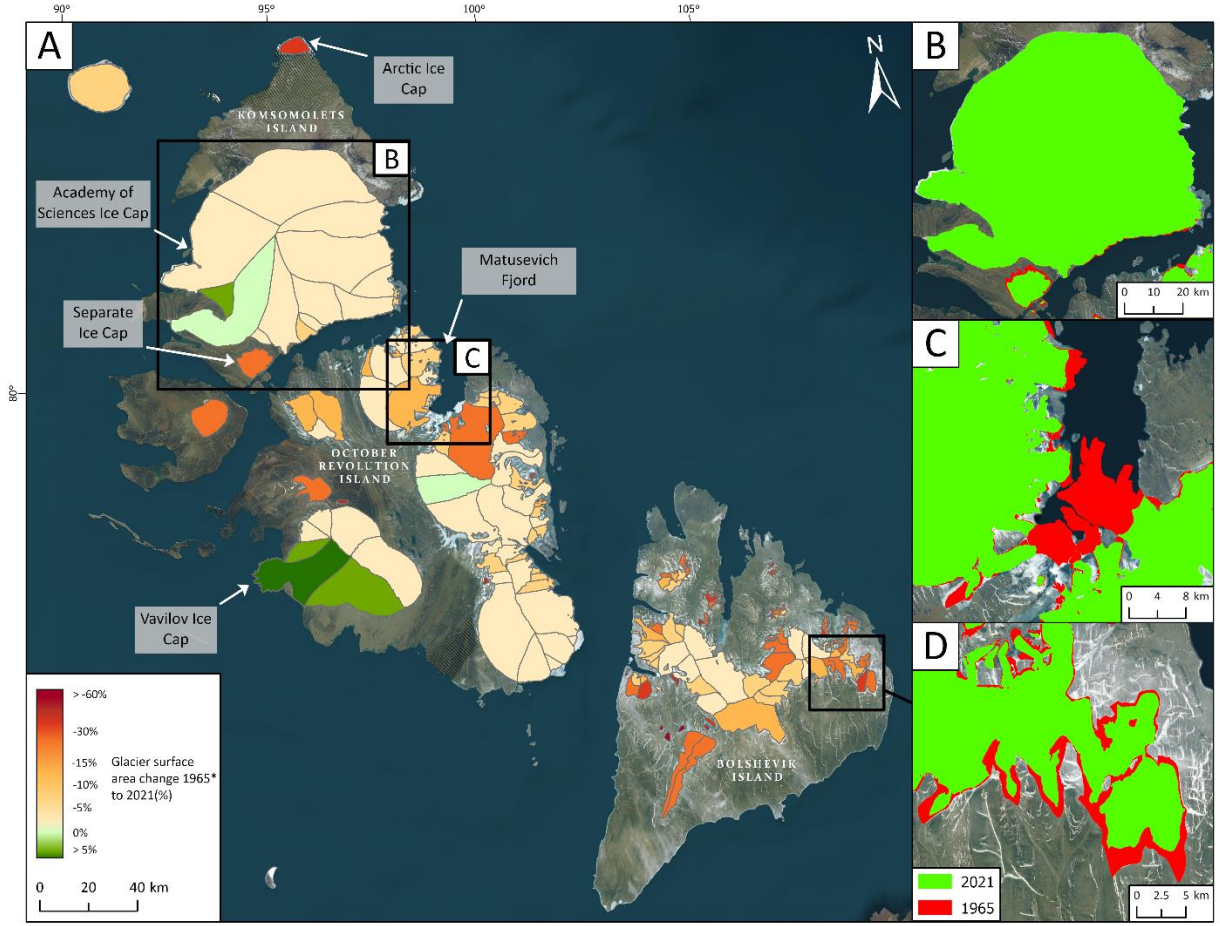

Fig. 5.3. *Overall glacier surface area changes between 1965 - 2021 (%). Negative (red) and positive (green) changes are scaled to reflect the amount of glacial change.*

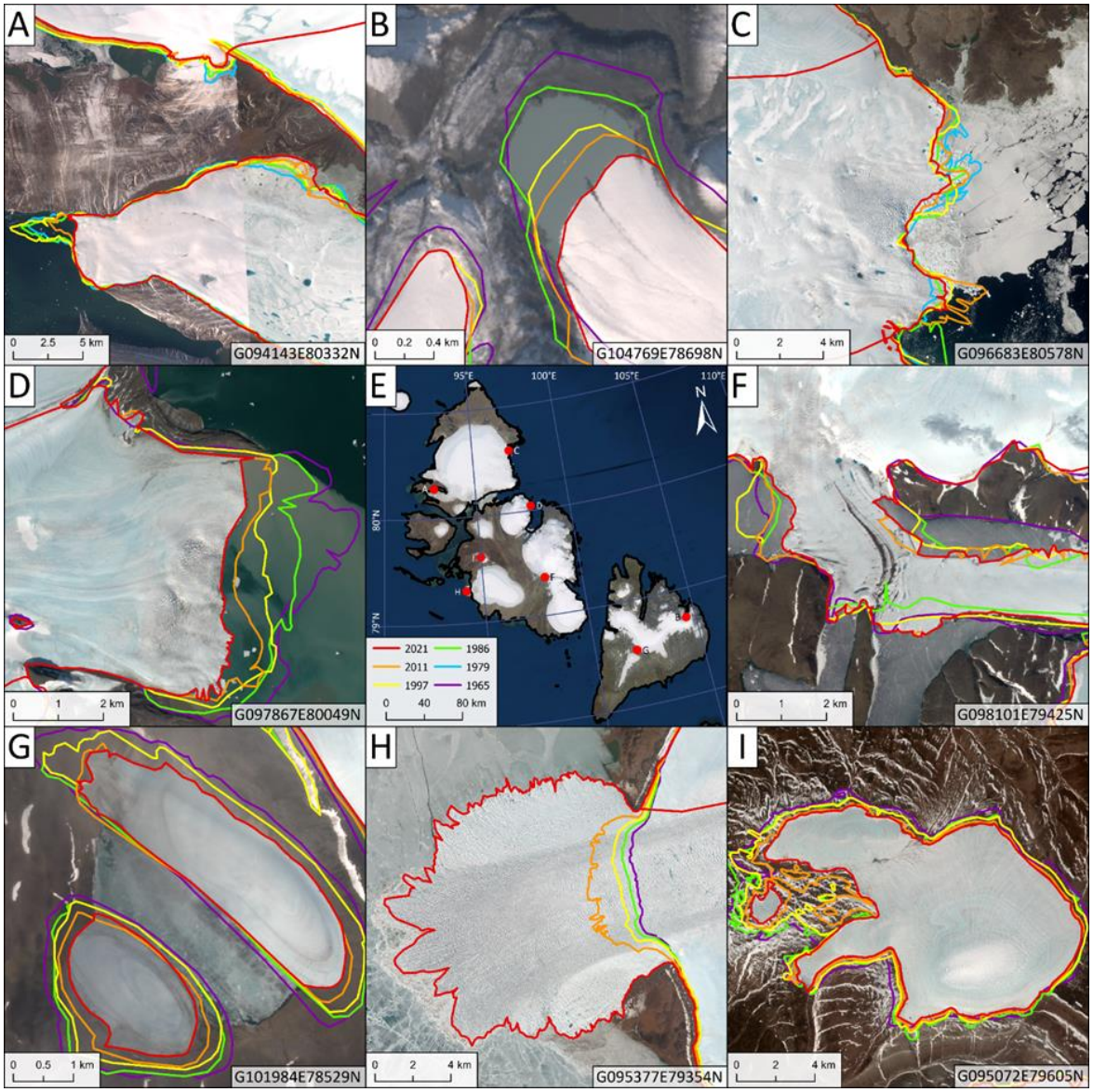

Fig. 5.4. *Glacier change outlines at dates from 1965 - 2021 overlayed on 2021 Sentinel 2 imagery, including RGI IDs. (A) Basin A of the AoSIC. (B) Glacier 41 - retreated from controlled moraines damming a proglacial lake. (C) Basin D of the AoSIC. (D) Glacier 1 - marine-terminating on the northeastern margin of the Rusanov Ice Cap. (E) Location of glaciers shown within SZ. (F) Glacier 105 - was observed to surge twice. (G) Glaciers 160 and 176 - lake terminating glaciers on Bolshevik Island (H) surge of the western Vavilov basin. (I) The separation of the Dezhnev Ice Cap.*

Glaciers on October Revolution Island have undergone the second-highest rate of area loss on SZ, with a -4.1 km^2 a^{-1} surface area loss (-3.0% area decrease) between 1965 and 2021 (Table 5.1). Net retreat between 1965 and 1986 (-5.8 km^2 a^{-1}) was interrupted by an increase in the overall area, attributed to an advance from a western basin of the Vavilov Ice Cap (41.18%

increase in km^2), which advanced 13.5 km from its 1965 position (Fig. 5.2; Fig 5.4H). Despite the continued advance of the Vavilov Ice Cap, the glaciated area of October Revolution Island declined post-1997, with the tributary glaciers feeding the former MIS experiencing rapid retreat post-2012 (Fig. 5.5). Between 2011 and 2021, glaciers on October Revolution Island showed a reduction in retreat rate (-1.5 km^2 a^{-1}), however, retreat rates are assumed to be higher because the rate of change is subdued due to a large gain in area from the advance of the Vavilov Ice Cap (Fig. 5.2; Fig. 5.4H).

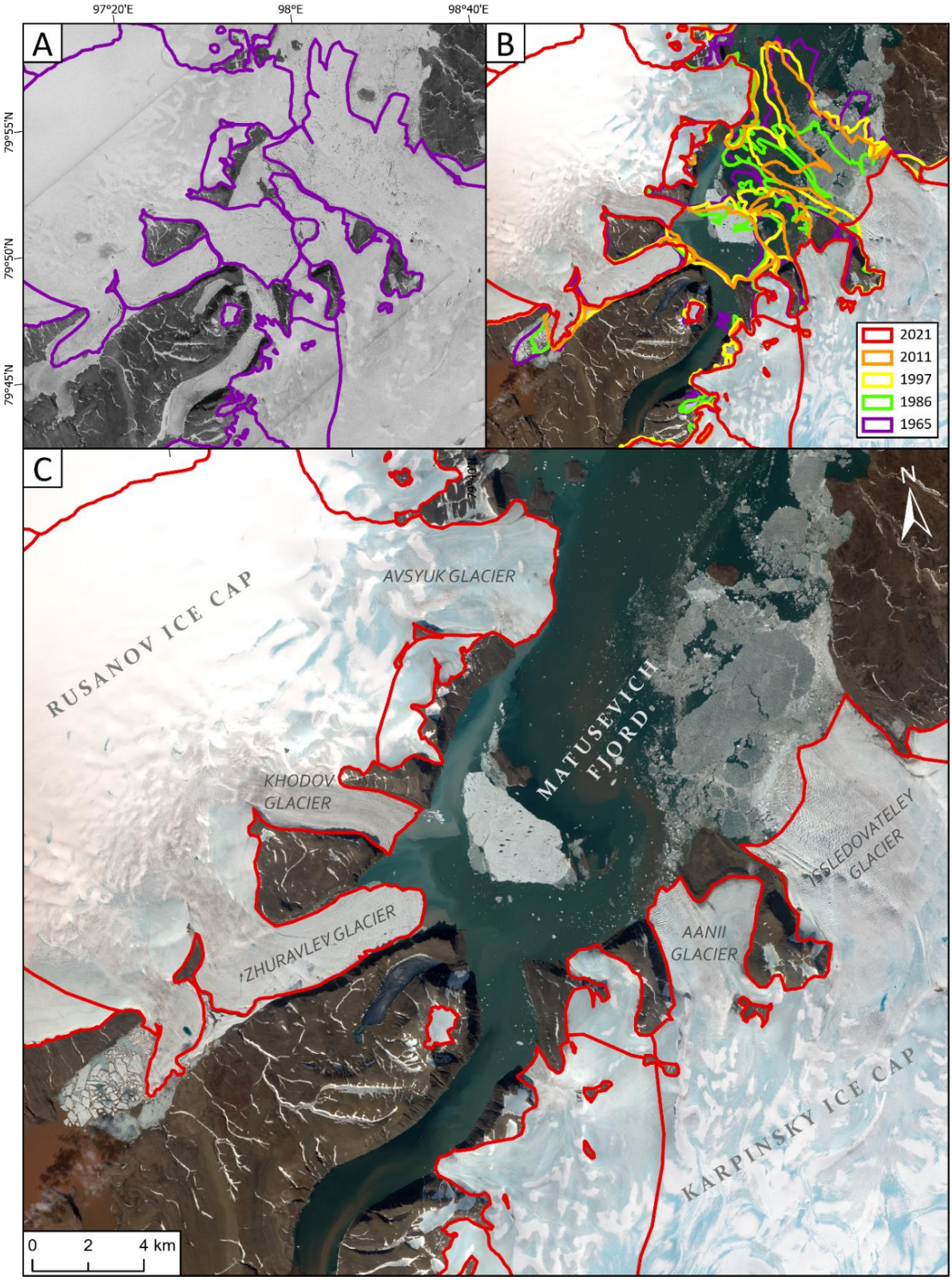

Fig. 5.5. *Changes in glacier extent surrounding the Matusevich Fjord. (A) The MIS in 1965 (KH-7 imagery) and glacier outlines (purple). (B) Changes in glacier extent (1965 - 2021) of MIS terminating glaciers. (C) The former MIS tributary glaciers in 2021 (red, Sentinel-2A imagery).*

The southernmost island, Bolshevik Island, has shown the greatest reduction in glacier area of -7.6 km^2 a^{-1} (-14.1% decrease, -426 km^2) from 1965 to 2021, with no advances recorded (Table 5.1). Between 1965 and 1986, glacier surface area declined at a rate of -8.2 km^2 a^{-1}, preferentially affecting small ice caps in the southwest of the island (Fig. 5.2; Fig. 5.3). Glacier retreat rates declined to -3.6 km^2 a^{-1} between 1986 and 1997, although the error margins are large due to the coarse imagery, so a significant deceleration is uncertain. Post-1997, the rate of glacier retreat increased at each date, with the greatest increase in retreat rates occurring between 1986 and 1997 (-3.6 km^2 a^{-1}) and 1997 and 2011 (-8.4 km^2 a^{-1}). The fastest rate of retreat occurred between 2011 and 2021 (-9.6 km^2 a^{-1}), which exceeded both Komsomolets (-4.3 km^2 a^{-1}) and October Revolution islands (-1.5 km^2 a^{-1}) during the same period.

The overall spatiotemporal trends in surface area change show a north-to-south gradient of increased retreat, concentrated on Bolshevik Island, where most glaciers are land-terminating (Fig. 5.3). Observations show a recent (post-1997) acceleration in retreat rates on northern SZ, albeit not strongly on October Revolution Island, whereas glaciers on Bolshevik Island have notably retreated across the entire observational period (1965 to 2021) (Fig. 5.1).

5.3 Climate Change

The coldest mean annual air temperatures are recorded at the more continentally influenced Im.E.K.Fedorova station, similar to the maritime influenced climate at Ostrov Golomjannyj (-14.1 °C, 1937 - 2021), which is 2 °C further north (Fig. 3.1, Fig. 5.6A-B). A stronger trend in mean annual warming temperature is recorded at Ostrov Golomjannyj, which has warmed by 3°C (R^2 = 0.24), 1 °C more than at Im.E.K.Fedorova (R^2 = 0.10) (Fig. 5.6A-B). Im.E.K.Fedorova is characterised by warmer summers (average -0.08 °C, 1936-2021) and is the only station beginning to trend towards summer warming (R^2 = 0.03) (Fig. 5.6 C). In contrast, Ostrov Golomjannyj is characterised by colder summers (-0.2°C, 1936-2021) and shows no discernible trend of summer warming (R^2 = 0.002; Fig. 5.6D). Ostrov Golomjannyj has warmer winters (-26.2 °C, 1937-2021) and experienced a stronger trend in winter warming (R^2 = 0.08) than Im.E.K.Fedorova (-26.9 °C), which has also undergone notable winter warming (R^2 = 0.02; Fig. 5.6E-F).

Long-term trends show that the mid-1930s to the mid-1950s were generally warmer than the 1936/7 to 2021 average (Im.E.K.Fedorova; -14.4 °C, Ostrov Golomjannyj; -14.1 °C) (Fig.

5.6A-F). Air temperatures were generally warmer at Im.E.K.Fedorova, which also recorded the highest air temperaturature anomalies, up to 4° C warmer than the long-term average (1936/7 to 2021), compared to Ostrov Golomjannyj, where temperatures were up to 2 °C warmer (Fig. 5.6A-F). Summer air temperatures were not anomalously warm during this period, with the largest air temperature anomalies during this period recorded in winter (max: +6°C warmer than average at Im.E.K Fedorova) (Fig. 5.6C-F). This was followed by a period of cooling between the mid-1950s and early 2000s, which similar to the prior warming, was more pronounced at Im.E.K.Fedorova on the Taymyr Penninsula than on Severnaya Zemlya (Ostrov Golomjannyj). Between 1965 to 1972, Im.E.K.Fedorova experienced the most anomalously cold summer air temperatures (-7.5 °C below average) on record, which is not recorded further north in Ostrov Golomjannyj (Fig. 5.6C-D). A shorter-lived summer cooling period of a lower magnitude is recorded from the mid-1980s to 2000, which is more pronounced on Severnaya Zemlya (Ostrov Golomjannyj) (Fig. 5.6C-D). Post-2006, annual air temperatures have progressively increased, which unlike warmer periods pre-2006, are not interrupted by a single negative air temperature anomaly (Fig. 5.6A-B).

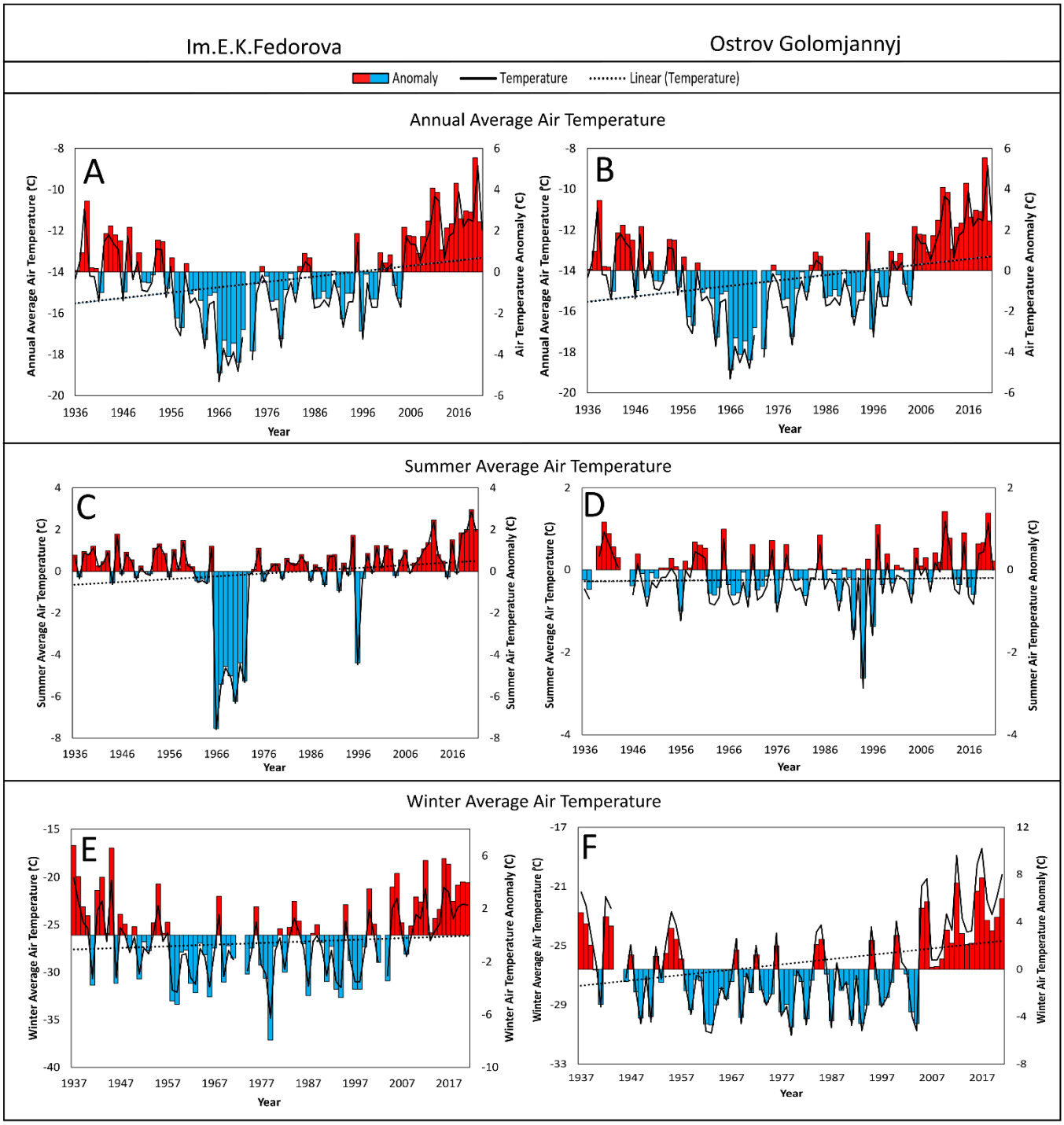

Fig. 5.6. *Seasonal and annual average air temperatures at Im.E.K.Fedorova (left) and Ostrov Golomjannyj (right). The location of each weather station is shown in figure 3.1. Negative anomalies (blue) and positive anomalies (red) are shown by the bar chart, along with linear trend lines in surface air temperatures which are plotted against a 1936/7 to 2021 mean. (A) Annual average air temperature at Im.E.K.Fedorova. (B) Annual average air temperature at Ostrov Golomjannyj. (C) Summer average*

air temperature at Im.E.K.Fedorova. (D) Summer average air temperature at Ostrov Golomjannyj. (E) Winter average air temperature at Im.E.K. Fedorova. (F) Winter average air temperature at Ostrov Golomjannyj.

Long-term (1981-2022) spatial trends in surface air temperature show that the warmest temperatures occurred in the southwest of SZ (western Bolshevik and southern October Revolution islands) on the Kara Sea coast (Fig. 5.7A). Temperatures decrease northwards towards Komsomolets Island and to the east of Bolshevik Island on the Laptev Sea coast (Fig. 5.7A). Since the 21st century, mean annual surface air temperature has increased across the entirety of SZ, with the strongest warming concentrated around the northern cape, and the weakest trends of warming occurring on Bolshevik Island (Fig. 5.7B). Spatial trends in SST mostly correspond with mean surface air temperature, with colder temperatures to the north and warmer temperatures on the Kara Sea coast (Fig. 5.7A, Fig. 5.7C). Note that the NCEP reanalysis dataset incorporates some classified meteorological stations (Kalnay and others, 1996), one of which, we attribute to the modelled isopleth bullseye effect of abnormally warm SSTs off northern Bolshevik Island, resulting from the sparsity of stations in the region. SST warming anomalies are strongest in the Arctic and Kara Seas, with evidence of warming but to a lesser extent in the Laptev Sea (Fig. 5.7D). Negative SST anomalies are confined to the northern coast of Bolshevik Island and eastern October Revolution Island (Fig. 5.7D). The highest rates of precipitation have been historically concentrated around northern Bolshevik Island and southern October Revolution Island (Fig. 5.7E). Since 2000, mean annual precipitation rates have increased compared to the climate normal timeperiod (1991 to 2020) on October Revolution and Komsomolets Islands, whereas they have undergone a slight decline around the precipitation high on Bolshevik Island (Fig. 5.7F).

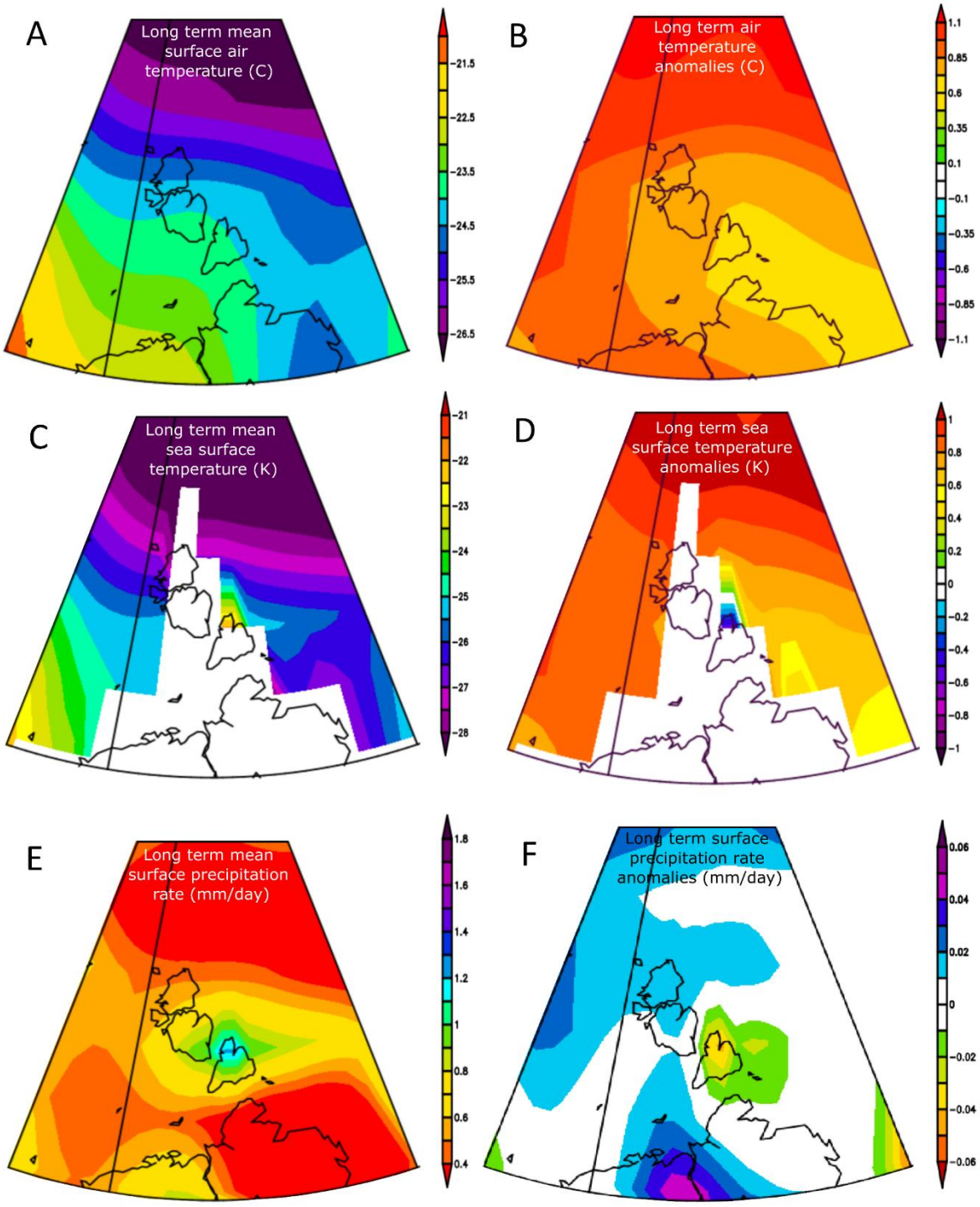

Fig. 5.7. *Long-term (1981-2022) mean annual climatologies (left) plotted using NOAA NCEP reanalysis monthly/seasonal climate composite tools (available at: https://psl.noaa.gov/cgi-bin/data/composites/printpage.pl). Anomaly plots that show recent 21st century (2000 to 2022) trends plotted against the new climate normal time period (1991 to 2020) (right). (A) Mean surface (2 m) air temperature (°C). (B) (2 m) air temperature anomalies (°C). (C) Mean sea surface temperature (°C).*

(D) Sea surface temperature anomalies (°C). (E) Mean annual precipitation (mm/day). (F) Mean annual precipitation anomalies (mm/day).

5.4 Identification of surge-type glaciers

The 190 glaciers on SZ were systematically investigated for evidence regarded as diagnostic of active and former surging. Using the criteria in Table 4.1, it is suggested that four glaciers are confirmed surge-type (2.1%), seven are likely to have surged (3.7%) and nine are possible surge-type (4.7%) (Table 5.2; Fig. 5.8). Glaciers classified as confirmed surge-type (active phase observed) comprise 10% of SZ's glacier surface area (mean size: 406 km^2), glaciers classified as likely to have surged cover 12% (mean size: 284 km^2) and possible surge type glaciers cover 16% (mean size: 293 km^2). The majority of glaciers on SZ are not of surge-type but, where they occur, the most commonly identified surge-diagnostic features include surface potholes, a localised abnormal ice-front advance, heavy surface crevassing and high surface velocities (Table 5.2).

Table 5.2. *The presence of surge-type glaciers on SZ. Lettering indicates the presence of a feature at an individual date: a. 1965, b. 1979, c. 1986, d. 1999, e.2011, f.2021. A weighted total of 0-3 = non-surge, 4-6 = possible surge-type, >7 = likely to have surged, with glaciers classified as confirmed surge-type if they score >10, an advance is observed (active phase), and 3 or more surge-indicative features are present. See Table 4.1 for the weighting of each criterion.*

Glacier	Terminus	2021 Area (km^2)	RGI ID	Looped/ deformed medial moraines	Deformed ice structures	Shear margins	Surface crevassing up-glacier	Heavy surface crevassing at the terminus	Localised abnormal advance	Highly digitate terminus	Surface potholes	Thrust-block/push moraines	Total (weighted)
105	lacustrine	350.7	G098101E79425N	a	cdef		def	acd	c-e		acdef		16
128	marine	493.6	G098527E79706N				f	acdef	c-d	acde	acdef		13
76	marine	485.1	G095377E79354N			f	f	ef	e-f		cd		11
93	marine	293.7	G097064E79876N				cdef	adef	c-e		acdef		10
138	land	56.9	G099222E79553N	acdef						acdef		acdef	12
161	marine	145.6	G099370E79446N	acdef				acdef			acdef	acdef	11
43	marine	411.1	G094682E80294N				abcdef	abcdef	a-b				9
67	land	24.7	G099506E79382N						a-c	acdef			8
38	marine	712.5	G094143E80332N					bcdef	b-f		bcdef		7
139	marine	168.1	G096735E80048N					ab	a-b		abcdef		7
143	marine	468.8	G096683E80578N					bcdef	d-e		bcdef		7
49	marine	196.5	G096576E80253N					abcdef	a-b				6
70	land	87.5	G098974E79688N	cdef	b								6
1	marine	120.6	G097867E80049N					a				acdef	5
137	marine	828.5	G096063E80433N				def	bdef			cdef		5
2	marine	275.4	G095561E80299N				aef	abcdef			c		5
31	land	93.3	G094665E79378N			f	f	f					5
77	land	511.3	G096205E79192N						c-f				5
104	land	419.0	G096481E79287N						c-f				5
154	land	103.8	G093581E80318N						d-f				5

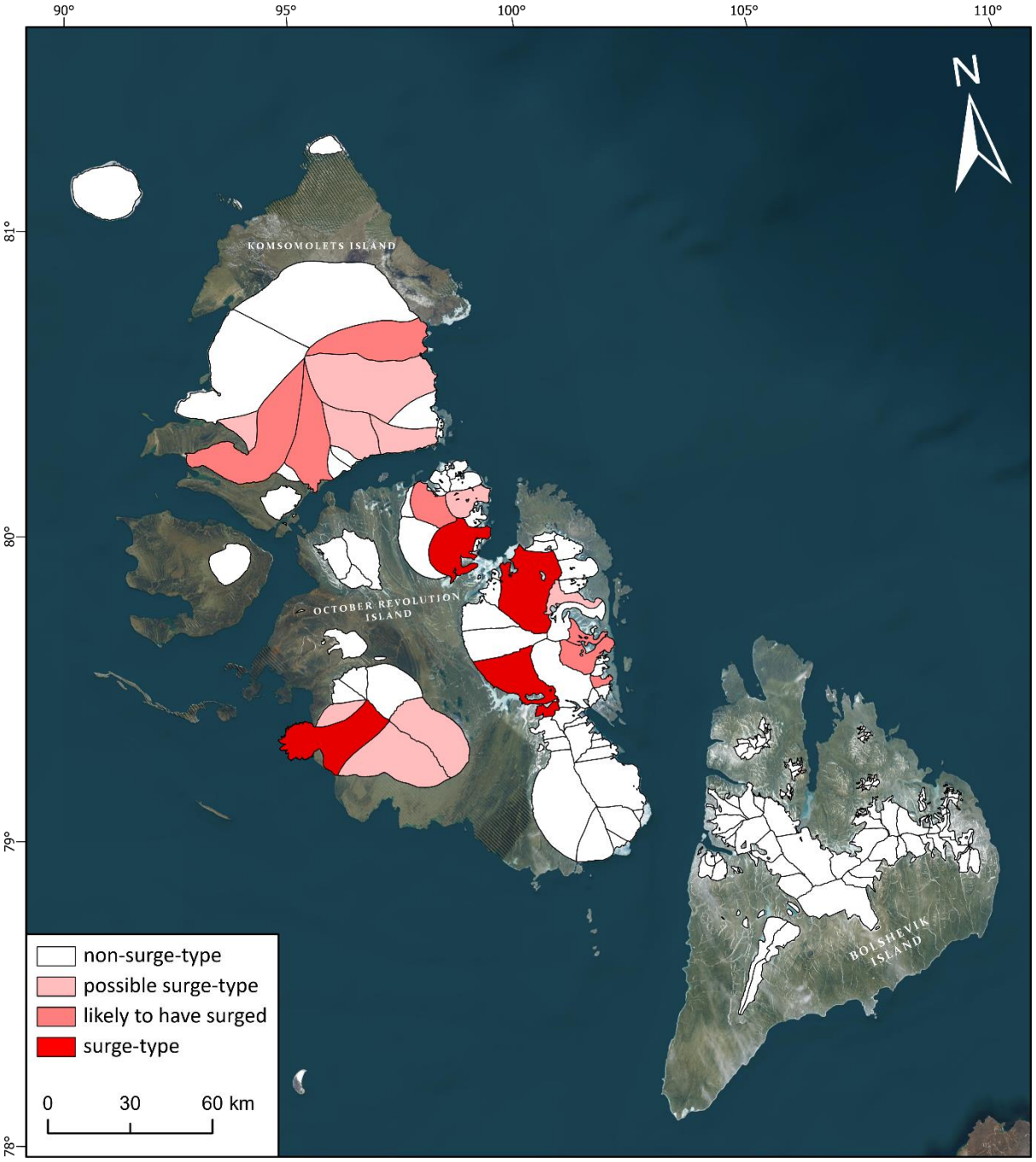

Fig. 5.8. *Classification of glaciers by likelihood of being surge-type based on a systematic identification of each glacier for surge-indicative features. Note that no glaciers on Bolshevik Island are classified as surge-type and that surging primarily occurs towards the north and east of SZ.*

Evidence of surging predominantly occurs north of 79°N on October Revolution Island and Komsomolets Island (Fig. 5.8). Surge-type glaciers (including possible and likely of surge-type) all originate from large ice caps, primarily clustered around the AoSIC, Rusanov Ice Cap and Karpinsky with no evidence of surging in the Albanov, University Ice Cap or on Bolshevik

Island. Glaciers with evidence of surging have a mean size of 312 km^2 (median: 284.5 km^2) compared to 86 km^2 for non-surge-type glaciers. All surge-type glaciers are marine/lake terminating, although this decreases to 65% when likely to have surged and possible surge-type glaciers are included (Table 5.2).

Between 1965 and 2021, 14 localised abnormal advances (>0.5 km^2) were observed at various times and of varying duration (see Appendix B). The western margins of the Vavilov Ice Cap exhibited the largest advance between any date, extending ~11 km further into the Kara Sea than its position in 2011 (Fig. 5.4H). The surrounding basins of the Vavilov Ice Cap underwent a minor advance as the western margin surged. The highest confidence classification is glacier 105, a lake-terminating glacier, which is observed to actively surge between 1987 - 2011 and shows evidence of having formerly surged at least twice; the evidence being a looped medial moraine observed on the glacier in 1965 prior to the observation of a surge between 1987 - 2011 (Fig. 5.9; Fig. 5.10C-D).

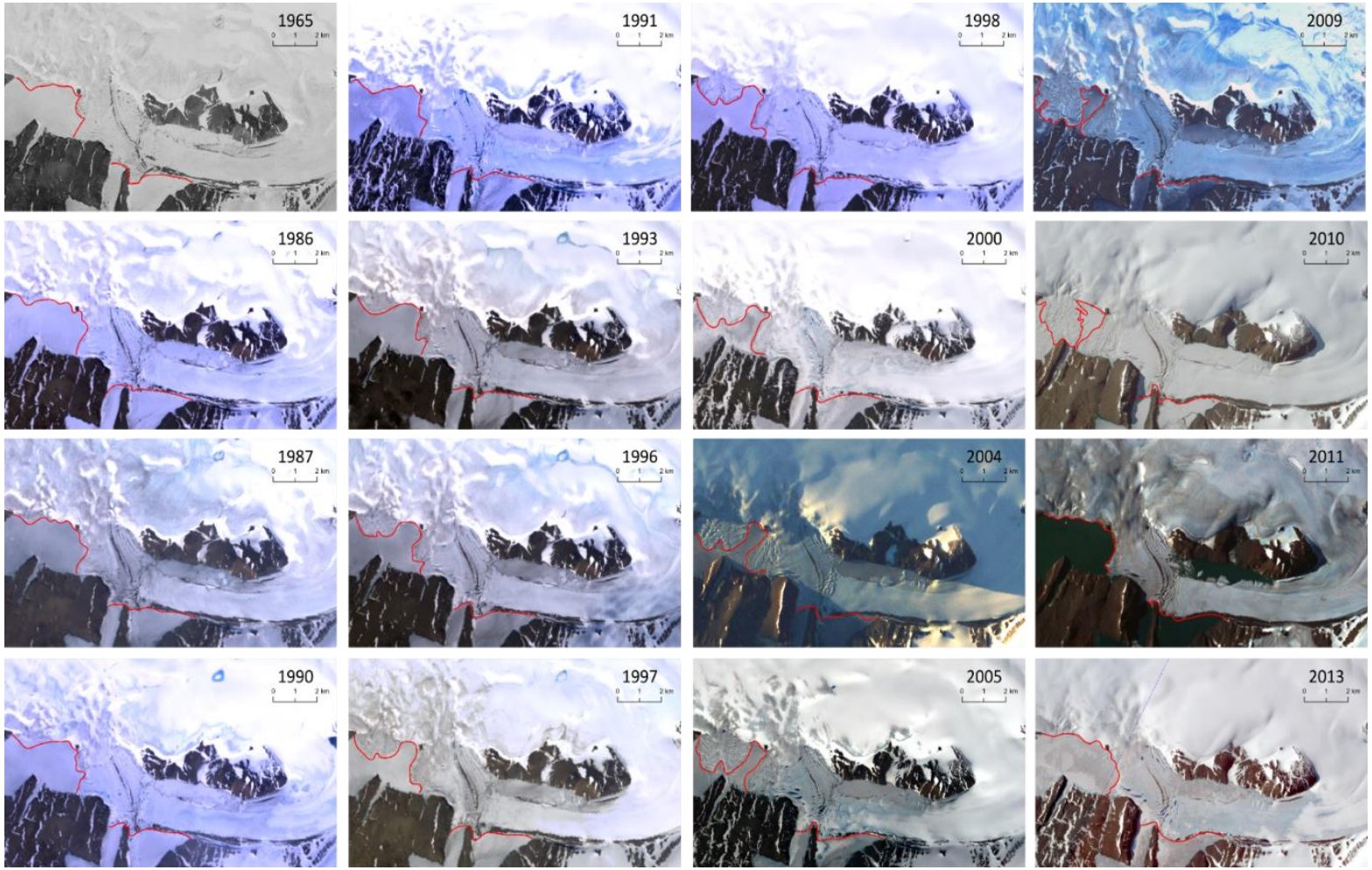

Fig. 5.9. *The surge of glacier 105 between 1965/86 to 2010. The terminus of the glacier is outlined (red) at each timestamp. A .gif of the glacier surge can be viewed at https://www.dropbox.com/s/zkdh6k6z2g02n43/Active_surge_phase.gif?dl=0*

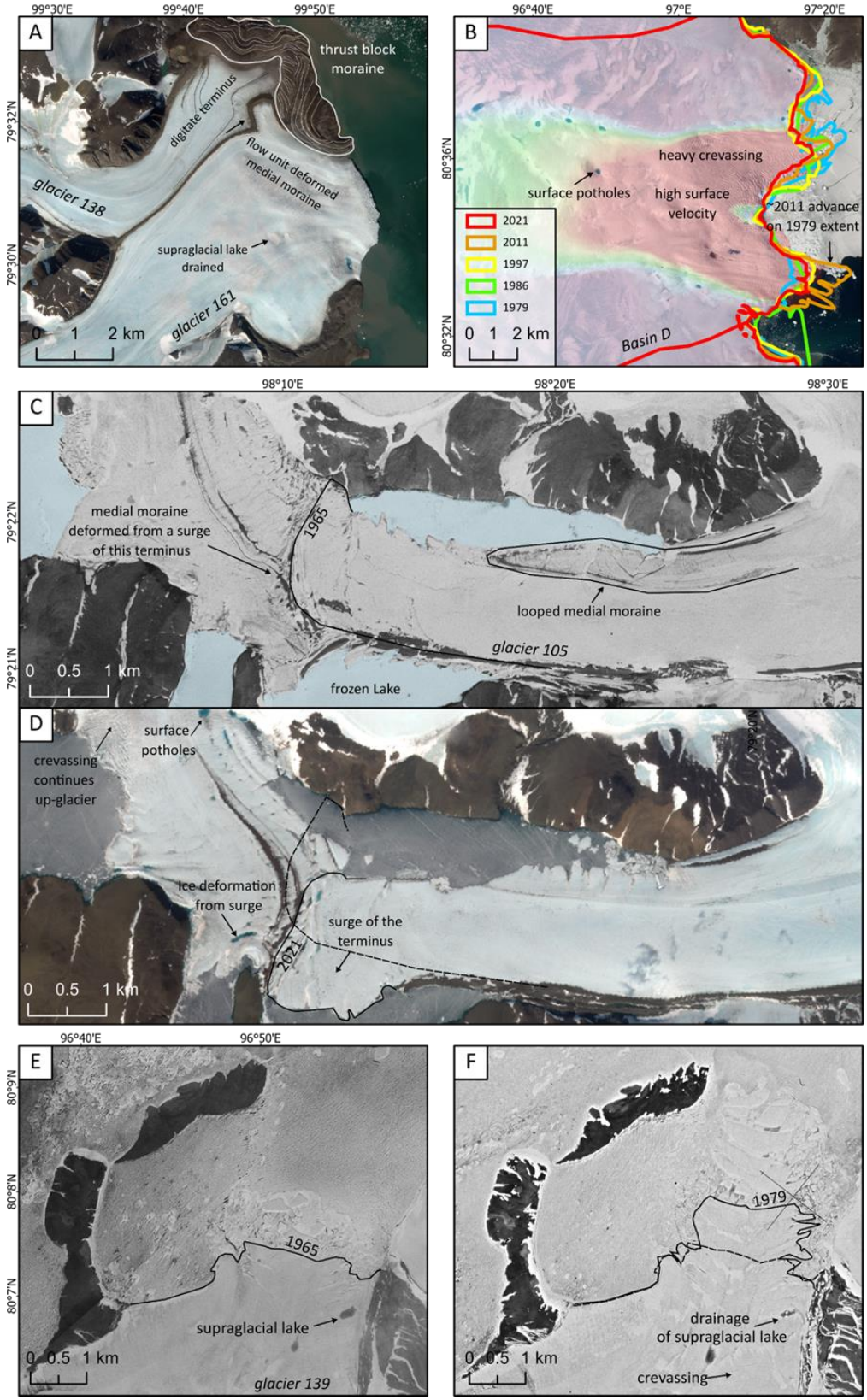

Fig. 5.10. *Evidence of surge-type glaciers. (A) Glacier 138 (north) and 161 (south) on the eastern Karpinsky Ice Cap, including the presence of a deformed medial moraine and a thrust block moraine*

in contact with the ice-margin at the terminus of glacier 138. (B) Localised advance to the south of Basin D of the AoSIC between 1979 and 2011, including heavy crevassing and surface potholes. (C) 1965 KH-7 imagery of glacier 105. The frozen lake is artificially coloured blue to aid visibility. Note the presence of a looped medial moraine. (D) 2021 Sentinel 2a imagery of glacier 105. (E) 1965 KH-7 imagery of glacier 139. (F) KH-9 1979 imagery showing a rapid localised advance of the terminus of glacier 139.

Pre-1965 surging is mainly recorded by preserved thrust block/glacitectonic composite moraines, with former surges superimposed, primarily on eastern October Revolution Island (e.g., Fig. 5.10A), which is one of the few areas to contain extensive forelands of deformable sediment. There are no preserved moraines beyond the limit of the possible surge moraines, most of which are still in contact with the ice front. As the surge diagnostic nature of thrust block/glacitectonic composite moraines is not entirely unequivocal (cf. Sharp 1985, 1988; Evans & Rea 1999, 2003; Fitzsimons 1996, 1997, 2003; Ingolfsson et al. 2016), their presence in the absence of other surge criteria is not regarded as sufficient evidence for a definite surge classification. On Bolshevik Island, four small cirque glaciers are classified as non-surge-type despite potential thrust-block/glacitectonic composite moraines at their termini due to a possible, alternative, controlled moraine interpretation of such forms based on aerial and satellite imagery alone (Fig 5.11; Evans, 2009).

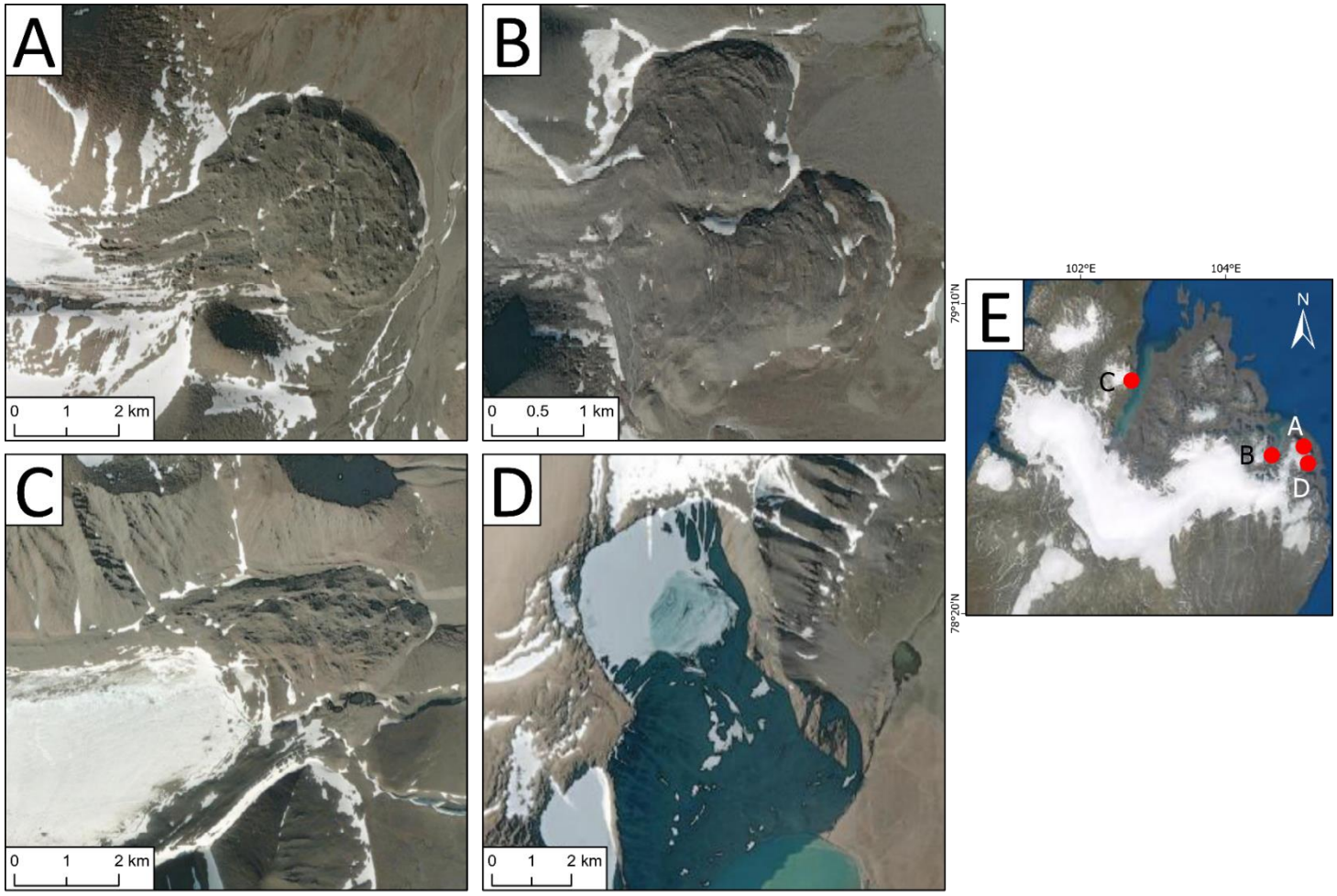

Fig. 5.11. *Potential thrust-block/glacitectonic composite moraines on eastern Bolshevik Island. (A) Glacier 189. (B) Glacier 180. (C) Glacier 28. (D) Glacier 183. (E) The location of panels A-D is shown on Bolshevik Island.*

5.5 Summary

Overall glacier surface area declined across all regions between 1965 and 2021 (5% overall decrease), although glaciers and ice caps on Komsomolets Island did not begin to retreat (outside of error margins) until post-1997. The intensity of glacier retreat (in percentage loss) varied regionally, increasing along a north-south gradient, with Bolshevik Island undergoing the largest decline in surface area (-14.1%, 1965-2021). Climatological long-term trends show that the warmest summer air surface temperatures have occurred towards the south, although the strongest trends in annual and winter warming have occurred towards the north. Evidence of surging is concentrated towards the north on October Revolution and Komsomolets Islands (20 glaciers of varying confidence levels), with no evidence of surging on Bolshevik Island. All ‘surge-type’ glaciers originate from larger ice caps and are more likely to be marine or lake terminating than non-surge-type glaciers.

Chapter 6: Discussion

6.1 Introduction

In this chapter, the results are contextualised with respect to the relevant literature to assess the trends and drivers of glacier change and surge-type behaviour. The first section outlines the spatiotemporal patterns of glacier change and interprets the significance of various possible climatic drivers (section 6.2.1). This is followed by a subsection on the trends and drivers of glacier retreat on SZ in comparison to the wider Arctic region (section 6.2.2). The second section details the significance of the identification of surge-type glaciers, their occurrence (section 6.3.1), characteristics (section 6.3.2), distribution (section 6.3.3), and mechanisms (6.3.4). The final section focuses on potential further work on SZ.

6.2 Glacier Change & Climatic Forcing

6.2.1 Spatiotemporal Trends

Overall, almost all glaciers on SZ have retreated between 1965 and 2021 (Fig. 5.3; Table 5.1). The reduction in glacierised area is attributed to atmospheric warming, with annual average air temperature increases of ~2-3 °C (1936-2021) and an increase in positive SST anomalies surrounding SZ (Fig. 5.6; Fig. 5.7). Glaciers and ice caps have retreated the least in the north of SZ, with retreat rates increasing along a southward gradient (Fig. 5.3; Table 5.1). Until 1997, glaciers on northern SZ were relatively stable, whereas on southern SZ they were already retreating as early as 1952/75 (Govorukha et al., 1987). Rates of glacier retreat notably accelerated in all regions post-1997, correlating with the transition between the colder period of the 1950s-90s and rapid warming at the end of the 20th century (Fig. 5.1; Fig. 5.6). If retreat was solely due to LIA readjustment, it is unlikely that a post-2000 acceleration in retreat rates would be observed, which can be attributed to increased warming in the 21st century,

Between 1965 and 2021, the largest losses in glacier area occurred on Bolshevik Island (-14.1%), in the south of SZ (Table 5.1). Retreat rates have increased between each time slice post-1997, peaking at -9.6 km^2 a^{-1} (2011 to 2021) and of a magnitude higher than retreat rates elsewhere on SZ (Table 5.1). Bolshevik Island is influenced by warmer surface air and SSTs on the Kara Sea coast and receives the most precipitation on SZ, but precipitation totals have fallen between 1981 and 2022 (Fig. 5.7). The closest weather station to Bolshevik Island,

Im.E.K.Fedorova, shows a trend towards summer warming, unlike Ostrov Golomjannyj on western SZ which shows no trend of summer warming (Fig. 5.6). Glacier mass balance is most strongly controlled by summer climate (Möller & Kohler, 2018) and when increased summer ablation is combined with a decrease in precipitation (Fig. 5.7E), glacier mass balance will become increasingly negative. This combination of summer atmospheric warming occurring at a magnitude higher than the rest of SZ and a slight decrease in precipitation on Bolshevik Island specifically, provides a likely explanation for the southwards increase in retreat rates. It should be noted that glaciers on Bolshevik Island are smaller, and retreat is likely to be exaggerated in percentage terms than larger glaciers, however, 55% of all 1965 to 2021 glacier area loss (-426 km^2) occurred there, thus showing that retreat is occurring faster to the south.

Northwards, glaciers and ice caps on October Revolution Island (-3.0%, 1965-2021) have retreated at a slower rate than on Bolshevik Island (-14.1%, 1965-2021), but recent observations indicate more dramatic changes. The region underwent slow but incremental retreat until 2011, when the westernmost basin of the Vavilov Ice Cap underwent a rapid advance (Fig. 5.4H; Willis et al., 2018) and the MIS collapsed (Fig. 5.3; Willis et al., 2015). Until its collapse, the MIS was the largest floating ice shelf in the RHA and had historically undergone cyclical terminus fluctuations due to large calving events and subsequent advances (Williams & Dowdeswell, 2001). In the three years preceding the collapse, surface air temperatures were 2, 4 and 5°C higher than normal, and one tributary glacier (Issledovateley) advanced, destabilising the MIS and leading to its collapse in 2012 (Fig. 5.5; Willis et al., 2015). Post-collapse (2012 to 2014), a reduction in buttressing from the MIS resulted in thinning rates that exceed the 30-year average rate for SZ (Willis et al., 2018). By 2021, imagery shows that a large tabular iceberg from the breakup of the Khodov terminus remains grounded in Matusevich Fjord and former MIS outlet glaciers show an increase in crevassing at their terminus (Fig. 5.5). Additionally, it is likely that the now exposed terminus of the Zhuravlev Glacier (Rusanov Ice Cap) is at risk of collapse from a lack of buttressing and increased exposure to submarine melt undercut and collapse, a process found to be a primary driver of frontal ablation on Svalbard (Fig. 5.5; Luckman et al., 2015). Due to warmer SSTs and a SZ-wide pattern of retreat (1965 to 2021), a regeneration of the MIS is deemed highly unlikely (Fig. 5.3; 5.7D). The exposure of marine-terminating (MIS-fed) outlet glaciers to warmer SSTs poses a risk to accelerated melting of the Rusanov and Karpinsky Ice Caps, which already have exhibited some of the highest rates of surface area loss on October Revolution

Island. However, without higher resolution SST data, it remains uncertain to what extent temperatures within the fjord differ from the Laptev Sea.

Komsomolets Island (northernmost SZ) shows the least overall change of the three main islands, having lost the least glacierised area between 1979 and 2021 (-1.9%; Table 5.1). The AoSIC occupies most of Komsomolets Island and has had a mass balance close to zero for the last four decades (Bassford et al., 2006a; Sánchez-Gámez et al., 2019). However, between 1965 and 2021, two basins have increased in surface area and multiple basins of the AoSIC show evidence of cyclical advance and retreat patterns (Moholdt et al., 2021b). The majority of advances observed in this study (from 1965 to 2021) are from one of the four fast-flowing AoSIC 'ice streams', which we classify as surge-type, albeit with varying degrees of certainty, each having velocities of a magnitude higher than the rest of SZ (Table 5.2; Fig. 5.8). It is not known what causes these ice streams to advance, although it has been argued that their sub-glacial geology, if deformable, could support transient subglacial deformation, or that drainage of water to the bed could explain glacier speed-up events (Moholdt et al., 2012b). Hence, it is suggested here that this is a viable explanation, as the drainage and re-appearance of large meltwater lakes on most 'ice streams' is observed, which may route meltwater to the glacier bed and result in glacier speed-up events. A climatic driver can also be dismissed, as these advances are asynchronous, and the ice cap is not gaining mass. Thus, it is most probable that the speed-up events are due to the characteristics of the ice cap or another mechanism (e.g., surging), rather than climate.

Overall, accelerated glacier retreat on SZ is attributed to a 2-3 °C increase in mean annual surface air temperatures on the Taymyr Peninsula and October Revolution Island (1936 to 2021; Fig. 5.6A-B). The highest rates of retreat occurred at land-terminating glaciers on Bolshevik Island and are likely due to atmospheric surface temperatures beginning to trend towards summer warming on the proximal Taymyr Peninsula (Fig. 5.6C). Summer warming is the primary control on glacier retreat, leading to increased ablation, which may be exacerbated by a lengthened melt season due to winter warming. Increased ablation, combined with the trend in reduced precipitation has likely resulted in an increasingly negative glacier mass balance, which has manifested as a reduction in glacier surface area (Fig. 5.7E-F). In contrast, further north there is no apparent trend in summer warming and the rate of precipitation (1936 to 2021) has remained steady or has increased (Fig. 5.6; Fig. 5.7E-F). Although winter warming may have lengthened the melt season in the north, retreat has occurred at a slower rate due to

lower rates of summer warming and ablation compared to Bolshevik Island (Fig. 5.6F). Additionally, there is evidence that declining sea ice concentrations due to oceanic warming may allow for increased heat flux transfer from the ocean to the atmosphere, with a statistically significant correlation between reduced late-summer sea ice concentrations and earlier surface snowpack melt (Rodrigues, 2008; Zhao et al., 2014; Tepes et al., 2021b). This trend in oceanic warming is attributed by Tepes et al. (2021b) to be the primary driver of mass loss on SZ. However, as the highest reductions in surface area are observed at land-terminating glaciers on Bolshevik Island, it is suggested that atmospheric warming is more influential than previously thought, especially on small, land-terminating glaciers in the south. It is anticipated that SZ will become increasingly negative in mass balance as summer warming trends are likely to increase, resulting in higher rates of ablation that cannot be sustained by the current rates of precipitation.

6.2.2 Comparison to other Arctic regions

The absence of summer warming trends in surface air temperature (1936 to 2021) on northern SZ is in accordance with NZ (1990 to 2011) (Carr et al., 2014), although NZ has since become a hotspot for warm anomalies (2011 to 2016) (Ciracì et al., 2018). South of SZ, the Taymyr peninsula on mainland Russia exhibits a trend in summer atmospheric warming, a trend that perhaps extends onto southern SZ (Fig. 5.6C). Similar to SZ, Svalbard exhibits a strong trend of winter warming (1.6°C decade^{-1}, 1961-2012) and, to a lesser degree, summer warming (0.2°C decade^{-1}, 1961-2012). The latter has been pinpointed as the key driver of glacier thinning on Svalbard and, when combined with the trend of declining summer precipitation, has resulted in glaciers being unable to maintain positive mass balance (van Pelt et al., 2016; Geyman et al., 2022). The warming trends and resulting glacier retreat observed in the western Barents-Kara region (i.e., Svalbard and western NZ) can be used as a predictor for the future glaciological changes on SZ, as its warming is delayed with respect to the western Barents-Kara Sea region (Tepes et al., 2021b). Thus, it might be expected that SZ glaciers will be increasingly less capable of sustaining their current mass balance characteristics under predicted stronger trends of summer warming.

Strong winter warming trends in the Barents Sea have been linked to sea ice decline and a subsequent acceleration of glacier retreat (Carr et al., 2014; Tepes et al., 2021b). In addition, the increased encroachment of warmer Atlantic waters into the Eurasian Basin has been

attributed to changes in the Atlantic Multi-decadal Oscillation and North Atlantic Oscillation, leading to further sea ice decline (Carr et al., 2017b; Carvalho & Wang, 2020). There is also evidence that, in recent decades, Ural blocking events have contributed to sea ice decline (Luo et al., 2016, 2019). The influx of warm waters into the Eurasian Basin and the resulting sea ice decline, has led to an eastward movement of winter convection, increased vertical mixing and reduced ocean stratification around NZ (Polyakov et al., 2017). Without blocking from sea ice, heat flux can rise into the atmospheric boundary layer from the water column, resulting in an ocean-atmospheric warming feedback loop, further reducing sea ice and increasing atmospheric warming (Polyakov et al., 2017). The effect of long-term sea ice decline has been observed in the Arctic, notably in Greenland, where retreat rates have increased during phases of low or no sea ice (Reeh et al., 2001; Amundson et al., 2010; Moon et al., 2015). At present, sea ice concentrations have declined around SZ, but still remain fairly high, thus there is no difference in retreat rates (outside of error margins) between land and marine-terminating glaciers(Rodrigues, 2008; Onarheim et al., 2018). In contrast, glacier retreat at marine-terminating outlets on neighbouring NZ and FJL is observed to have occurred at a disproportionally faster rate compared to land-terminating glaciers (Carr et al., 2014; Moon et al., 2015; Zheng et al., 2018). On NZ, marine-terminating glaciers have retreated 3.5 times faster than land-terminating glaciers (Carr et al., 2017b). The results presented here show that the largest reductions in glacier surface area have occurred at land-terminating glaciers in the far south of SZ (Fig. 5.2). This is likely to change as warming on SZ is delayed compared to NZ, hence NZ can be used as a predictor of future change. For example, it is probable that in the coming decades, a climatic gradient, similar to what is currently observed between the Barents and Kara Seas, will emerge between the Kara and Laptev Seas. At present, observations of SST remain limited surrounding SZ, hence, it remains unknown as to whether warmer SSTs are penetrating into fjords, nor have grounding lines been mapped, which would aid future research on ice-climate interactions on SZ. It is anticipated that under continued sea ice decline, the magnitude of marine-terminating glacier retreat on SZ will greatly exceed that of land-terminating glaciers.

6.3 Identification of Surge-Type Glaciers

6.3.1 Occurrence

Within the RHA, glacier surging has been perceived to be confined to the more temperate climate of NZ (Grant et al., 2009). In contrast, predominantly cold-based glaciers, as seen further east (e.g., SZ), have not traditionally been associated with surge-type behaviour, despite some clear evidence to the contrary (e.g., Hattersley-Smith 1969; Copland et al. 2003). Models predict that surging should occur on SZ and note the need for further investigation in the region (Sevestre & Benn, 2015). The notion that surging occurs on SZ is supported by the identification of two looped medial moraines by Dowdeswell & Williams (1997) from 30 m imagery on the eastern Karpinsky Ice Cap. More recently, a large destabilisation of the western Vavilov Ice Cap in 2012 implied that surge-like behaviour may be more widespread on SZ than previously thought (Willis et al., 2018). This 'surge', or more correctly "speed-up event", shared similar properties to that of a large fast-flow event at Austfonna, Svalbard (Dunse et al., 2011; Gong et al., 2018) and numerous other active phases of surging observed in more temperate Svalbard. Contrary to the Svalbard polythermal glacier regime, glaciers on SZ are thought to be predominantly cold-based and receive less precipitation, meaning the quiescent period is likely to be longer. However, given the presence of the looped medial moraines observed by Dowdeswell & Williams (1997), it is likely that surging has and does occur on SZ and this is confirmed in the present study. Indeed, it is proposed that surging is more widespread on SZ than initially thought, with 20 glaciers possibly of surge-type (Table 5.2; Fig. 5.8). When sub-divided by confidence, four glaciers are classified as confirmed surge-type, seven are likely to have surgedand nine are possible surge-type. The recent availability of higher resolution imagery (e.g., ArcticDEM, 2m, Sentinel 2, 10m) and the use of multiple dates (1965, 1979, 1986, 1999, 2011 & 2021) is attributed to the increased detection of surge-type glaciers compared to previous attempts (Dowdeswell & Williams, 1997).

Surging occurs less frequently on SZ than NZ and Svalbard, but compared to NZ, surge-type glaciers (including likely to have surged and possible) on SZ occupy a disproportionate portion of its glacierised area. As a percentage of glacierised area, the 38% surge-type glacier coverage of SZ exceeds that of NZ (~18%; Grant et al., 2009), but is lower than Svalbard (~46.5%; Jiskoot et al., 1998). The difference in surge-type glacierised area between SZ and NZ is attributed to many surge-type glaciers on SZ being concentrated around the outlets of large ice domes, which are substantially larger than any ice cap on NZ. Additionally, the difference in surge frequency is perhaps due to higher rates of precipitation further west, affecting the

duration needed for a glacier to gain enough mass to surge. As precipitation is a control on the length of the quiescent period (Eisen et al., 2001), it makes identifying multiple surges unlikely in colder, dryer climates like SZ. Based on traditional definitions, advances must be cyclical for a glacier to be surge-type. Thus, without observing cyclical behaviour it cannot be confirmed whether externally forced one-off speed-up events rather than cyclical/repeated surges occur on SZ. It is also possible that under climate change one-off surge events may be possible, whereby a glacier is unable to regain sufficient mass to surge again (Małecki et al., 2013). Despite this, one glacier (105) is observed in its active phase (~1986 to 2010) and has a looped medial moraine in 1965 imagery, which presumably formed before the active phase commenced. Hence, it is likely a relic from a prior surge, implying that the glacier has surged at least twice, conforming to traditional definitions of surging (Fig. 5.10C-D). This strengthens the notion that at least some glaciers on SZ are of surge-type and it may be more commonplace here than previously thought.

The presence of surge-indicative features is less common on SZ than Svalbard, with notable differences in foreland geomorphology. Any record of surging on SZ is likely represented by superimposition of proglacial thrust masses, illustrated by the thrust block moraines on eastern October Revolution Island (Fig. 5.10A). Many glaciers remain in contact with thrust blocks at their terminus, with no inner zone in which to identify other surge diagnostic forms such as long flutings, geometric ridge networks or zig-zag eskers (Evans & Rea, 2003; Ingolfsson et al., 2016). Where forelands are exposed, they contain no such clear evidence of glacier surging. In some cases, this is possibly due to imagery resolution, but it is also likely that the landsystem signature of predominantly cold-based surging glaciers will contain less subglacially-derived components such as crevasse-squeeze and infill landforms, such as geometric ridges and zig-zag eskers and flutings. A similar scenario occurs in the Canadian High Arctic where glaciers that have constructed thrust moraines are not traditionally interpreted as surge-type (cf. Evans & England 1991, 1992; Copland et al. 2003; Ó Cofaigh et al. 1999, 2003). Consequently, future research needs to further investigate the landsystem imprint typical of cold-based glacier systems in order to assess the presence, both former and contemporary, of High Arctic glacier surges.

6.3.2 Distribution

Surging on SZ is primarily clustered around north-eastern SZ, on the AoSIC, Karpinsky and Rusanov Ice Caps (Fig. 5.8). Within these ice caps, individual basins classified as surge-type display no preferential aspect. The geomorphological imprint of surging is primarily clustered around the Karpinsky Ice Cap, in eastern SZ, where glaciers descend from areas of higher elevation down to areas of deformable sediment on the Laptev Sea coast. Glaciers on the Laptev Sea coast are more likely to be marine-terminating, as this coastal zone is characterised by colder surface air temperatures even though there are warmer SSTs on the continental shelf here than on the Kara Sea coast (Fig. 5.7A, Fig. 5.7C). However, it is clear that surging is not restricted to a climatic envelope on the Laptev Sea coast due to the ice-marginal speed-up event on the Vavilov Ice Cap and the post-surge geometry of Basin A, both of which are on the Kara Sea coast (Fig. 5.4A, Fig. 5.4H).

If warmer ice temperatures and polythermal glacier regimes increase the likelihood of glacier surging, surging should be most prevalent on the warmer, southernmost, Bolshevik Island, which contains small glaciers and ice caps. However, there is no explicit evidence of past surging on the Island, with the exception of four small (~0.5-1.5 km^2) cirque glaciers (classified as non-surge-type) that have disproportionally large ice-cored, potentially thrust-block, terminal moraines (Fig. 5.11). These small cirques differ from the characteristics typical of surge-type glaciers on SZ, NZ and on Svalbard, which typically are predominantly long, have relatively steep slopes and occupy larger basins (Jiskoot et al., 2000; Grant et al., 2009; Sevestre & Benn, 2015). However, small cirque glaciers have been observed to surge in northern Iceland (Brynjólfsson et al., 2012; Ingólfsson et al., 2016) and, despite differing basal thermal regimes between Iceland and SZ, these glaciers may have once surged. Notwithstanding this evidence for possible surging cirque glaciers, there is a lack of unequivocal surging activity on Bolshevik Island.

The existence of surge-type glaciers on Komomolets Island has been debated (e.g., Moholdt et al., 2012). However, it is suggested that evidence is sufficient to assume that surging has most likely occurred in the AoSIC. Previous research has found no evidence of past surge activity within the residency time of the ice, in the form of looped medial moraines, heavy surface crevassing or rapid changes in extent (Dowdeswell et al., 2002). Previous studies (Moholdt et al., 2012b; Sánchez-Gámez et al., 2019) show that the ice streams of the AoSIC (Basins B, BC, C, D) alternate between periods of slow and fast flow (e.g., Fig. 5.10B), which is recorded by

periodic advances seen in the glacial change mapping from this thesis. The mechanism driving this cyclical behaviour is unknown, but the notion that they are surge-type is supported by two basins (A & B) which have undergone surge-like elevation changes (Moholdt et al., 2012b). These changes were followed by a deceleration in ice flow velocity in Basin A, which is characterised by a typical post-surge geometry (Moholdt et al., 2012b). In addition, observations show a small but constant advance of Basin A at the north-eastern margin of its low-gradient lobe and a small advance between 1979-1997 at its terminus (Fig. 5.4A). Despite there being alternative explanations for the existence of some surge-indicative features (e.g., shear margins and high surface velocities are also typical of ice streams), some features, such as the large low-gradient lobe characteristic of a post-surge terminus, are difficult to attribute to another mechanism. Thus, it is deemed likely that surging has occurred in the AoSIC, but there is no chronological constraint on when it occurred.

Similar issues of equifinality exist when determining whether the glaciers that fed the former MIS on October Revolution Island are of surge-type, or if the presence of surge-indicative features is a result of externally forced ice dynamics (i.e., speed-up event) as a result of ice shelf collapse. Before its collapse in 2012, there was evidence of an acceleration in ice flow velocity in the ice shelf's tributary glaciers between 1965 and 1995 (Sharov et al., 2015). As this velocity speed-up was synchronous with other glaciers this behaviour can be dismissed as surging. Additionally, observations show a notable localised advance of one tributary glacier (Issledovateley) between 1986 and 1997, which in conjunction with its heavy crevassing classifies this glacier as surge-type using the protocol outlined in this thesis (Fig. 5.5; see section 4.5). Nevertheless, it is suggested that this advance may not be due to surging *sensu stricto* as the ice shelf is known to undergo cyclical patterns of disintegration and re-establishment every 30 years (Williams & Dowdeswell, 2001). As the last advance was between 1962 and 1973 (Willis et al., 2015), the advance recorded between 1986 and 1997 is ~30 years later and therefore appears to be part of the cyclical behaviour that drives speed-up events. Moreover, it is unlikely that a quiescent phase would be as short as ~30 years when such phases are 50 to 100 years in duration on Svalbard (Dowdeswell et al., 1991).

6.3.3 Characteristics

Surge-type glaciers are typically characterised by an imbalance whereby they are not able to efficiently regulate mass, resulting in a surge/quiescent cycle (Sevestre & Benn, 2015; Benn et al., 2019). Glacier length and slope appear to be the key differentiators between surge-type and non-surge-type glaciers, with surge-type glaciers in cold-dry climates (e.g., Arctic Canada, NZ, SZ) most likely to be longer with shallower slope angles (Clarke et al., 1986; Jiskoot et al., 1998; Grant et al., 2009; Sevestre & Benn, 2015). The results show that surging on SZ is mainly restricted to long outlet glaciers descending from larger ice caps, notably around Mount Karpinsky, the highest point on SZ (Fig. 5.8). Marine and lake terminating glaciers are most likely to surge on SZ and account for 65% of glaciers classified as potential surge-type. However, the number of marine-terminating surge-type glaciers may be underestimated due to the absence of bathymetric datasets, hence the inability to identify surge-diagnostic landform evidence around SZ.

It is assumed that surge-type glaciers on SZ are characterised by a longer quiescent and active surging phase than glaciers in warmer climates with higher rates of precipitation. The observation of active surging on glacier 105 occurred for ~24 years between 1986 to 2010. Additionally, the surge of the Vavilov ice cap has continued for >10 years post-destabilisation in 2011, whereas the active phase of surge-type glaciers on Svalbard is typically 3-10 yrs. If these advances are due to surging, as assumed, the active phase duration may be similar to glaciers in the cold, dry Canadian High Arctic, where the active phase has exceeded 40-50 years for some glaciers (Copland et al., 2003). Despite the fact that surging has not been observed enough to accurately constrain the duration of the active and quiescent phases, it can be assumed that the duration required for replenishing the mass to enable surging would take longer than in areas with higher rates of precipitation (e.g., Svalbard and Alaska). Thus, it is suggested that surging occurs less frequently on SZ than in areas westward towards the Barents Sea, where rates of precipitation are higher.

6.3.4 Mechanisms

The protocol used in this study classifies Basin A of the AoSIC as likely of surge-type, concurring with the previous proposals of Moholdt et al. (2012b) and Sánchez-Gámez et al. (2019). The basin has undergone surge-like patterns of surface elevation change and has been advancing on the northern margin of its terminus at each timestamp post-1965. The advance of

Basin A is of a very low magnitude compared to the Vavilov surge, and it has been suggested to have an inefficient subglacial drainage system (Nela et al., 2019). Its drainage system has likely led to low-pressure sub-glacial conditions and slow basal ice movement, providing a mechanism for its low-magnitude advance. As most observations of surge-type glaciers are of faster flowing, warmer temperate and polythermal glaciers, predominantly in Svalbard, North America and High Mountain Asia (e.g., Fowler et al., 2001; Bhambri et al., 2017), it is unknown whether this advance should be classified as surging due to limited observations of mostly cold-based glacier surging. However, it is important to note here that variable speeds of surging have been identified for colder, polythermal glaciers glaciers (Frappé & Clarke 2007). Therefore, it is suggested that Basin A is likely of surge-type but highlight the need for further investigations on the dynamics of mostly cold-based surge-type glaciers.

Mechanisms of polythermal glacier surging include the thermal switch model, which suggests that increased accumulation during the quiescent phase results in increased driving stresses and creep rates, thereby generating heat and increasing the proportion of warm ice (Fowler et al., 2001; Benn and Evans, 2010). Meltwater production at the bed and the propagation of warm-ice down-glacier then triggers a surge when basal sliding can start (Fowler et al., 2001). This transition from a mostly stable cold-based regime to a rapid surge-like advance was observed at the Vavilov Ice Cap, with high ice flow velocities requiring basal sliding in modelled scenarios (Fig. 5.4H; Willis et al., 2018). Future ice cap instability can be anticipated in cold, dry climates where basal conditions may change more permanently as a result of climatic warming. However, it is acknowledged that identifying ice caps at risk of surge-like behaviour is difficult without clear identifiable criteria. In the case of the Vavilov Ice Cap, it may be unlikely that it will ever regain sufficient mass to surge again. Indeed, it has been suggested that it has now transitioned into an ice stream in that velocity is of a magnitude higher than surrounding glaciers and it efficiently drains mass from the ice cap (Zheng et al., 2019). Nevertheless, should surging become more prevalent under climatic warming it poses a risk to accelerated rates of glacier mass loss and resulting SLR.

6.4 Further Research

Research in the Arctic has historically focused on the GrIS, Svalbard, the Canadian Arctic and, more recently, NZ, in the RHA (see section 2.1). In recent years, interest in SZ has increased,

notably due to the Vavilov surge and the collapse of the large former-MIS, leading to studies focusing on these individual events and the production of an up-to-date assessment of glacier mass balance (see section 2.3.2). Hence, due to the lack of research on SZ numerous avenues for further research have been identified that were outside of the scope of this project and these are now outlined in turn.

6.4.1 Supraglacial lakes

Numerous surface meltwater lakes and streams have been identified during the process of surveying each glacier for surge indicative features (Fig. 6.1). On Komsomolets Island, Basin A of the AoSIC contains large surficial meltwater lakes, which often exceed 1 km in length, interconnected by meltwater streams that can exceed 0.2 km in width (Fig. 6.1A). Similar, but smaller, meltwater lakes and streams exist in high concentration on the northern Karpinsky Ice Cap, on the glaciers formerly feeding the MIS (Fig. 6.1B). Additionally, glacier 105 (southern Karpinsky Ice Cap) formed and drained multiple supraglacial lakes during its active surge phase (Fig. 5.9). All of these glaciers are classified, with varying levels of confidence, as surge-type, yet it is unknown if or how meltwater production and potential surface-to-bed drainage events might be influencing predominantly cold-based glacier surging. However, research has suggested that routing of supraglacial meltwater to the bed of the AoSIC 'ice streams' is unlikely to be the cause of ice flow variability (see section 6.2) as monthly ice flow variability is still observed during winter (Strozzi et al., 2017; Tepes et al., 2021b). Additionally, no correlation was found between summer air temperatures and ice dynamics (Sánchez-Gámez et al., 2019). Thus, alternate mechanisms may be needed to explain glacier ice flow variability.

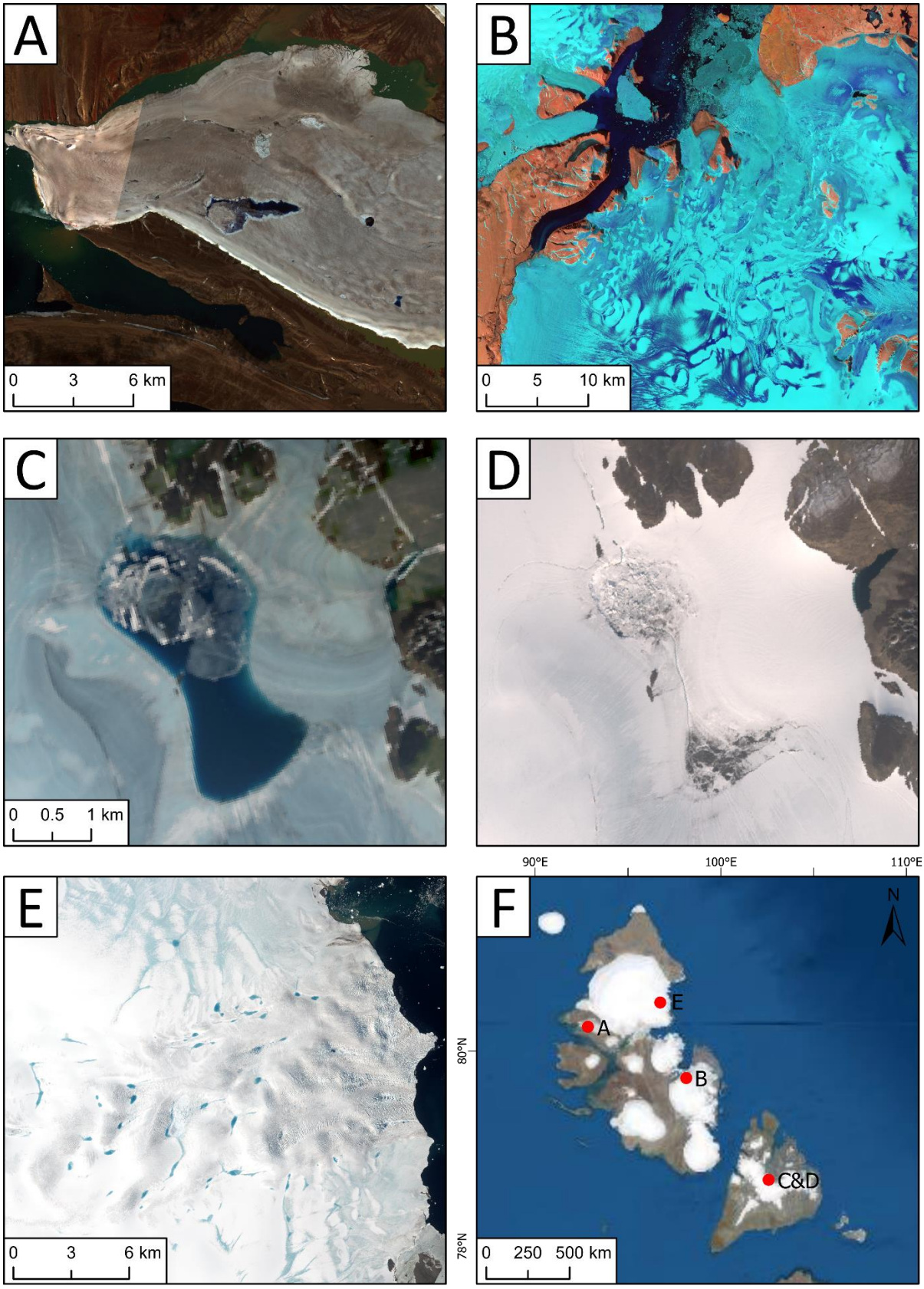

Fig. 6.1. *Supraglacial streams and lakes identified on SZ. (A) Basin A of the AoSIC. Note the large meltwater lakes and streams in 2011 ASTER imagery acquired at the end of the melt season. (B)*

Supraglacial streams surrounding Matusevich Fjord shown in a false colour composite 2021 Sentinel 2A image. (C) A supraglacial lake on the Leningrad Ice Cap on Bolshevik Island in 2019 at the end of the melt season. (D) Drainage of the lake in panel C, shown in 2021 Landsat 8 imagery. (E) Basin C of the AoSIC. Note the presence of numerous small lakes and streams in 2021 Sentinel 2A imagery. (F) The location of panels A-E shown within SZ.

On Bolshevik Island, where surging has not been observed, two large (~1.5 km and 3.5 km) supraglacial meltwater lakes exist and appear to have undergone large fluctuations in volume (Fig. 6.1C-D). Supraglacial lakes on Bolshevik Island have been observed during conducting this thesis as early as 1965 and are not noted in any English language literature. Further research would be beneficial to assess how these lakes have evolved over time as increased lake coverage would reduce surface albedo, accelerating glacier mass loss. Thus, as glacier hydrology is a control on glacier mass loss, it is vital that glacier hydrology on SZ is understood for predicting future rates of SLR contributions.

6.4.2 Bathymetric data

Most surge-type glaciers on SZ identified in this study are marine-terminating. Despite this, there is a bias for classifying land-terminating surge-type glaciers as they contain more surge-indicative features in their forelands. If bathymetric datasets were available, it is probable that even more marine-terminating surge-type glaciers could be identified or the confidence in potential surge-type glaciers could be increased. In Svalbard, high-resolution swath bathymetry was used to establish a landsystem model for tidewater surge-type glaciers (Ottesen and Dowdeswell, 2006; Ottesen et al., 2008; Flink et al., 2015). This provides additional criteria to identify surge-type glaciers and is beneficial for surge-type glacier identification in areas with long quiescent periods and limited long-term observations. Additionally, such datasets could be useful for establishing the maximum extent of the Barents-Kara Ice Sheet during the LGM, which remains disputed on its eastern margins (Svendsen, 2004).

6.4.3 Chronologies of moraine formation

On NZ and FJL, chronologies of moraine formation have been established with neoglacial advances dated to 1300 and 800 yr BP and ca. 1 kyr, respectively, followed by LIA advances

in both regions (see section 3.2). Additionally, both regions are known to have been covered by the Barents-Kara Ice Sheet during the LGM (Svendsen et al., 1999, 2004; Polyak et al., 2008; Hughes et al., 2015). In contrast, as SZ has no established chronology for moraine stabilisation, periods of glacier advance and retreat remain unknown; nor is it known whether the Barents-Kara Ice Sheet did extend to SZ. Oxygen isotope data from a core extracted from the AoSIC suggests that the Medieval Climate Anomaly and the LIA may not have been pronounced on SZ (Opel et al., 2013). However, without a chronology, it is unknown when glaciers on SZ last advanced and how they have responded to climatic perturbations. The best location for dating is suggested to be the terminal moraines on eastern October Revolution Island as they are the best preserved and most accessible. Importantly, establishing a chronology on SZ may help to resolve whether the disputed eastern Barents-Kara Ice Sheet margin did indeed extend to SZ, and if not, what was the style of glaciation during the LGM.

6.4.4 Precipitation data

Further research could benefit from using precipitation data available (albeit with numerous gaps) from Ostrov Golomjannyj and Im.E.K.Fedorova to assess how changes in precipitation (snow and rain) are affecting rates of glacier retreat. Precipitation (snow) is a key component in glacier mass balance and can result in a glacier retreat or advance. Additionally, changes to precipitation can result in an unsteady state if the glacier is no longer able to keep ice discharge and accumulation in equilibrium, resulting in surging. Precipitation can also determine the duration of the quiescent period, as it affects the rate at which mass is acquired for a glacier to surge.

Whilst increasing Arctic temperatures have led to accelerated glacier retreat and sea ice decline, they have also resulted in increased moisture in the atmosphere due to sea ice decline, which has been found to increase precipitation rates in the Arctic by >100% between the 20th and 21st century (Higgins & Cassano, 2009). Increased precipitation has the potential to compensate for the impact of increasing temperatures if precipitation is in sufficient quantity to allow glacier mass balance to remain above or close to zero. However, an increase in rainfall may accelerate glacier melt and decrease the surface albedo (Vihma et al., 2016). Thus, it is important to understand changes in Arctic precipitation in order to accurately predict future scenarios of SLR and glacier mass loss.

6.4.4 Modelling future scenarios

The data provided in this thesis provides the longest-term record of past glacier surface area changes for SZ, but the future evolution of glaciers on SZ remains unknown. There is potential to use modelling, calibrated with the record provided by this thesis, to assess how glaciers will evolve under Representative Concentration Pathways (RCP) emission scenarios (e.g., Hock et al., 2019; Zekollari et al., 2019). This would allow for the identification of potential tipping points and help inform predictions of future SLR. Additionally, as the Arctic-wide trend in declining sea ice has been identified to be a control on retreat rates (see sections 2.1.2.3 and 6.2.2), it may be important to integrate these variables, along with predicted changes to Arctic precipitation patterns (see section 6.4.4). When combined, the data from this thesis and the shorter record of widely available mass balance estimates for SZ (e.g., Moholdt et al., 2012a; Sommer et al., 2022), provides sufficient data to calibrate modelling of future SLR and glacier change scenarios.

Chapter 7: Conclusions

This study has produced the longest (1965 to 2021) digital record of glacier surface area change on SZ to date and contributes to an improved understanding of glacier dynamics in the RHA, specifically in terms of the prevalence of surge-type glaciers. Since 1965, glaciers and ice caps on SZ have undergone substantial surface area loss (-778 km^2, -5%), covering an area of 16,275 ± 69 km^2 in 2021. Spatiotemporal trends show that rates of retreat have not been universal across SZ, with retreat mostly concentrated on southernmost SZ (Bolshevik Island). In contrast, glaciers on northern SZ did not begin to retreat outside of error margins until after 1997. It is evident that climatic warming is having an irreversible impact on glaciers on SZ, judging from the increasing evidence of large-scale cryospheric change (e.g., the collapse of the MIS) and the trend of glacier retreat.

Changes in glacier surface area can be linked to patterns of surface air temperature trends and rising ocean temperatures. Long-term records (1936 to 2021) show that mean annual surface air temperatures have increased by ~2-3 °C and there is evidence of winter warming on both the Taymyr Peninsula (R^2 = 0.02, Im.E.K.Fedorova) and on SZ (R^2 = 0.08, Ostrov Golomjannyj). The high rates of retreat on Bolshevik Island are attributed to evidence of summer atmospheric warming on the proximal Taymyr Peninsula (R^2 = 0.03, Im.E.K.Fedorova), whereas northern SZ has not yet begun to trend towards summer warming. As land-terminating glaciers also retreated further north, albeit to a lesser degree, it is probable that annual and winter atmospheric warming has lengthened the melt season. Whilst oceanic warming has already been identified as a control on glacier retreat on SZ (Tepes et al., 2021b), it is suggested that atmospheric warming may be more influential in driving glacier retreat on SZ than previously thought, especially in the south.

The findings of this study suggest that surging is more common on SZ than previously thought, building upon the previous identification of two potential surge-type glaciers on SZ (Dowdeswell and Williams, 1997). Most glaciers on SZ are non-surge-type, but it is suggested that four glaciers are surge-type (2.1% of glaciers on SZ), seven are probable (3.7%) and nine are possible (4.7%). Surge-type glaciers on SZ occupy large, long, marine- or lake-terminating basins and are primarily concentrated around the Karpinsky Ice Cap. The quiescent phase is assumed to be longer than NZ and Svalbard due to lower rates of precipitation, colder climate and the observation of very few active surge phases between 1965 and 2021 on glaciers confidently classified as surge-type. From the few active phases observed, it can be suggested

that the active phase of surging on SZ is longer than other clusters where this is well constrained, but further observation and monitoring of these glaciers is required.

Under continued amplification of Arctic warming, accelerated rates of glacier mass loss can be anticipated from the RHA. On SZ, the increase in negative precipitation anomalies around northern Bolshevik Island and south-eastern Bolshevik Island is likely to result in increasingly negative glacier mass balance due to an inability to re-gain mass lost to increasing glacier melt. This also has implications for the rate of reservoir build-up required for surge initiation, with a likely decline in surge frequency. However, under continued warming, a transition from mostly cold-based thermal regimes to polythermal is probable, which may result in a change in glacier dynamics on SZ. This regime shift may result in the destabilisation of larger ice caps and increased surge-like behaviour, increasing the rate of sea level rise contributions from the RHA.

References:

Andreev, A.A. and Klimanov, V.A., 2000. Quantitative Holocene climatic reconstruction from Arctic Russia. *Journal of Paleolimnology*, 24(1), pp.81-91.

Asbjørnsen, H., Årthun, M., Skagseth, Ø. and Eldevik, T., 2020. Mechanisms underlying recent arctic atlantification. *Geophysical Research Letters*, 47(15), e2020GL088036.

Bamber, J.L., Oppenheimer, M., Kopp, R.E., Aspinall, W.P. and Cooke, R.M., 2019. Ice sheet contributions to future sea-level rise from structured expert judgment. *Proceedings of the National Academy of Sciences*, 116(23), pp.11195-11200.

Bassford, R.P., Siegert, M.J. and Dowdeswell, J.A., 2006b. Quantifying the mass balance of ice caps on SZ, Russian High Arctic. II: Modeling the flow of the Vavilov Ice Cap under the present climate. *Arctic, Antarctic, and Alpine Research*, 38(1), pp.13-20.

Bassford, R.P., Siegert, M.J. and Dowdeswell, J.A., 2006c. Quantifying the mass balance of ice caps on SZ, Russian High Arctic. III: Sensitivity of ice caps in SZ to future climate change. *Arctic, Antarctic, and Alpine Research*, 38(1), pp.21-33.

Bassford, R.P., Siegert, M.J., Dowdeswell, J.A., Oerlemans, J., Glazovsky, A.F. and Macheret, Y.Y., 2006a. Quantifying the mass balance of ice caps on SZ, Russian High Arctic. I: Climate and mass balance of the Vavilov Ice Cap. *Arctic, Antarctic, and Alpine Research*, 38(1), pp.1-12.

Benn, D.I. and Evans, D.J.A. 2010. *Glaciers and Glaciation*. Hodder, London.

Benn, D.I., Fowler, A.C., Hewitt, I. and Sevestre, H., 2019. A general theory of glacier surges. *Journal of Glaciology*, 65(253), pp.701-716.

Bevan, S.L., Luckman, A.J., Benn, D.I., Cowton, T. and Todd, J., 2019. Impact of warming shelf waters on ice mélange and terminus retreat at a large SE Greenland glacier. *The Cryosphere*, 13(9), pp.2303-2315.

Bhambri, R., Hewitt, K., Kawishwar, P. and Pratap, B., 2017. Surge-type and surge-modified glaciers in the Karakoram. *Scientific reports*, 7(1), pp.1-14.

Brynjolfsson, S., Ingólfsson, Ó. and Schomacker, A., 2012. Surge fingerprinting of cirque glaciers at the Tröllaskagi peninsula, North Iceland. *Jökull*, 62, pp.151-166.

Carr, J.R., Bell, H., Killick, R. and Holt, T., 2017b. Exceptional retreat of Novaya Zemlya's marine-terminating outlet glaciers between 2000 and 2013. *The Cryosphere*, 11(5), pp.2149-2174.

Carr, J.R., Stokes, C.R and Vieli, A., 2014. Recent retreat of major outlet glaciers on Novaya Zemlya, Russian Arctic, influenced by fjord geometry and sea-ice conditions. *Journal of Glaciology*, 60(219), pp.155-170.

Carr, J.R., Stokes, C.R. and Vieli, A., 2017a. Threefold increase in marine-terminating outlet glacier retreat rates across the Atlantic Arctic: 1992–2010. *Annals of Glaciology*, 58(74), pp.72-91.

Carr, J.R., Vieli, A. and Stokes, C., 2013. Influence of sea ice decline, atmospheric warming, and glacier width on marine-terminating outlet glacier behaviour in northwest Greenland at seasonal to interannual timescales. *Journal of Geophysical Research: Earth Surface*, 118(3), pp.1210-1226.

Carvalho, K.S. and Wang, S., 2020. Sea surface temperature variability in the Arctic Ocean and its marginal seas in a changing climate: Patterns and mechanisms. *Global and Planetary Change*, 193, 103265.

Catalogue of Glaciers of the USSR (Katalog lednitov USSR), 1965-82. *Leningrad: Gidrometeoizdat*, Volume 1-69. (in Russian).

Cherezova, A.A., Fedorov, G.B., Raschke, E.A., Rethemeyer, J., Bolshiyanov, D.Y., Yozhikov, I.S., Spiridonov, I.G., Bazhenova, E.A., Sokolov, V.T. and Melles, M., 2020. Lateglacial and Holocene palaeoenvironments on Bolshevik Island (Severnaya Zemlya), Russian High Arctic. *Boreas*, 49(2), pp.375-388.

Chernov, R.A. and Muraviev, A.Y., 2020. Catastrophic outburst-flood of the Spartakovskoye glacier-dammed lake on the Bolshevik Island (Severnaya Zemlya). *Earth's Cryosphere*, 24(4), pp.50-59.

Ciracì, E., Velicogna, I. and Sutterley, T.C., 2018. Mass balance of Novaya Zemlya archipelago, Russian High Arctic, using time-variable gravity from grace and altimetry data from ICESat and Cryosat-2. Remote Sensing, 10(11), p.1817.

Ciracì, E., Velicogna, I. and Swenson, S., 2020. Continuity of the mass loss of the world's glaciers and ice caps from the GRACE and GRACE Follow-On missions. *Geophysical Research Letters*, 47*(9)*, 2019GL086926.

Clarke, G.K.C., Schmok, J.P., Ommanney, C.S.L. and Collins, S.G., 1986. Characteristics of surge-type glaciers. *Journal of Geophysical Research: Solid Earth*, 91(B7), pp.7165-7180.

Cook, A.J., Copland, L., Noël, B.P., Stokes, C.R., Bentley, M.J., Sharp, M.J., Bingham, R.G. and van den Broeke, M.R., 2019. Atmospheric forcing of rapid marine-terminating glacier retreat in the Canadian Arctic Archipelago. *Science Advances*, 5(3), eaau8507.

Copland, L., Sharp, M.J. and Dowdeswell, J.A., 2003. The distribution and flow characteristics of surge-type glaciers in the Canadian High Arctic. *Annals of Glaciology*, 36, pp.73-81.

Cullather, R.I., Andrews, L.C., Croteau, M.J., Digirolamo, N.E., Hall, D.K., Lim, Y.K., Loomis, B.D., Shuman, C.A. and Nowicki, S.M., 2020. Anomalous circulation in July 2019 resulting in mass loss on the Greenland Ice Sheet. *Geophysical Research Letters*, 47(17), e2020GL087263.

DeBeer, C.M. and Sharp, M.J., 2007. Recent changes in glacier area and volume within the southern Canadian Cordillera. *Annals of glaciology*, 46, pp.215-221.

Dowdeswell, J.A., Hamilton, G.S. and Hagen, J.O., 1991. The duration of the active phase on surge-type glaciers: contrasts between Svalbard and other regions. *Journal of Glaciology*, 37(127), pp.388-400.

Dowdeswell, J.A. and Williams, M., 1997. Surge-type glaciers in the Russian High Arctic identified from digital satellite imagery. *Journal of Glaciology*, 43(145), pp.489-494.

Dowdeswell, J.A., Hagen, J.O., Björnsson, H., Glazovsky, A.F., Harrison, W.D., Holmlund, P., Jania, J., Koerner, R.M., Lefauconnier, B., Ommanney, C.S.L. and Thomas, R.H., 1997. The mass balance of circum-Arctic glaciers and recent climate change. *Quaternary research*, 48(1), pp.1-14.

Dowdeswell, J.A., Bassford, R.P., Gorman, M.R., Williams, M., Glazovsky, A.F., Macheret, Y.Y., Shepherd, A.P., Vasilenko, Y.V., Savatyuguin, L.M., Hubberten, H.W. and Miller, H., 2002. Form and flow of the Academy of Sciences Ice Cap, SZ, Russian High Arctic. *Journal of Geophysical Research: Solid Earth*, 107(B4), EPM-5.

Dowdeswell, J.A. and Ottesen, D., 2016. Eskers formed at the beds of modern surge-type tidewater glaciers in Spitsbergen. *Geological Society, London, Memoirs*, 46(1), pp.83-84.

Dowdeswell, J.A., 2017. Eurasian Arctic ice shelves and tidewater ice margins. In *Arctic ice shelves and ice islands* (pp. 55-74). Springer, Dordrecht.

Dunse, T., Greve, R., Schuler, T.V. and Hagen, J.O., 2011. Permanent fast flow versus cyclic surge behaviour: numerical simulations of the Austfonna ice cap, Svalbard. *Journal of Glaciology*, 57(202), pp.247-259.

Edwards, T.L., Nowicki, S., Marzeion, B., Hock, R., Goelzer, H., Seroussi, H., Jourdain, N.C., Slater, D.A., Turner, F.E., Smith, C.J. and McKenna, C.M., 2021. Projected land ice contributions to twenty-first-century sea level rise. *Nature*, 593(7857), pp.74-82.

Eisen, O., Harrison, W. & Raymond, C., 2001. The surges of Variegated Glacier, Alaska, U.S.A., and their connection to climate and mass balance. *Journal of Glaciology*, 47(158), pp. 351-358.

Evans, D.J.A and Rea, B.R., 1999. Geomorphology and sedimentology of surging glaciers: a land-systems approach. *Annals of Glaciology*, 28, pp.75-82.

Evans, D.J.A and Rea, B.R., 2003. Surging glacier landsystem. In: Evans, D.J.A. (ed.), *Glacial Landsystems*. Arnold, London, pp. 259-288.

Evans, D.J.A, 2009. Controlled moraines: origins, characteristics and palaeoglaciological implications. *Quaternary Science Reviews*, 28(3-4), pp.183-208.

Evans, D.J.A, Twigg, D.R., Rea, B.R. and Shand, M., 2007. Surficial geology and geomorphology of the Brúarjökull surging glacier landsystem. *Journal of Maps*, 3(1), pp.349-367.

Evans, D.J.A. and England, J. 1991. Canadian Landform Examples - 19: High arctic thrust block moraines**.** *Canadian Geographer*, 35, pp. 93-97.

Evans, D.J.A. and England, J. 1992. Geomorphological evidence of Holocene climatic change from northwest Ellesmere Island, Canadian high arctic. *The Holocene*, 2, pp.148-158.

Evans, D.J.A, Storrar, R.D. and Rea, B.R., 2016. Crevasse-squeeze ridge corridors: diagnostic features of late-stage palaeo-ice stream activity. *Geomorphology*, 258, pp.40-50.

Farnsworth, W.R., Ingólfsson, Ó., Retelle, M. and Schomacker, A., 2016. Over 400 previously undocumented Svalbard surge-type glaciers identified. *Geomorphology*, 264, pp.52-60.

Fitzsimons, S.J., 1996. Formation of thrust-block moraines at the margins of dry-based glaciers, south Victoria Land, Antarctica. *Annals of Glaciology*, 22, pp.68-74.

Fitzsimons, S.J. 1997. Glaciotectonic deformation of glaciomarine sediments and formation of thrust block moraines at the margin of an outlet glacier, Vestfold Hills, East Antarctica. *Earth Surface Processes and Landforms*, 22, pp.175-187.

Fitzsimons, S.J. 2003. Ice-marginal terrestrial landsystems: polar continental glacier margins. In: Evans, D.J.A. (ed.), *Glacial Landsystems*. Arnold, London, pp. 89-110.

Flink, A.E., Noormets, R., Kirchner, N., Benn, D.I., Luckman, A. and Lovell, H., 2015. The evolution of a submarine landform record following recent and multiple surges of Tunabreen glacier, Svalbard. *Quaternary Science Reviews*, 108, pp.37-50.

Forman, S.L., Lubinski, D.J., Zeeburg, J.J., Polyak, L., Miller, G.H., Matishov, G. and Tarasov, G., 1999. Postglacial emergence and late Quaternary glaciation on northern Novaya Zemlya, Arctic Russia. *Boreas*, 28(1), pp.133-145.

Fowler, A., 1987. A theory of glacier surges. *Journal of Geophysical Research: Solid Earth*, 92(B9), pp. 9111-9120.

Fowler, A.C., Murray, T. and Ng, F.S.L., 2001. Thermally controlled glacier surging. *Journal of Glaciology*, 47(159), pp.527-538.

Frappé, T.P. and Clarke, G.K., 2007. Slow surge of Trapridge Glacier, Yukon Territory, Canada. *Journal of Geophysical Research: Earth Surface*, 112(F3).

Gardner, A.S., Moholdt, G., Cogley, J.G., Wouters, B., Arendt, A.A., Wahr, J., Berthier, E., Hock, R., Pfeffer, W.T., Kaser, G. and Ligtenberg, S.R., 2013. A reconciled estimate of glacier contributions to sea level rise: 2003 to 2009. *science*, 340(6134), pp.852-857.

Geyman, E.C., JJ van Pelt, W., Maloof, A.C., Aas, H.F. and Kohler, J., 2022. Historical glacier change on Svalbard predicts doubling of mass loss by 2100. *Nature*, 601(7893), pp.374-379.

Glazovsky, A., Bushueva, I. and Nosenko, G., 2015, March. Slow 'surge' of the Vavilov Ice Cap, SZ. In *Proceedings of the IASC Workshop on the Dynamics and Mass Balance of Arctic Glaciers, Obergurgl, Austria*, pp.23-25.

Gong, Y., Zwinger, T., Åström, J., Altena, B., Schellenberger, T., Gladstone, R. and Moore, J.C., 2018. Simulating the roles of crevasse routing of surface water and basal friction

on the surge evolution of Basin 3, Austfonna ice cap. *The Cryosphere*, 12(5), pp.1563-1577.

Govorukha, L.S., Bol'shiyanov, D.Y., Zarkhidze, V.S., Pinchuk, L.Y. and Yunak, R.I., 1987. Changes in the glacier cover of Severnaya Zemlya in the twentieth century. *Polar Geography*, 11(4), pp.300-305.

Grant, K.L., Stokes, C.R. and Evans, I.S., 2009. Identification and characteristics of surge-type glaciers on Novaya Zemlya, Russian Arctic. *Journal of Glaciology*, 55(194), pp.960-972.

Grosval'd, M.G. and Kotlyakov, V.M., 1969. Present-day glaciers in the USSR and some data on their mass balance. *Journal of Glaciology*, 8(52), pp.9-22.

Hambrey, M.J., Huddart, D., Bennett, M.R. and Glasser, N.F., 1997. Genesis of 'hummocky moraines' by thrusting in glacier ice: evidence from Svalbard and Britain. *Journal of the Geological Society*, 154(4), pp.623-632.

Hamilton, G. & Dowdeswell, J., 1996. Controls on glacier surging in Svalbard. *Journal of Glaciology*, 42(140), pp. 157-168.

Hanna, E., Mernild, S.H., Cappelen, J. and Steffen, K., 2012. Recent warming in Greenland in a long-term instrumental (1881–2012) climatic context: I. Evaluation of surface air temperature records. *Environmental Research Letters*, 7(4), p.045404.

Hewitt, K., 2007. Tributary glacier surges: an exceptional concentration at Panmah Glacier, Karakoram Himalaya. *Journal of Glaciology*, 53(181), pp.181-188.

Higgins, M.E. and Cassano, J.J., 2009. Impacts of reduced sea ice on winter Arctic atmospheric circulation, precipitation, and temperature. *Journal of Geophysical Research: Atmospheres*, 114(D16).

Hock, R., Bliss, A., Marzeion, B.E.N., Giesen, R.H., Hirabayashi, Y., Huss, M., Radić, V. and Slangen, A.B., 2019. GlacierMIP–A model intercomparison of global-scale glacier mass-balance models and projections. *Journal of Glaciology*, 65(251), pp.453-467.

Holmes, F.A., Kirchner, N., Kuttenkeuler, J., Krützfeldt, J. and Noormets, R., 2019. Relating ocean temperatures to frontal ablation rates at Svalbard tidewater glaciers: Insights from glacier proximal datasets. *Scientific reports*, 9(1), pp.1-11.

Howat, I.M., Joughin, I., Fahnestock, M., Smith, B.E. and Scambos, T.A., 2008. Synchronous retreat and acceleration of southeast Greenland outlet glaciers 2000–06: ice dynamics and coupling to climate. *Journal of Glaciology*, 54(187), pp.646-660.

Hubberten, H.W., Andreev, A., Astakhov, V.I., Demidov, I., Dowdeswell, J.A., Henriksen, M., Hjort, C., Houmark-Nielsen, M., Jakobsson, M., Kuzmina, S. and Larsen, E., 2004. The periglacial climate and environment in northern Eurasia during the Last Glaciation. *Quaternary Science Reviews*, 23(11-13), pp.1333-1357.

Hugonnet, R., McNabb, R., Berthier, E., Menounos, B., Nuth, C., Girod, L., Farinotti, D., Huss, M., Dussaillant, I., Brun, F. and Kääb, A., 2021. Accelerated global glacier mass loss in the early twenty-first century. *Nature*, *592*(7856), pp.726-731.

Humphrey, N.F. and Raymond, C.F., 1994. Hydrology, erosion and sediment production in a surging glacier: Variegated Glacier, Alaska, 1982–83. *Journal of Glaciology*, 40(136), pp.539-552.

Ingólfsson, Ó., Benediktsson, Í.Ö., Schomacker, A., Kjær, K.H., Brynjólfsson, S., Jónsson, S.A., Korsgaard, N.J. and Johnson, M.D., 2016. Glacial geological studies of surge-type glaciers in Iceland—Research status and future challenges. *Earth-Science Reviews*, 152, pp.37-69.

IPCC, 2022. Climate Change 2022: Impacts, Adaptation, and Vulnerability. Contribution of Working Group II to the Sixth Assessment Report of the Intergovernmental Panel on Climate Change [H.-O. Pörtner, D.C. Roberts, M. Tignor, E.S. Poloczanska, K. Mintenbeck, A. Alegría, M. Craig, S. Langsdorf, S. Löschke, V. Möller, A. Okem, B. Rama (eds.)]. Cambridge University Press. In Press.

Jiskoot, H., Boyle, P. and Murray, T., 1998. The incidence of glacier surging in Svalbard: evidence from multivariate statistics. *Computers & Geosciences*, 24(4), pp.387-399.

Jiskoot, H., Murray, T. & Boyle, P., 2000. Controls on the distribution of surge-type glaciers in Svalbard. *Journal of Glaciology*, 46(154), pp. 412-422.

Kalnay, E., Kanamitsu, M., Kistler, R., Collins, W., Deaven, D., Gandin, L., Iredell, M., Saha, S., White, G., Woollen, J. and Zhu, Y., 1996. The NCEP/NCAR 40-year reanalysis project. *Bulletin of the American meteorological Society*, 77(3), pp.437-472.

Kamb, B., 1987. Glacier surge mechanism based on linked cavity configuration of the basal water conduit system. *Journal of Geophysical Research: Solid Earth*, 92(B9), pp. 9083-9100.

Kamb, B., Raymond, C.F., Harrison, W.D., Engelhardt, H., Echelmeyer, K.A., Humphrey, N., Brugman, M.M. and Pfeffer, T., 1985. Glacier surge mechanism: 1982-1983 surge of Variegated Glacier, Alaska. *Science*, 227(4686), pp.469-479.

Khromova, T., Nosenko, G., Kutuzov, S., Muraviev, A. and Chernova, L., 2014. Glacier area changes in Northern Eurasia. *Environmental Research Letters*, 9(1), 015003.

Kochtitzky, W., Winski, D., McConnell, E., Kreutz, K., Campbell, S., Enderlin, E.M., Copland, L., Williamson, S., Main, B. and Jiskoot, H., 2020. Climate and surging of Donjek glacier, Yukon, Canada. *Arctic, Antarctic, and Alpine Research*, 52(1), pp.264-280.

Kim, K.Y., Hamlington, B.D., Na, H. and Kim, J., 2016. Mechanism of seasonal Arctic sea ice evolution and Arctic amplification. *The Cryosphere*, 10(5), pp.2191-2202.

Lawson, W., 1996. Structural evolution of variegated Glacier, Alaska, USA, since 1948. *Journal of Glaciology*, 42(141), pp.261-270.

Leigh, J.R., Stokes, C.R., Carr, R.J., Evans, I.S., Andreassen, L.M. and Evans, D.J.A., 2019. Identifying and mapping very small (< 0.5 km^2) mountain glaciers on coarse to high-resolution imagery. *Journal of Glaciology*, 65(254), pp.873-888.

Lingle, C. & Fatland, D., 2003. Does englacial water storage drive temperate glacier surges?. *Annals of Glaciology*, 36, pp. 14-20.

Lovell, H. and Boston, C.M., 2017. Glacitectonic composite ridge systems and surge-type glaciers: an updated correlation based on Svalbard, Norway. *arktos*, 3(1), pp.1-16.

Lubinski, D.J., Forman, S.L. and Miller, G.H., 1999. Holocene glacier and climate fluctuations on Franz Josef Land, Arctic Russia, 80 N. *Quaternary Science Reviews*, 18(1), pp.85-108.

Luckman, A., Benn, D.I., Cottier, F., Bevan, S., Nilsen, F. and Inall, M., 2015. Calving rates at tidewater glaciers vary strongly with ocean temperature. *Nature communications*, 6(1), pp.1-7.

Luo, B., Wu, L., Luo, D., Dai, A. and Simmonds, I., 2019. The winter midlatitude-Arctic interaction: effects of North Atlantic SST and high-latitude blocking on Arctic sea ice and Eurasian cooling. *Climate dynamics*, 52(5), pp.2981-3004.

Luo, D., Xiao, Y., Yao, Y., Dai, A., Simmonds, I. and Franzke, C.L., 2016. Impact of Ural blocking on winter warm Arctic–cold Eurasian anomalies. Part I: Blocking-induced amplification. *Journal of Climate*, 29(11), pp.3925-3947.

Małecki, J., Faucherre, S. and Strzelecki, M., 2013. Post− surge geometry and thermal structure of Hørbyebreen, central Spitsbergen. *Polish Polar Research*, 34(3), pp.305-321.

Matsuo, K. and Heki, K., 2013. Current ice loss in small glacier systems of the Arctic Islands (Iceland, Svalbard, and the Russian High Arctic) from satellite gravimetry. *Terrestrial, Atmospheric and Oceanic Sciences*, 24(4-1), pp.657-670.

Meier, M.F. and Post, A., 1969. What are glacier surges?. *Canadian Journal of Earth Sciences*, 6(4), pp.807-817.

Mengel, M., Levermann, A., Frieler, K., Robinson, A., Marzeion, B. and Winkelmann, R., 2016. Future sea level rise constrained by observations and long-term commitment. *Proceedings of the National Academy of Sciences*, 113(10), pp.2597-2602.

Meredith, M., M. Sommerkorn, S. Cassotta, C. Derksen, A. Ekaykin, A. Hollowed, G. Kofinas, A. Mackintosh, J. Melbourne-Thomas, M.M.C. Muelbert, G. Ottersen, H. Pritchard, and E.A.G. Schuur., 2019. Polar Regions. In: IPCC Special Report on the Ocean and Cryosphere in a Changing Climate [H.-O. Pörtner, D.C. Roberts, V. Masson-Delmotte, P. Zhai, M. Tignor, E. Poloczanska, K. Mintenbeck, A. Alegría, M. Nicolai, A. Okem, J. Petzold, B. Rama, N.M. Weyer (eds.)]. Cambridge University Press, Cambridge, UK and New York, NY, USA, pp. 203–320. https://doi.org/10.1017/9781009157964.005.

Moholdt, G., Heid, T., Benham, T. and Dowdeswell, J.A., 2012b. Dynamic instability of marine-terminating glacier basins of Academy of Sciences Ice Cap, Russian High Arctic. *Annals of Glaciology*, 53(60), pp.193-201.

Moholdt, G., Wouters, B. and Gardner, A.S., 2012a. Recent mass changes of glaciers in the Russian High Arctic. *Geophysical Research Letters*, 39(10).

Möller, M. and Kohler, J., 2018. Differing climatic mass balance evolution across Svalbard glacier regions over 1900–2010. *Frontiers in Earth Science*, 6, p.128.

Moon, T., Ahlstrøm, A., Goelzer, H., Lipscomb, W. and Nowicki, S., 2018. Rising oceans guaranteed: Arctic land ice loss and sea level rise. *Current climate change reports*, 4(3), pp.211-222.

Moon, T., Joughin, I. and Smith, B., 2015. Seasonal to multiyear variability of glacier surface velocity, terminus position, and sea ice/ice mélange in northwest Greenland. *Journal of Geophysical Research: Earth Surface*, 120(5), pp.818-833.

Murray, T., Dowdeswell, J.A., Drewry, D.J. and Frearson, I., 1998. Geometric evolution and ice dynamics during a surge of Bakaninbreen, Svalbard. *Journal of Glaciology*, 44(147), pp.263-272.

Nela, B.R., Bandyopadhyay, D., Singh, G., Glazovsky, A.F., Lavrentiev, I.I., Kromova, T.E. and Arigony-Neto, J., 2019. Glacier flow dynamics of the Severnaya Zemlya archipelago in Russian high arctic using the differential SAR interferometry (DInSAR) technique. *Water*, 11(12), p.2466.

Niessen, F., Hong, J.K., Hegewald, A., Matthiessen, J., Stein, R., Kim, H., Kim, S., Jensen, L., Jokat, W., Nam, S.I. and Kang, S.H., 2013. Repeated Pleistocene glaciation of the East Siberian continental margin. *Nature Geoscience*, 6(10), pp.842-846.

Noël, B., Van De Berg, W.J., Lhermitte, S., Wouters, B., Schaffer, N. and van den Broeke, M.R., 2018. Six decades of glacial mass loss in the Canadian Arctic Archipelago. *Journal of Geophysical Research: Earth Surface*, 123(6), pp.1430-1449.

Nordli, Ø., Przybylak, R., Ogilvie, A.E. and Isaksen, K., 2014. Long-term temperature trends and variability on Spitsbergen: the extended Svalbard Airport temperature series, 1898–2012. *Polar research*, 33(1), p.21349.

Ó Cofaigh, C., Evans, D.J.A. and England, J. 2003. Ice marginal terrestrial landsystems: sub-polar glacier margins of the Canadian and Greenland high arctic. In: Evans D.J.A. (ed.), *Glacial Landsystems*. Arnold, London, pp. 44-64.

Ó Cofaigh, C., Lemmen, D.S., Evans, D.J.A. and Bednarski J. 1999. Glacial landform-sediment assemblages in the Canadian high arctic and their implications for late Quaternary glaciation. *Annals of Glaciology*, 28, 195-201.

Oerlemans, J., Bassford, R.P., Chapman, W., Dowdeswell, J.A., Glazovsky, A.F., Hagen, J.O., Melvold, K., de Wildt, M.D.R. and Van de Wal, R.S.W., 2005. Estimating the contribution of Arctic glaciers to sea-level change in the next 100 years. *Annals of Glaciology*, 42, pp.230-236.

Onarheim, I.H., Eldevik, T., Smedsrud, L.H. and Stroeve, J.C., 2018. Seasonal and regional manifestation of Arctic sea ice loss. *Journal of Climate*, 31(12), pp.4917-4932.

Opel, T., Fritzsche, D. and Meyer, H., 2013. Eurasian Arctic climate over the past millennium as recorded in the Akademii Nauk ice core (SZ). *Climate of the Past*, 9(5), pp.2379-2389.

Ottesen, D. and Dowdeswell, J.A., 2006. Assemblages of submarine landforms produced by tidewater glaciers in Svalbard. *Journal of Geophysical Research: Earth Surface*, 111(F1).

Ottesen, D., Dowdeswell, J.A., Benn, D.I., Kristensen, L., Christiansen, H.H., Christensen, O., Hansen, L., Lebesbye, E., Forwick, M. and Vorren, T.O., 2008. Submarine landforms characteristic of glacier surges in two Spitsbergen fjords. *Quaternary Science Reviews*, 27(15-16), pp.1583-1599.

Ottesen, D., Dowdeswell, J.A., Bellec, V.K. and Bjarnadóttir, L.R., 2017. The geomorphic imprint of glacier surges into open-marine waters: examples from eastern Svalbard. *Marine Geology*, 392, pp.1-29.

Paul, F., 2015. Revealing glacier flow and surge dynamics from animated satellite image sequences: examples from the Karakoram. *The Cryosphere*, 9(6), pp.2201-2214.

Pfeffer, W.T., Arendt, A.A., Bliss, A., Bolch, T., Cogley, J.G., Gardner, A.S., Hagen, J.O., Hock, R., Kaser, G., Kienholz, C. and Miles, E.S., 2014. The Randolph Glacier Inventory: a globally complete inventory of glaciers. *Journal of glaciology*, 60(221), pp.537-552.

Polyak, L., Niessen, F., Gataullin, V. and Gainanov, V., 2008. The eastern extent of the Barents–Kara ice sheet during the Last Glacial Maximum based on seismic-reflection data from the eastern Kara Sea. *Polar Research*, 27(2), pp.162-172.

Polyakov, I.V., Pnyushkov, A.V., Alkire, M.B., Ashik, I.M., Baumann, T.M., Carmack, E.C., Goszczko, I., Guthrie, J., Ivanov, V.V., Kanzow, T. and Krishfield, R., 2017. Greater role for Atlantic inflows on sea-ice loss in the Eurasian Basin of the Arctic Ocean. *Science*, 356(6335), pp.285-291.

Quincey, D.J., Braun, M., Glasser, N.F., Bishop, M.P., Hewitt, K. and Luckman, A., 2011. Karakoram glacier surge dynamics. *Geophysical Research Letters*, 38(18).

Raab, A., Melles, M., Berger, G.W., Hagedorn, B. and Hubberten, H.W., 2003. Non-glacial paleoenvironments and the extent of Weichselian ice sheets on SZ, Russian High Arctic. *Quaternary Science Reviews*, 22(21-22), pp.2267-2283.

Raymond, C., 1987. How do glaciers surge? A review. *Journal of Geophysical Research: Solid Earth*, 92(B9), pp. 9121-9134.

Reeh, N., Thomsen, H.H., Higgins, A.K. and Weidick, A., 2001. Sea ice and the stability of north and northeast Greenland floating glaciers. *Annals of Glaciology*, 33, pp.474-480.

Rea, B.R. and Evans, D.J.A, 2011. An assessment of surge-induced crevassing and the formation of crevasse squeeze ridges. *Journal of Geophysical Research: Earth Surface*, 116(F4).

RGI Consortium, 2017. Randolph Glacier Inventory - A Dataset of Global Glacier Outlines, Version 6. Boulder, Colorado USA. NSIDC: National Snow and Ice Data Center. doi: https://doi.org/10.7265/4m1f-gd79

Roberts, D.H., Yde, J.C., Knudsen, N.T., Long, A.J. and Lloyd, J.M., 2009. Ice marginal dynamics during surge activity, Kuannersuit Glacier, Disko Island, West Greenland. *Quaternary Science Reviews*, 28(3-4), pp.209-222.

Rodrigues, J., 2008. The rapid decline of the sea ice in the Russian Arctic. *Cold Regions Science and Technology*, 54(2), pp.124-142.

Sánchez-Gámez P., Navarro F.J., Dowdeswell J.A., De Andrés E., 2020. Surface velocities and calving flux of the Academy of Sciences Ice Cap, SZ. *Ice and Snow*. 2020, 60(1). pp.19-28.

Sánchez-Gámez, P., Navarro, F.J., Benham, T.J., Glazovsky, A.F., Bassford, R.P. and Dowdeswell, J.A., 2019. Intra-and inter-annual variability in dynamic discharge from the Academy of Sciences Ice Cap, SZ, Russian Arctic, and its role in modulating mass balance. *Journal of Glaciology*, 65(253), pp.780-797.

Schaefer, K., Lantuit, H., Romanovsky, V.E., Schuur, E.A. and Witt, R., 2014. The impact of the permafrost carbon feedback on global climate. *Environmental Research Letters*, 9(8), 085003.

Schomacker, A., Benediktsson, Í.Ö. and Ingólfsson, Ó., 2014. The Eyjabakkajökull glacial landsystem, Iceland: geomorphic impact of multiple surges. *Geomorphology*, 218, pp.98-107.

Screen, J.A. and Williamson, D., 2017. Ice-free Arctic at 1.5° C?. *Nature Climate Change*, 7(4), pp.230-231.

Sevestre, H. and Benn, D.I., 2015. Climatic and geometric controls on the global distribution of surge-type glaciers: implications for a unifying model of surging. *Journal of Glaciology*, 61(228), pp.646-662.

Sevestre, H., Benn, D.I., Hulton, N.R. and Bælum, K., 2015. Thermal structure of Svalbard glaciers and implications for thermal switch models of glacier surging. *Journal of Geophysical Research: Earth Surface*, 120(10), pp.2220-2236.

Sharov, A., Nikolskiy, D., Troshko, K. and Zaprudnova, Z., 2015, May. Interferometric control for mapping and quantifying the 2012 breakup of Matusevich Ice Shelf, Severnaya Zemlya. In *Proc. of the International Workshop Fringe*.

Sharov, A.I. and Tyukavina, A.Y., 2009, November. Mapping and interpreting glacier changes in SZ with the aid of differential interferometry and altimetry. In *Proc. of the International Workshop 'Fringe 2009 Workshop', Frascati, Italy* (Vol. 30).

Sharp, M., 1988. Surging glaciers: geomorphic effects. *Progress in Physical Geography*, 12(4), pp.533-559.

Smith, A.M., Murray, T., Davison, B.M., Clough, A.F., Woodward, J. and Jiskoot, H., 2002. Late surge glacial conditions on Bakaninbreen, Svalbard, and implications for surge termination. *Journal of Geophysical Research: Solid Earth*, 107(B8), ESE-1.

Sommer, C., Seehaus, T., Glazovsky, A. and Braun, M.H., 2022. Brief communication: Increased glacier mass loss in the Russian High Arctic (2010–2017). *The Cryosphere*, 16(1), pp.35-42.

Stroeve, J.C., Serreze, M.C., Holland, M.M., Kay, J.E., Malanik, J. and Barrett, A.P., 2012. The Arctic's rapidly shrinking sea ice cover: a research synthesis. *Climatic change*, 110(3), pp.1005-1027.

Strozzi, T., Paul, F., Wiesmann, A., Schellenberger, T. and Kääb, A., 2017. Circum-Arctic changes in the flow of glaciers and ice caps from satellite SAR data between the 1990s and 2017. *Remote Sensing*, 9(9), p.947.

Sun, Z. and Qiao, G., 2021. a Review of Surge-Type Glaciers. *The International Archives of Photogrammetry, Remote Sensing and Spatial Information Sciences*, 43, pp.503-508.

Svendsen, J.I., Astakhov, V.I., Bolshiyanov, D.Y., Demidov, I., Dowdeswell, J.A., Gataullin, V., Hjort, C., Hubberten, H.W., Larsen, E., Mangerud, J.A.N. and Melles, M., 1999. Maximum extent of the Eurasian ice sheets in the Barents and Kara Sea region during the Weichselian. *Boreas*, 28(1), pp.234-242.

Svendsen, J.I., Gataullin, V., Mangerud, J. and Polyak, L., 2004. The glacial history of the Barents and Kara Sea region. *Quaternary glaciations—extent and chronology*, 1, pp.369-378.

Tepes, P., Gourmelen, N., Nienow, P., Tsamados, M., Thherd, A. and Weissgerber, F., 2021a. Changes in elevation and mass of Arctic glaciers and ice caps, 2010–2017. *Remote Sensing of Environment*, 261, p.112481.

Tepes, P., Nienow, P. and Gourmelen, N., 2021b. Accelerating ice mass loss across Arctic Russia in response to atmospheric warming, sea ice decline, and Atlantification of the Eurasian Arctic Shelf Seas. *Journal of Geophysical Research: Earth Surface*, 126(7), e2021JF006068.

The IMBIE Team., 2020. Mass balance of the Greenland Ice Sheet from 1992 to 2018. *Nature*, 579, pp 233-239.

Thøgersen, K., Gilbert, A., Schuler, T.V. and Malthe-Sørenssen, A., 2019. Rate-and-state friction explains glacier surge propagation. *Nature communications*, 10(1), pp.1-8.

Timokhov, L.A., 1994. Regional characteristics of the Laptev and the East Siberian seas: climate, topography, ice phases, thermohaline regime, circulation. *Berichte zur Polarforschung*, 144, pp.15-31.

van Pelt, W.J., Kohler, J., Liston, G.E., Hagen, J.O., Luks, B., Reijmer, C.H. and Pohjola, V.A., 2016. Multidecadal climate and seasonal snow conditions in Svalbard. *Journal of Geophysical Research: Earth Surface*, 121(11), pp.2100-2117.

Van Wijngaarden, W.A., 2015. Temperature trends in the Canadian arctic during 1895-2014. *Theoretical and Applied Climatology*, 120(3), pp.609-615.

Vihma, T., Screen, J., Tjernström, M., Newton, B., Zhang, X., Popova, V., Deser, C., Holland, M. and Prowse, T., 2016. The atmospheric role in the Arctic water cycle: A review on processes, past and future changes, and their impacts. *Journal of Geophysical Research: Biogeosciences*, 121(3), pp.586-620.

Wang, M. and Overland, J.E., 2009. A sea ice free summer Arctic within 30 years?. *Geophysical research letters*, 36(7).

Williams, M. and Dowdeswell, J.A., 2001. Historical fluctuations of the Matusevich ice shelf, Severnaya Zemlya, Russian high Arctic. *Arctic, Antarctic, and Alpine Research*, 33(2), pp.211-222.

Willis, M.J., Melkonian, A.K. and Pritchard, M.E., 2015. Outlet glacier response to the 2012 collapse of the Matusevich Ice Shelf, Severnaya Zemlya, Russian Arctic. *Journal of Geophysical Research: Earth Surface*, 120(10), pp.2040-2055.

Willis, M.J., Zheng, W., Durkin IV, W.J., Pritchard, M.E., Ramage, J.M., Dowdeswell, J.A., Benham, T.J., Bassford, R.P., Stearns, L.A., Glazovsky, A.F. and Macheret, Y.Y., 2018. Massive destabilization of an Arctic ice cap. *Earth and Planetary Science Letters*, 502, pp.146-155.

Wouters, B., Gardner, A.S. and Moholdt, G., 2019. Global glacier mass loss during the GRACE satellite mission (2002-2016). *Frontiers in earth science*, *7*, p.96.

Wunderling, N., Willeit, M., Donges, J.F. and Winkelmann, R., 2020. Global warming due to loss of large ice masses and Arctic summer sea ice. *Nature communications*, 11(1), pp.1-8.

Yadav, J., Kumar, A. and Mohan, R., 2020. Dramatic decline of Arctic sea ice linked to global warming. *Natural Hazards*, 103(2), pp.2617-2621.

Zemp, M., Huss, M., Thibert, E., Eckert, N., McNabb, R., Huber, J., Barandun, M., Machguth, H., Nussbaumer, S.U., Gärtner-Roer, I. and Thomson, L., 2019. Global glacier mass changes and their contributions to sea-level rise from 1961 to 2016. *Nature*, 568(7752), pp.382-386.

Zhao, M., Ramage, J., Semmens, K. and Obleitner, F., 2014. Recent ice cap snowmelt in Russian High Arctic and anti-correlation with late summer sea ice extent. *Environmental Research Letters*, 9(4), 045009.

Zheng, W., Pritchard, M.E., Willis, M.J. and Stearns, L.A., 2019. The possible transition from glacial surge to ice stream on Vavilov Ice Cap. *Geophysical Research Letters*, 46(23), pp.13892-13902.

Zheng, W., Pritchard, M.E., Willis, M.J., Tepes, P., Gourmelen, N., Benham, T.J. and Dowdeswell, J.A., 2018. Accelerating glacier mass loss on Franz Josef Land, Russian Arctic. *Remote Sensing of Environment*, 211, pp.357-375

Appendix A: Imagery

Table 1. *The imagery used for glacier area delineation and surge-type glacier identification. The table details the individual sensors, ground pixel resolution (m), date of acquisition, area coverage, tiles used, and source information.*

Sensor	Spatial Resolution	Spectral bands	Date(s)	Coverage	Tiles	Source
KH-7	4.9 m	N/A	7th July 1965	All except Komsomolet & Schmidt	DS1022-1005DA010 DS1022-1005DA011 DS1022-1005DA012 DS1022-1005DA013 DS1022-1005DA014 DS1022-1005DA015 DS1022-1005DA016 DS1022-1005DA017 DS1022-1005DA018 DS1022-1005DA019 DS1022-1005DA0120 DS1022-1005DA021	USGS (https://earthexplorer.usgs.gov/)
KH-9	7 m	N/A	22nd June 1979	Only Komsomolet & N. October Revolution	DZB1215-500454L003001	USGS (https://earthexplorer.usgs.gov/)
Landsat TM	30 m	B1: (0.45 - 0.52 µm) B2: (0.52 - 0.60 µm) B3: (0.63 - 0.69 µm)	21st – 24th July 1986	Full coverage	LT05_L2SP_169002_19860723_20200917_02_T1 LT05_L2SP_162003_19860722_20200918_02_T1 LT05_L2SP_160003_19860724_20200918_02_T1 LT05_L2SP_171001_19860721_20200917_02_T1	USGS (https://earthexplorer.usgs.gov/)
			Various dates in July/Aug 1997	Full coverage	LT05_L2SP_167002_19970723_20200910_02_T1 LT05_L1TP_179001_19970711_20200910_02_T1 LT05_L1TP_167003_19970723_20200910_02_T1 LT05_L2SP_177001_19970830_20200909_02_T1 LT05_L2SP_158004_19970724_20200910_02_T1 LT05_L2SP_157004_19970802_20200910_02_T1	
ASTER	v15 m	B1: (0.52 - 0.60 µm) B2: (0.63 - 0.69 µm) B3N: (0.78 - 0.86 µm)	Various dates in July/Aug 2011 (Schmidt Island 20th June)	Full coverage	AST_07_00308162011121734_20211123091415_30482 AST_07_00308212011123556_20211123091324_28626 AST_07_00308212011123605_20211123091314_28293 AST_07_00308212011123547_20211123091314_28299 AST_07_00308122011124210_20211019044822_1490 AST_07_00308162011072436_20211123085034_7322 AST_07_00309012011121753_20211123085753_19671 AST_07_00308202011070009_20211025122709_5827 AST_07_00308122011074912_20211018094530_15987 AST_07_00308122011074921_20211018094510_15738 AST_07_00308122011124228_20211018094530_15995 AST_07_00308202011070018_20211019063322_31230 AST_07_00308122011124219_20211018094530_15982 AST_07_00308122011124201_20211019063322_31233 AST_07_00307082011121208_20211018094540_16065 AST_07_00308192011075520_20211018094500_15606 AST_07_00308122011110445_20211019063252_30941 AST_07_00308192011075529_20211019063222_30830 AST_07_00308172011112316_20211123091435_30746 AST_07_00308112011115948_20211123091435_30740 AST_07_00308172011112307_20211123115146_784 AST_07_00306202011104629_20220220043307_17570	NASA (https://earthdata.nasa.gov/)
Arctic DEM	2 m		12th July 2018	Full coverage	N/A	Arctic DEM (https://doi.org/10.7910/DVN/OHHUKH)
Landsat 8	15 m	B2: (0.45 - 0.51 µm) B3: (0.53 - 0.59 µm) B4: (0.64 - 0.67 µm)	3rd and 6th August 2021	Bolshevik Island	LC08_L1TP_198241_20210803_20210811_02_T1 LC08_L1TP_203240_20210806_20210811_02_T1	USGS (https://earthexplorer.usgs.gov/)
Sentinel 2A	10 m	B2: (490 µm) B3: (560 µm) B4: (665 µm)	Various dates in July, August and September	October Revolution & Komsomolets Islands	L1C_T46XEQ_A031879_20210730T092553 L1C_T46XEP_A031935_20210803T072618 L1C_T47XMH_A031935_20210803T072618 L1C_T47XMJ_A031935_20210803T072618 L1C_T47XNJ_A031935_20210803T072618 L1C_T46XER_A031936_20210803T090557 L1C_T46XDP_A032250_20210825T080608 L1C_T46XDQ_A032422_20210906T084559	USGS (https://earthexplorer.usgs.gov/)

Appendix B: Individual Glacier Data

Data for each glacier is available using the link (below) and includes individual error margins, glacier surface area at each timestamp, glacier names and terminus classifications: https://www.dropbox.com/s/sg86vl3xa70wul6/Supplementary_Data_SZ.xlsx?dl=0